Investigating Uncertainty in Coastal Flood Risk Assessment in Small Island Developing States

A Case Study in São Tomé and Príncipe

Matteo Ulisse Parodi

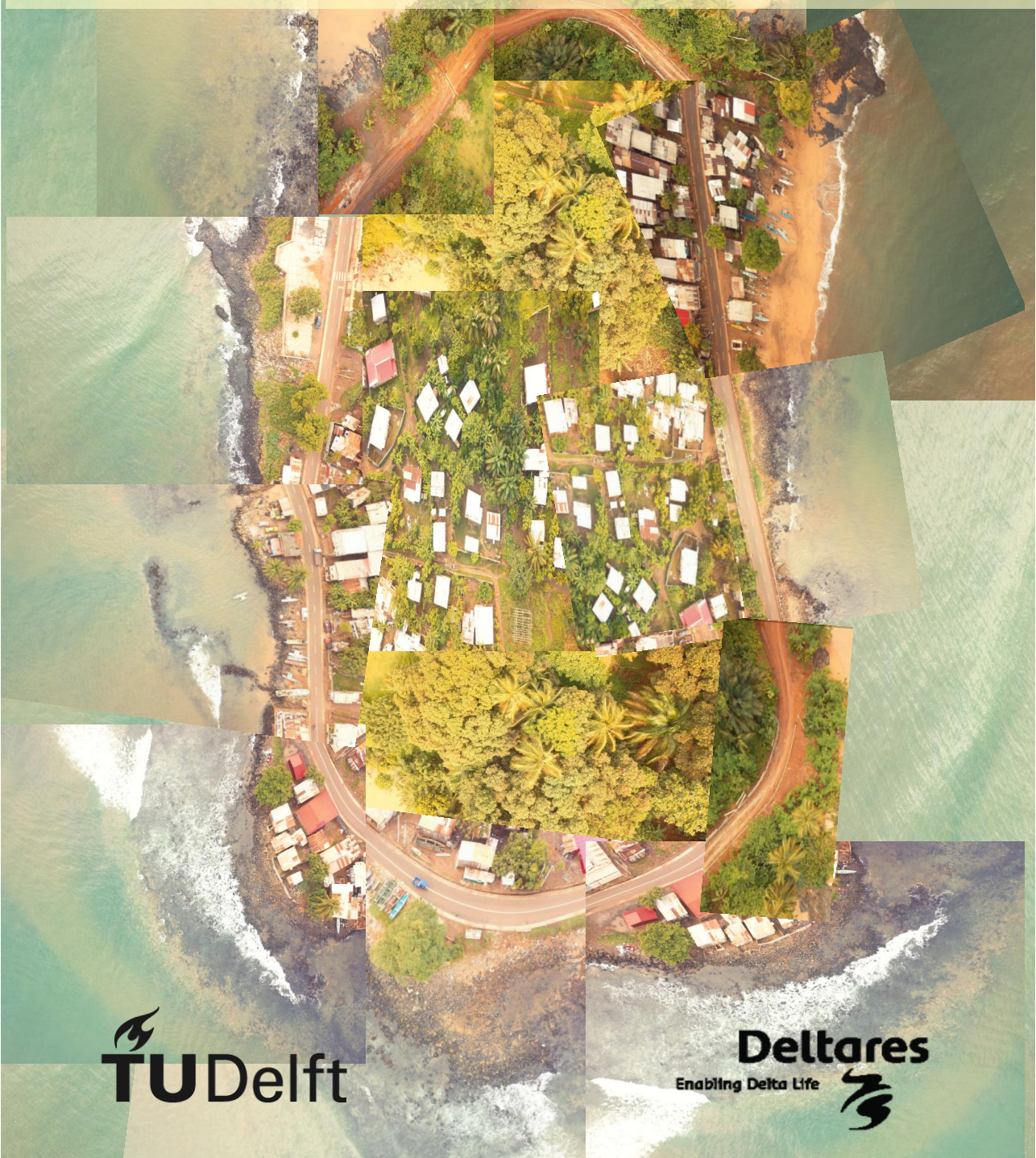

TU Delft

Deltares
Enabling Delta Life

INVESTIGATING UNCERTAINTY IN COASTAL FLOOD RISK ANALYSES IN SMALL ISLANDS DEVELOPING STATES

A CASE STUDY: SÃO TOMÉ AND PRÍNCIPE

by

Matteo Ulisse PARODI

in partial fulfillment of the requirements for the degree of

Master of Science
Coastal & Marine Engineering and Management

at the Delft University of Technology,
to be defended publicly on Wednesday July 17th, 2019 at 08:30 AM.

Thesis committee:
Prof. dr. ir. A.J.H.M. Reniers, Delft University of Technology
Dr.ir. J.D.Bricker, Delft University of Technology
Ir. S.G. Pearson, Delft University of Technology & Deltares
Dr. ir. A.R. van Dongeren, Deltares
Dr. ir. A. Giardino, Deltares

An electronic version of this thesis is available at http://repository.tudelft.nl/
Correspondence with the author may be directed to: parodi.mat@gmail.com
In collaboration with:

Delft University of Technology

Deltares
Enabling Delta Life

Cover: Collage of aerial images of São Tomé and Príncipe ©Deltares & CDR
Back Cover: Aerial image of Príncipe ©www.timbuktutravel.com

The Erasmus+: Erasmus Mundus MSc in Coastal and Marine Engineering and Management is an integrated programme including mobility organized by five European partner institutions, coordinated by Norwegian University of Science and Technology (NTNU).

The joint study programme of 120 ECTS credits (two years full-time) has been obtained at two or three of the five CoMEM partner institutions:

- Norges Teknisk- Naturvitenskapelige Universitet (NTNU) Trondheim, Norway
- Technische Universiteit (TU) Delft, The Netherlands
- Universitat Politècnica de Catalunya (UPC). BarcelonaTech. Barcelona, Spain
- University of Southampton, Southampton, Great Britain
- City University London, London, Great Britain

During the first three semesters of the programme, students study at two or three different universities depending on their track of study. In the fourth and final semester an MSc project and thesis has to be completed. The two-year CoMEM programme leads to a multiple set of officially recognized MSc diploma certificates. These will be issued by the universities that have been attended by the student. The transcripts issued with the MSc Diploma Certificate of each university include grades/marks and credits for each subject.

Information regarding the CoMEM programme can be obtained from the programme coordinator:

Øivind A. Arntsen, Dr.ing. Associate Professor in Marine Civil Engineering
Department of Civil and Transport Engineering
NTNU Norway
Telephone: +4773594625 Cell: +4792650455 Fax: + 4773597021
Email: oivind.arntsen@ntnu.no
URL: https://www.ntnu.edu/studies/mscomem

A bubi.
Ho sempre piú cose da raccontarti, ma scommetto anche tu.

The flood is threat'ning
My very life today
Gimme, gimme shelter
Or I'm gonna fade away.

Rolling Stones

SUMMARY

Small Island Developing States (SIDS) are increasingly under threat of coastal flooding, which challenges the safety of their societies and vulnerable economies. The emergency of this issue, exacerbated by climate change, has alarmed international organisations and national governments that have been demanding for robust risk assessments to guide the development of resilient adaptation strategies. In SIDS, the paucity of local data, required to perform such kind of coastal risk analyses, hinders the application of highly detailed models that therefore need to rely on inaccurate and publicly available data, thus introducing uncertainty in the assessment. This thesis aims to investigate the uncertainty in input data and its impact on coastal flood damage estimates.

This study examines prominent uncertainty sources in the coastal flood risk modeling chain, namely: the stochastic variability of (i) significant wave height and (ii) storm surge water level, the quality of (iii) bathymetry data and (iv) digital elevation models and (v) the choice of depth-damage function. To account for risk temporal changes, two other inputs are included, specifically (vi) different sea level rise projections and (vii) socioeconomic developments. A methodology is developed to test the afore-mentioned inputs through global sensitivity analysis, using an ensemble of hydrodynamic models (XBeach and SFINCS) coupled with an impact model (Delft-FIAT). The impacts of these sources on the flood damage estimates are evaluated in a case study on the islands of São Tomé and Príncipe.

Model results indicate, for the current time horizon, depth-damage functions and digital elevation models as the inputs with the most significant contribution to the overall damage estimation uncertainty, yielding a variation in the output prediction of a factor 16 and 10, respectively. As future climate and socioeconomic development uncertainties are introduced in the system, sea level rise projection becomes, followed by digital elevation models and depth-damage functions, the most relevant input for the year 2100. Neglecting economic growth in the risk analysis leads to an extremely high underestimation of damages. However, given the constrained intrinsic uncertainty for the projected societal trends, its sensitivity on the risk output is limited.

The scarcity of accurate input data proves to have an enormous impact on risk assessments in Small Island Developing States, leading to considerable prediction error and affecting the model outcome uncertainty. New emerging data collection techniques, such as unmanned aerial vehicles, could augment the trustworthiness of risk assessments by providing more accurate datasets for bathymetry and topography. Furthermore, research efforts could be directed towards developing knowledge on the physics of damages and their implementation in a risk modeling scheme. The uncertainty framework presented could be applied in projects with the aim to support risk communication

to stakeholders by portraying the implications of the various inputs used and assumptions made, but also to guide the allocation of limited economic resources towards the acquisition of the input data that matters the most in terms of reliability of damage estimates.

CONTENTS

List of Figures

LIST OF TABLES

List of Acronyms

Abbreviation	Description
ASTER	Advanced Spaceborne Thermal Emission and Reflection Radiometer
CDF	Cumulative Density Function
CFR	Coastal Flood Risk
DASM	Damage Scanner Model
DEM	Digital Elevation Model
DDF	Depth Damage Function
DRR	Disaster Risk Reduction
DSM	Digital Surface Model
DTM	Digital Terrain Model
EAD	Expected Annual Damage
EVA	Extreme Value Analysis
GDP	Gross Domestic Product
GEBCO	General Bathymetric Chart of the Oceans
GEV	Gumbel Extreme Value
GPD	Generalised Pareto Distribution
HF	High Frequency
IG	Infragravity
IPCC	Intergovernmental Panel on Climate Change
JONSWAP	Joint North Sea Wave Project
JRC	Joint Research Centre
MC	Monte Carlo
ME	Mean Error
PDF	Probability Density Function
POT	Peak Over Threshold
RCP	Representative Concentration Pathway
SD	Standard Deviation
SIDS	Small Island Developing States
SLR	Sea Level Rise
SSP	Shared Socio-economic Pathway
SRTM	Shuttle Radar Topography Mission
STD	Sao Tomean Dobras
UAV	Unmanned Aerial Vehicle

ACKNOWLEDGEMENTS

As I write these words, the journey that I began two years ago comes to an end. It has been special, to say the least. Going through it in my mind brings a lot of memories and people that I would like to thank.

First, an extremely certain thank you to my graduation committee. Thank you Ad, for chairing the committee and providing me with useful feedbacks throughout my research timeline. Thank you Jeremy for sharing your ideas and opinions on my project. Stuart, thank you very much for your contagious enthusiasm. Witnessing your energy for research has kept me motivated throughout the past five months. Your willingness to help is inspirational. You pushed me to be always critical about my assumptions and findings. A special thank you goes to my Deltares supervisors, Alessio and Ap. Thank you Alessio, firstly for providing me with the data necessary for this study and secondly for continuously encouraging me to look at my research from a broader perspective. Thank you Ap, for initially taking me as a student and being always available to share your great knowledge on flood risk modeling, pointing me in the right direction.

To my fellow master students here at Deltares, I am grateful for the many lunch and coffee talks, through which we shared ideas and encouragement. You have eased the hours of work and I wish you the best of luck with the beginning of your careers.

Tusen takk, Dank je wel & Thank you to my CoMEM family. From the Norwegian waffles, through the Portswood pubs and all the way to the Dutch canals we have shared countless laughs, memories, trips, ideas and special moments. Thanks to you, I have learned a bit more about the rest of the world. A special mention goes to the Track 4 soldiers that managed to cope with my loud voice and pranks during our stay in Holyrood 16, thank you so much Ingrid, Nikos and Hassan. You will be deeply missed.

Cheers to the Boys. I have been thinking for a while to find the right words to describe what you ended up representing for me. Writing it in a few sentences would not make it justice. Within a couple of days, three legends will set sail to their adventurous journeys, looking forward to seeing where that will take them in a few years. Till the next one Fred and Flo.

Saving the best for last, GRAZIE to my big family: Mamma, Papá and everyone else that has joined it in these last 24 years. You have given my a sense of dedication that has never left me. Receiving your support and love is a gift that I bring with me every day.

Matteo Ulisse Parodi
Delft, July 2019

1

INTRODUCTION

CHAPTER SUMMARY

Small Island Developing States are increasingly under threat of coastal flooding, which challenges the safety of their societies and vulnerable economies. The consequences that they will face due to climate change, particularly considering the risk of coastal floods, are disproportionate to the amount of greenhouse gases produced by them in the past century. This situation has led to numerous global initiatives aiming to increase the resilience of insular communities, which require robust coastal flood risk assessment to develop resilient adaptation strategies. Accurate data on hydrodynamic and damage models is scarce for many of these islands, due to their remoteness and limited size. Indeed, knowing what input data matters the most would be beneficial for increasing the reliability of models. Therefore, this thesis investigates the impact of uncertainty sources on flood damage estimates, in order to improve the trustworthiness of risk analyses in SIDS.

1

1.1. MOTIVATION

This study is motivated by the increasing threat of coastal flooding that many communities around the world are facing, particularly in the view of climate change. A group of countries that will be most impacted by climate change are Small Island Developing States (SIDS). Their fragile environmental safety has been recognised and many initiatives have been launched to support them.

SMALL ISLAND DEVELOPING STATES DISASTER VULNERABILITY

SIDS comprise more than 50 countries around the world (see Figure 1.1), with varying geographical and economic characteristics. SIDS are very vulnerable to a range of different environmental hazards due to many factors, among which the most important ones are their small size and remoteness (Pelling and Uitto, 2001), (OECD World Bank, 2016). These features amplify their vulnerability, often leading to a relatively narrow resource base that minimises their economic diversification and hinders their development (UN-OHRLLS, 2015), (Hongbo, 2014), (Méheux et al., 2007).

Figure 1.1: Small Island Developing States, from Osiris, at https://en.wikipedia.org/wiki/Small_Island_Developing_States/File:SIDS_map_en.svg

Several coastal communities around the world will experience increasing coastal flood risk owing to climate change induced sea level rise (Nicholls et al., 2007). These consequences will be particularly felt in SIDS (UN-OHRLLS, 2015), (Storlazzi et al., 2018). Indeed, most island communities live within few meters from the waterline and accommodation space is scarce, thereby their exposure exacerbates the damages of coastal floods. Furthermore, the frequency and intensity of extreme weather events is increasing, as is the exposure of poor and vulnerable communities of SIDS (Kaly et al., 2002), (IPCC, 2001), (McGranahan et al., 2007), which reduces the liveability of such areas. Indeed, the number of natural disasters impacting SIDS has already been increasing since 1960 (OECD World Bank, 2016), see Figure 1.2. Climate change will also negatively impact different economic sectors, like fisheries and tourism. Tourism alone is responsible for more than 30% of the Gross Domestic Product (GDP) for several SIDS, particularly in

the Caribbean (UN-OHRLLS, 2015). As an example, the tourism industry in Caribbean SIDS is projected to loose 3 billion USD by 2100 as a consequence of climate change (UN-OHRLLS, 2015),(Moore, 2010).

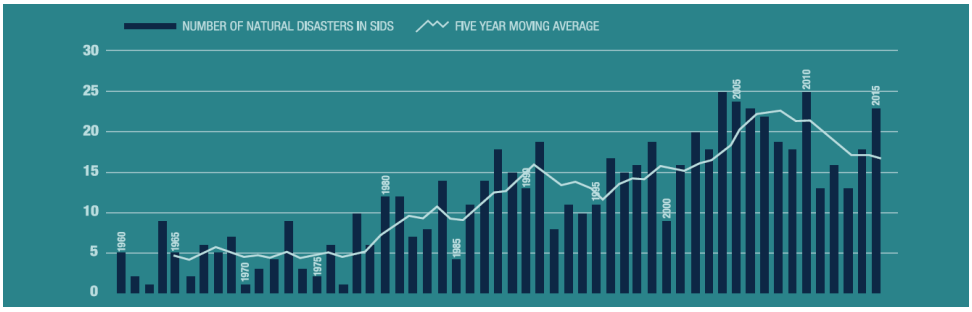

Figure 1.2: Occurrence of major natural disasters in SIDS since 1960, from (OECD World Bank, 2016)

Even though SIDS are considered among the countries most impacted by climate change, they are dealing with many other issues. These include rapid rural-to-urban migration (Chilunga et al., 2017) and a lack of appropriate infrastructure (Kelman and West, 2009), hence increasing the number of assets that can be affected by coastal floods.

These factors highlight the growing importance of investing in Disaster Risk Reduction (DRR) and building resilience of SIDS (GFDRR; The World Bank; ISDR, 2016). Indeed, in recent years numerous initiatives have been started that aim at developing a sustainable future for SIDS. For example, the Small Islands States Resilience Initiative (SISRI), a global program launched by the Global Facility for Disaster Risk Reduction (GFDRR). The objective of the program is to provide technical and operational support to help island nations increase the effectiveness of their resilience actions, in order to reduce climate and disaster risks to SIDS populations, assets, ecosystems and economies. Such programs call for a more robust assessment of coastal flood risk.

CHALLENGES IN COASTAL FLOOD RISK ASSESSMENTS

The need for coastal flood risk analyses has increased in the past years (GFDRR The World Bank, 2014). However, these analyses have generally been lacking for SIDS compared to more developed countries (Méheux et al., 2007). These assessments are required for planning adaptation and engineering activities, since they provide insights of the potential threats to populated areas by computing expected damages from the flooding hazards. Thanks to these kinds of analyses, the optimal investment option that reduces the risk can be selected. In recent times, the benefit of investing in nature based solutions and exploiting local knowledge to adapt to climate change has been highlighted (Mercer et al., 2012).

For the relevance of these purposes, an appropriate and robust risk assessment is recommended. At the present state, for regional and local scale analyses, hydrodynamic models can achieve acceptable levels of accuracy. Nevertheless, trying to reproduce reality with models comes at the cost of simplifying and introducing errors in the system (Vousdoukas et al., 2018a). Moreover, because precise input data are often not available

in developing countries (Monioudi et al., 2018), (GFDRR The World Bank, 2014), all output values are subject to imprecision. A large amount of the uncertainties comes from the quality of input data and the methods used to collect it. Especially for data-poor environments, such as SIDS and other oceanic islands, the lack of locally retrieved data often forces the use of publicly available information for environmental risk analyses. Although, the degree of precision of globally available datasets is usually not enough for hydrodynamic models (Van de Sande et al., 2012). Furthermore, to develop long term adaptation plans, future risk estimates that include temporal changes are required (De Moel et al., 2012), which introduces further assumptions and uncertainty. Indeed, if both climate change and societal developments are included in the analysis, they can carry a significant amount of additional uncertainty towards the model outcome (Wahl et al., 2017), (Bouwer et al., 2010). Therefore, the final outcome of a risk analysis is imperfect and uncertain.

The usefulness of any model partly depends on the accuracy and reliability of its output. Investigating which model inputs matter the most for current and future risk estimates can guide the allocation of limited financial resources to collect new data (Loucks and Van Beek, 2017), ultimately improving the risk assessment. At the same time, estimating the consequences of inaccurate data and modeling assumptions can improve the communication of risk to the stakeholders (Thompson, 2002).
This thesis will aim to identify and estimate uncertainties in the assessment of coastal flood risk (CFR), especially in data-poor environments, like SIDS.

Main Motivation for Research:

- Many SIDS are already facing high risk of coastal flooding
- Climate change and societal developments will pose unique challenges to islands residents
- Lack of accurate input data to perform robust CFR assessments for SIDS

1.2. RESEARCH SIGNIFICANCE

Traditionally, flood management has been focusing on identifying the most suitable flood mitigation strategy for a given (deterministic) scenario, where a single probability of occurrence is taken into account (Jonkman et al., 2016). However, recently there has been an increasing shift towards a more risk-based approach to flood management (Kron, 2005), (Nicholls et al., 2007), (Apel et al., 2006) where multiple undesired events and their probabilities are investigated and combined. Nonetheless, there is still a knowledge gap regarding the uncertainty in the assessment of flood risk (Apel et al., 2004). As previously mentioned, input data and model assumptions are, at least, imperfect and therefore risk analyses are subject to error and wrong estimations. Currently, studies on flood risk uncertainty are growing in number (Jacobsen, 2005), (Merz et al., 2004), (Merz and Thieken, 2009), (De Moel et al., 2012), (Uusitalo et al., 2015), (Wagenaar et al., 2016), (Vousdoukas

et al., 2018a). However, most of these studies focus only on one part of the whole risk assessment chain, such as the hydrodynamic modeling or damage modeling. Moreover, research studies which have investigated inputs uncertainty have mainly focused on developed countries. To the author's knowledge, the relative importance of different inputs has not been thoroughly studied for developing countries, where often accurate data is lacking. Furthermore, uncertainty analyses for risk assessments that consider future scenarios are scarce and only a few integrate temporal changes in risk predictions (Vousdoukas et al., 2018a). Societal and economic developments alter the exposure and vulnerability of the assets, ultimately changing the risk. While climate change impacts on projected flood damages, such as sea level rise, are being accounted for, socioeconomic changes have often been overlooked in several studies.

The present study aims to fill the knowledge gaps regarding uncertainty propagation in risk analyses. First, a methodology is developed (see Section 3), which could be applied to different risk analyses. Furthermore, we seek to bride the gap in assessing uncertainty in coastal flood risk. Indeed, most of precedent studies have only focused on one aspect of risk, whereas here we attempt to investigate uncertainty along the whole risk analysis (see Section 2.1). The temporal evolution of risk is investigated, by including climate and socioeconomic changes and their impacts on CFR. The outcomes of this study could also support decision-making in data-poor environments. In fact, if we improve our understanding of the uncertainties in flood modeling, we can build public confidence in the output, communicate implications of limitations in the analyses and provide the best possible background for efficient decision making.

1.3. RESEARCH OBJECTIVES

In this section, the research objectives and questions are presented. To answer these questions, we hope to give new insights on what inputs are most important for local scale flood risk assessment. The main research objective that has been set for this research is:

Main Objective:
Investigate input uncertainty in the calculation of flood damage and risk in data-poor environments

Sub-Objectives:

1. Develop a methodology to reproduce input uncertainty for coastal flood risk assessments
2. Identify and estimate uncertainties in the assessment of coastal flood risk
3. Investigate the change of uncertainties for future risk estimates

4. Investigate the importance of input data for coastal flood risk assessments

The main objectives will be fulfilled by answering the following question:

Main Question:
How can we estimate relative uncertainties in input data for coastal flood risk assessments and their impact on damages evaluation?
Sub-Questions:

1. *Can we estimate uncertainties by varying input distributions and data in a train of models?*
2. *What are the most important inputs that drive uncertainties in coastal flood risk assessment?*
3. *How important are inputs interactions to estimate uncertainties and how do they vary under future conditions?*
4. *What is the minimum required quality of input data to have a satisfactory assessment of risk?*

1.3.1. RESEARCH APPROACH

To tackle the fore-mentioned sub-questions, the following tasks will be performed:

1. *Can we reproduce uncertainties by varying input distributions and parameters in a train of models?*
   - Identify inputs that can have a significant impact in the uncertainty of the outcome
   - Establish ranges of input values and datasets using literature, field and publicly available data to conduct a sensitivity analysis
2. *What are the most important inputs that drive uncertainties in coastal flood risk assessment?*
   - Analyse uncertainty propagation in the risk assessment
   - Quantify the impact of uncertainties on the risk outcome
   - Identify to which inputs risk estimates are most sensitive to
   - Define guidelines for potential use of the analysis for risk uncertainty reduction

3. *How important are inputs interactions in estimating uncertainties and how do they vary under future conditions?*
    - Assess the interactions between variables and how they reflect on output uncertainty
    - Identify variables that can represent climate and socioeconomic changes for future conditions
    - Estimate the variation of relative importance of the analysed input over different time horizons
4. *What is the minimum required quality of input data to have a satisfactory assessment of risk?*
    - Assess the variation of uncertainty and error in the model output from the variation of input data
    - Suggest guidelines for utility decision in flood risk management

1.4. THESIS OUTLINE

Chapter 1 lists the main motivation for the research and the approach used to tackle the research questions. The processes that lead to coastal hazards and the main steps of a coastal flood risk assessments are described in Chapter 2, which also defines uncertainty (2.4). From that, the uncertainty sources considered for this study are also illustrated. In Chapther 3, first the modeling approach is defined, followed by a description of the set of inputs included. The results are presented in Chapter 4 and discussed in Chapter 5. Conclusions are drawn in Chapter 6, were also some recommendations for future research are proposed. The Appendixes include preliminary sensitivity tests results and detailed model setup (A-C). Appendix E shows some preliminary results of the impact of interpolating techniques.

2

LITERATURE REVIEW

CHAPTER SUMMARY

In this chapter the most relevant information necessary to understand the concept of coastal flood risk is given. The components of risk are defined (Section 2.1) together with its main drivers in the coastal environment (Section 2.2). Then, the main steps that comprise a typical flood risk assessment are briefly outlined in Section 2.3. Uncertainty analysis and the possible approaches are described in Sections 2.4, highlighting the advantages and disadvantages of each method. The most important input data that are used in the assessment of coastal flood risk, which comprises hazard, topography and damage variables, are treated in the last Sections 2.5, 2.6 and 2.7. For each input type, its most important uncertainties identified from literature are also defined.

2.1. FLOOD RISK

It is important, before starting to address the methodology, to give clear definitions on a few concepts that will be used in this work and that could give rise to confusion. Indeed, the term risk is understood in different ways by different people. In the scientific community, it is generally agreed that risk is the product of a hazard and its consequences. In this work, the definition given by (Kron, 2005) will be used. According to (Kron, 2005), three components determine the risk: hazard, exposure and vulnerability, see Figure 2.1. The hazard encompasses the physical aspect of risk, whereas exposure and vulnerability are related to socioeconomic characteristics.

Figure 2.1: Disaster Risk definition, from http://www.un -spider.org/risks-and- disasters/disaster -risk-management

Hazard is the probability and magnitude of an event with negative impacts. From (UNISDR, 2016):

"*A process, phenomenon or human activity that may cause loss of life, injury or other health impacts, property damage, social and economic disruption or environmental degradation.*"

A hazard is usually identified by a set value for a set return period. For example, a flood depth inland resulting from the combination of water levels and waves represents a coastal flooding hazard. In other fields of flood risk, such as river flooding, hazards can also be quantified by inundation depths and flow velocity (Merz et al., 2007).

Following from (UNISDR, 2016), also exposure can be defined :

"*The situation of people, infrastructure, housing, production capacities and other tangible human assets located in hazard-prone areas.*"

Exposure, therefore, entails the assets that are exposed to the natural hazard. Measures of exposure can include the number of people, or they can be estimated through

spatial information, by looking for instance at land cover maps and infrastructure distributions.

The last component is vulnerability (UNISDR, 2016):

"*The conditions determined by physical, social, economic and environmental factors or processes which increase the susceptibility of an individual, a community, assets or systems to the impacts of hazards. .*"

Vulnerability allows to compute the damages received by a receptor given its hazard and exposure. It constitutes a fundamental stage in a risk analysis. Two different receptors may be subjected to the same environmental hazard but experience different damages (e.g. two buildings with different flood resistance). The schematics of this definition are shown in Figure 2.2 for a simplified case. The top panel in this figure shows different exposures, where all three elements including the industrial plant, residential buildings and the buildings on high ground have high exposure (as their asset value is considered high). The middle panel shows the possible hazard resulting from higher water level and waves. In this case, 2 of the 3 receptors will be damaged (high vulnerability) but the buildings on the high ground, will not be affected and therefore even with high exposure, their vulnerability under the same hazard is lower (lower panel in the figure).

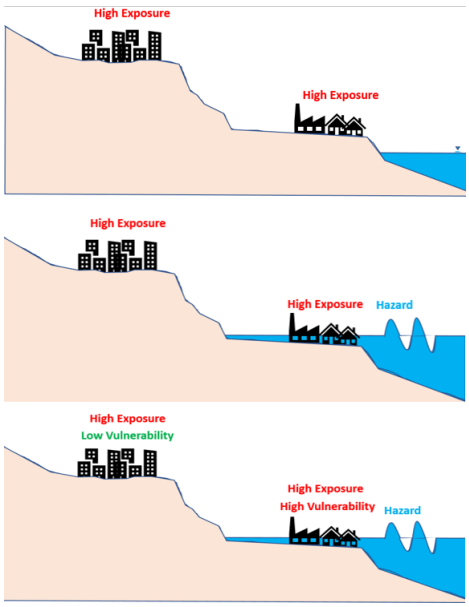

Figure 2.2: Simplified description of the three risk components.

2.1.1. FLOOD DAMAGES

Another very crucial part of flood risk's taxonomy is the definition of its unit of measure. Risk is often seen as the probability of an undesired event, multiplied by its consequences. Therefore, the unit of risk directly follows from the definition of the units of probability and consequences. The unit of measure for the probability is usually given, in flood analyses, by the return period of the event, in this case the hazard (Jonkman et al., 2016). For example, an extreme water level with an estimated occurrence of once every 100 years, will have a $0.01/year$ probability. The consequence of a specific hazard can be measured differently according to the targets, such as the number of fatalities, economic loss or natural habitat loss. In most studies and applications, consequences are expressed in monetary terms, for example €. The unit of risk (or expected value $E(d)$) then becomes € per year. A flood event with a 0.01 year probability that would cause damages for a value of 100.000 € has a risk of $1.000\ €/year$, also known as Expected Annual Damage (EAD) (Olsen et al., 2015).

From a general perspective, damages can be divided in *direct*, which relate to the immediate physical contact of flood water to people and assets, and *indirect* damages, which occur in an area that is not directly impacted during the flood. Most indirect losses refer to the temporary or permanent interruption to economic sectors that sustain the communities, including the damaging of roads for goods transport or the failure of factories upon which workers rely for their income (Scawthorn et al., 2006). Another relevant distinction is given by the possibility to express the damage in monetary terms or not. *Tangible* damages can, indeed, be expressed in monetary terms (e.g. the value of a flooded infrastructure). This is not the case for *intangible* damages. Intangible damages refer to targets and assets whose value is difficult, if not impossible, to quantify. Human fatalities or environmental losses represent some of the most common intangible damages. Table 2.1 presents an overview of the mentioned damage classification, based on (Jonkman et al., 2016) and (Penning-rowsell, 2004).

Table 2.1: Possible direct and indirect damages from flooding.

	Tangible	**Intangible**
Direct	• Vehicles • Buildings • Infrastructures •Contents	• Loss of life • Loss of natural habitat • Injuries and health effects
Indirect	• Loss of tourism activity • Traffic disruption • Emergency measures costs •Loss of industrial production	•Post-disaster mental disturbance • Increased vulnerability of survivors • Damage to government

Many risk analyses only concentrate on estimating direct damages, mostly for the sake of simplicity and often indirect damages are simply estimated by using a percentage of the direct damages (Messner and Meyer, 2005). Nevertheless, discarding other types of damages substantially underestimates the overall risk. Social losses and induced dam-

ages can represent a considerable share of the consequences of coastal floods. People that will be displaced in the occurrence of a flood will have shelter needs with their relative costs. Moreover, the tertiary industry of a country would be damaged in the event of a flood, as flooding prone areas may be temporarily inaccessible and would attract fewer tourists (Moore, 2010).

Unfortunately, due to the lack of necessary data, this study is constrained to direct and tangible damages, where only the economic effects on buildings are considered.

2.2. DRIVERS OF FLOOD RISK

In this section the different processes that can cause or change flood risk are presented. These mainly refer to the various mechanisms that can cause the occurrence of a flood hazard, but also other activities that can alter the exposure or the vulnerability of the flood targets. The review is conducted looking at the development of the three aspects of risk for future time horizons, under a varying climate and socioeconomic system.

2.2.1. COASTAL FLOODING PROCESSES

Water surface oscillations have a considerable complexity and variety in the ocean. Many different hydrodynamic processes can occur at different spatial and temporal scales along coastlines, thus it becomes essential to have a sound understanding of the various mechanisms and to set the scope of the analysis. In this section, we will first briefly describe the main hydrodynamic processes that occur in the nearshore zone, with a particular focus on those that are likely to cause floods. Then we will narrow down the range of processes that will be included in this study, as a complete analysis of all the different processes would not have been sustainable for the time of this project.
Water surface oscillations can be generated in different ways and span different frequencies. This is shown in Figure 2.3 taken from (Holthuijsen, 2009), which includes a classification of these processes based on their period. Tides and surges, described in the next section, can as well be regarded as waves that have a period which ranges from a few hours to more than a day.

WATER LEVELS

Water levels pose a high threat for many islands and coastlines around the world. Generally, water level variations have a periodicity and can mainly be attributed to tides generated by the gravitational forces of the sun and the moon. Nevertheless, water levels can also vary episodically with pressure induced storm surges, and, at longer time scales, sea level rise.

TIDES

Tides are periodical variations brought from gravitational forces on water from the Moon and the Sun. Their period, intensity and variability of tides varies globally due to many interferences such as land-mass or the axis of earth (Bosboom and Stive, 2011). During the moon cycle, also the magnitude of tides varies, generating neap and spring tides. For low-lying countries, spring tides can be already occasion of temporary flooding, as the tidal excursion can be rather consistent.

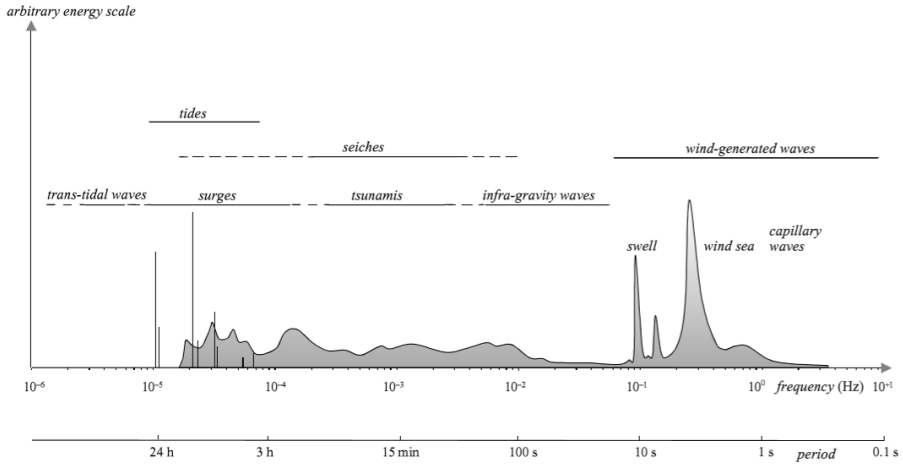

Figure 2.3: Frequency spectrum for water surface motions, from (Holthuijsen, 2009).

STORM SURGE

Wind pressure induced sea level variations are another main contributor of coastal flooding, referred as storm surges. Storm surges consist in a local water level change due to an atmospheric pressure difference that is compensated by an increase in surface elevation. High wind speeds during sea storms and cyclones exert high shear stresses on the water surface, that result in piling up of the water near the coast. Usually, storm surges have a stronger impact on coastlines with a wide and shallow shelf, which allows for higher water volumes to pile up on the coast. Narrow and steep shelves would encounter smaller surges, although they might still generate flooding. Oceanic islands that are located away from land, experience generally smaller storm surges compared to islands that are closer, as the water is less constrained by the surrounding land mass.

SEA LEVEL RISE

Sea level rise is considered one of the most prominent consequences of climate change and threats to coastal cities and civilizations around the world(Nicholls et al., 2007), (IPCC, 2001). The study of sea level rise is strongly complicated by the different processes that contribute to it. Indeed, sea level rise (SLR), or relative SLR, where relative indicates the relative change of the sea level in relation to the coastline position, is a combination of absolute sea level rise and coastal response (Curray, 1964). For example, absolute sea level rise may be sustained by a coastline if enough sediment input is fed to it, in order to build a dynamic balance with the water level (Nichols, 1989). At the same time, land subsidence may result in a relative SLR, even though the absolute sea level rise stays constant. From now on, we will refer to relative SLR as SLR.

Sea level rise is influenced by many processes, including gravitational attraction from land and ice masses or isostatic uplift or subsidence of the earth's crust (Mitrovica and Milne, 2002). The study of all these processes goes beyond the scope of this research, although sea level rise represents one of the main components of coastal flooding and car-

ries a considerable amount of uncertainty (Wahl et al., 2017), (Vousdoukas et al., 2018b) which should then be taken care of in flood risk analyses. One dangerous consequence of sea level rise is its interactions with wave dynamics. Many atolls and islands around the globe have very little accommodation space and sea level rise will allow for higher waves to reach the shores, thus exacerbating the risk of flooding (Storlazzi et al., 2018). These consequences are strongly coupled with the limited fresh water resources in these locations. Coastal flooding and rising sea level contaminate groundwater in SIDS and other islands around the world (White and Falkland, 2010), posing big threats to the local communities.

Sea level rise predictions are primarily based on future climate scenarios. The Intergovernmental Panel on Climate Change (IPCC) has defined four different greenhouse gas Representative Concentration Pathway (RCP) (IPCC, 2013). They describe different scenarios, namely RCP 2.6, RCP 4.5, RCP 6 and RCP 8.5, labelled after a possible range of radiative forcing values for the year 2100. The RCP 4.5 assumes emissions to peak around 2040 and then decline, whereas, in RCP 8.5, emissions continue to rise throughout the 21st century. According to each different scenario, different sea level rises for coming years have been predicted (see Figure 2.4). The figure shows the global projections of mean sea level rise over the 21st century, for the scenarios RCP 2.6 and RCP 8.5, from (IPCC, 2013). The shaded bands indicate the likely range of SLR. On the right, the likely ranges over the period 2081-2100 for all four RCP scenarios are given as coloured vertical bars. Such predictions are based on climate models that consider different environment variables and that require numerous assumptions. These assumptions yield different results and developments that ultimately increase the uncertainty surrounding these predictions.

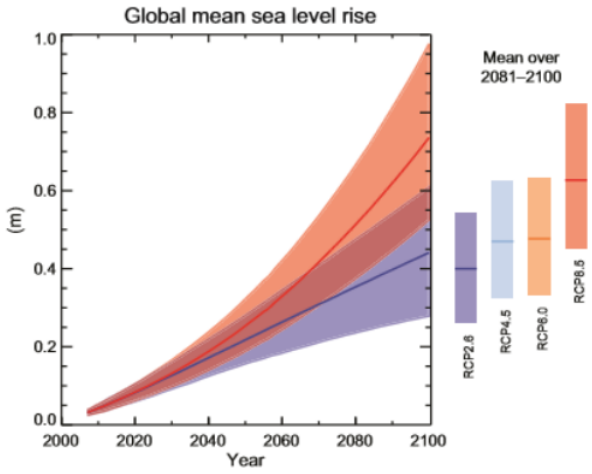

Figure 2.4: Projections of global mean sea level rise over the 21st century , relative to 1986-2005, for the scenarios RCP 2.6 and RCP 8.5. From (IPCC, 2013).

WAVES

WIND GENERATED WAVES

Wind waves are locally generated waves that originate from a storm. These storm waves typically have shorter periods and higher steepness. The sea surface under storm waves is generally rough. Their impact during storms is usually exacerbated by a water level increase that allows them to travel further onshore.

Contrarily from wind waves, swell waves are generated from distant wind fields and travel long distances before reaching the shore. Their generation comes from frequency and directional dispersion, which consists of different frequency waves travelling at different speeds. These different travelling speeds result in grouped lower frequency waves that travel further from the storm origin. Remotely generated swell waves are one of the main drivers of flooding for Pacific Islands. (Hoeke et al., 2013) have highlighted the impacts of this phenomena, also referred to as “Blue sky” event, that can produce heavy consequences with almost no warning and are challenging to forecast, as they travelled from a remote area.

INFRAGRAVITY WAVES

Infragravity (IG) waves have much longer periods than wind generated waves. Typically, the frequency cut-off to define IG waves is at 0.05 Hz, which corresponds to a wave period of 20 seconds. In literature, two main generating mechanisms have been identified. The relation between the presence of short-wave groups and low frequency motions at the shoreline was firstly observed by (Munk, 1949) and (Tucker, 1950), although (Biésel, 1952) was the first to demonstrate it mathematically. This process creates a ’bound’ long wave that travels with the high frequency (HF) waves group. The second generating mechanism was proposed by (Symonds et al., 1982). In their theory, the varying location of the break-point for short waves is responsible for generating long waves.

Bound long waves are generated offshore, due to the amplitude variability of the short waves within a single wave group. Indeed, higher HF waves will exert a stronger force on the water surface than smaller waves, thus pushing the water level lower. This entails a relative water level set up at the location of the smaller waves. This varying set up motion is small in offshore water depths but grows substantially in size in shallower waters. Figure 2.5 depicts the time series of short waves and the related bound wave (in red). Note that at the location of highest short waves, there is a bound wave trough.

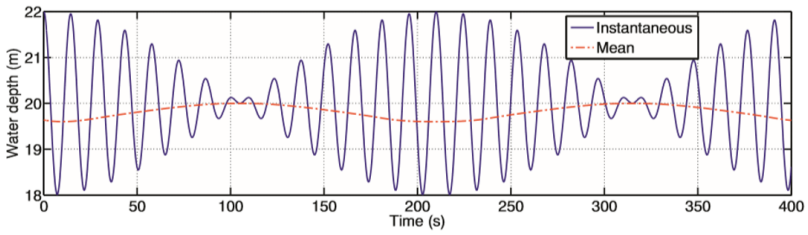

Figure 2.5: Free surface elevation (blue) and mean sea level oscillations (bound wave), over time.

The second mechanism is still related to wave groupiness. The amplitude variance over the group scale results in a varying break point in the surf zone, as higher waves will break further offshore. The dissipation of wave energy at varying position produces a time-varying gradient of the radiation stress. This time-varying gradient stress is balanced by a time-varying set-up (Symonds et al., 1982). These two mechanisms can be present simultaneously on a coastline, although (Baldock et al., 2000) have demonstrated that the break-point mechanism tends to dominate on steeper slopes, whereas for milder slopes, the shoaling of incoming bound waves is the governing process (Battjes, 2004). This is because, on steeper slopes, bound long waves have a "shorter" amount of time to shoal and much of their energy is reflected from the shore rather than dissipated.

IG waves heavyly influence run up at the shore, as they can directly increase the set up and allow for HF waves to travel closer to shore (during a long wave crest, the water depths will be higher and short waves will break further onshore). Finally, besides the cross-shore influence of long waves on set up and set down, these motions can also result in long-shore processes, such as edge waves. (Bertin et al., 2018) provides an exhaustive review of the literature on infra-gravity waves, for further reading.

TSUNAMIS AND METEOTSUNAMIS

Tsunamis can have devastating impacts along the coastline. Referring in Japanese to "big wave", the term tsunami has been used by oceanographers to describe earthquake's induced sea level motions. Tsunamis can have varying wave periods from a few minutes to hours and travel towards shore at very high velocities. As they reach shallow water, they are highly influenced by the local bathymetry and their wave height can increase abruptly. Land-slides and meteorites clashes are also considered generating processes.

Meteotsunamis are very long ocean waves in the tsunami frequency band that are originated by pressure disturbances (from here the name meteotsunamis). The research interest around meteotsunamis has been growing in recent years, as experts have been trying to describe their generating mechanism. These phenomenons, which have an amplitude of only a few centimeters offshore, can grow exponentially when they enter shallower waters. The main point of difference between meteotsunamis and seismic-induced tsunami is their spatial scale of impact. Being generated from highly energetic tectonic movements, tsunamis carry a more significant amount of momentum which results in their impacts being felt at very large scales (Leone et al., 2011). On the other hand, meteotsunamis can have smaller spatial scales, affecting only small bays or lagoons. Meteotsunamis have been noticed to occur frequently in certain areas of the world where they received specific names from the local population: "rissaga" in the Balearic Islands, "marubbio" in Sicily (Candela et al., 2002) and "abiki" in Japan((Hibiya and Kajiura, 1982)). The barometric anomalies that form meteotsunamis can only generate high water level oscillations when they are in resonance with the shelf resonance frequency. This resonance can be further increased in enclosed bays and harbours if the resonance periods of the atmospheric forcing and of the harbour depth match.

RUN-UP

A widespread indicator of coastal flooding hazard is the water level run-up. An accurate determination of this parameter is necessary for flood risk analyses, as underestimating it would result in an overall underestimation of the flood risk.

Runup and rundown are the up and down motions of the waterline at the shore. According to (Stockdon et al., 2006), runup can be divided into two components: maximum setup, the time-averaged water level elevation at the shoreline and swash, the time-varying vertical fluctuations about the temporal mean surface. Water level set up (onshore) and set down (offshore) are due to the gradient of radiation stresses in the cross-shore direction resulting from wave breaking (Bosboom and Stive, 2011). The effect of swash motions to runup can be further divided into infragravity swash and incident swash, resulting from low and high frequency waves respectively. The influence of one frequency band over runup varies accordingly to the beach type. On dissipative beaches, the runup will be dominated by infragravity motions, as they dominate the swash zone. On the other hand, as the influence of short, incident frequencies becomes more important on more reflective beaches, so will the influence of incident swash on the total runup.

For the scope of our research, modeling all the above processes would not be feasible. In our analysis, only swell waves generated from distant storms will be modeled, together with infragravity waves, which allowed us to consider their different contribution to the runup. Regarding water levels, also the impact of storm surges and tides will be included, which allowed us to look at their different contributions to hazards and flooding. Furthermore, to assess the temporal changes of the hazard, sea level rise predictions are considered.

2.2.2. CHANGES IN EXPOSURE AND VULNERABILITY

Changes in exposure are linked to socioeconomic development within the flood-prone zone. Many studies have estimated the impacts of population growth and increases in wealth on the increasing losses from natural disasters. In their study, (Bouwer et al., 2010) have found that socioeconomic changes, mainly relating to the change in land-use due to urbanization, appear to affect flood risk at least as much as climate change.

Changes in exposure can be linked to migration movements and rapid urbanization (Chilunga et al., 2017). Such global trends lead to an increase in the population of large coastal cities, which ultimately increases the already elevated risk of coastal flooding. This is occurring in SIDS, where often unplanned urbanization has lead to a higher likelihood of flood-related deaths (Chilunga et al., 2017). Other social and economic aspects can influence risk. For example, the distribution of welfare in the impacted community can result in different vulnerability, as poorer people are typically more vulnerable and affected by floods (Cannon, 2000). These factors are often left out in risk analyses.

The vulnerability of some areas and assets may well be enhanced or reduced, both through artificial or natural processes. Heightening coastal houses would ensure that,

for the same flooding event, the damages will be smaller and thus reducing the risk. At the same time, land subsidence could increase the relative flood depth for the same hazard, leading to greater damages. Other vulnerability changes are linked to policy measures that involve the introduction of mitigation actions in the coastal flood-prone area. Indeed, adopting a safer building code or defensive measures may reduce significantly the overall risk in a specific area (Vousdoukas et al., 2018a).
Despite being very relevant, these factors are often left out in risk analyses, owing to time constraints or to their challenging model implementation.

Since changes in vulnerability and exposure are strictly linked to the societal development of human societies, an important aspect that needs to be considered for future predictions of risk are the societal development scenarios. Societal developments can be described both quantitatively or qualitatively. Quantitative components provide assumptions for elements such as population or economic growth. Qualitative elements, on the other hand, describe the evolution of aspects of society like political stability or quality of life. In the past decades a joint effort to develop sets of integrated future societal developments has been made, in parallel with the creation of RCP scenarios described previously (Riahi et al., 2017), (van Vuuren et al., 2011), (O'Neill et al., 2017). These possible developments are described as Shared Socioeconomic Pathways (SSP). These pathways provide both quantitative and qualitative metrics for different variables that allow to predict future flood risk. These scenarios are designed to span a wide range of uncertainty in future developments and are defined based on the nature of the *outcomes*, rather than the *inputs*, (Riahi et al., 2017). In other words, a particular outcome is first defined and, consequently, the inputs that could lead to it are identified. SSPs are based mainly on two outcomes: the efforts that will be necessary either to mitigate or to adapt to climate change for future years. Figure 2.6, from (Riahi et al., 2017), shows the classification focused on challenges to mitigation and to adaption.

A list of the SSPs is shown below from (O'Neill et al., 2017)

- **SSP 1** - Sustainability:
  A gradual shift towards a more sustainable path is predicted. Reduced inequality both across and within countries, as well as educational and health investment that accelerate the demographic transition. This world is making relatively good progress towards sustainability, with ongoing efforts to achieve development goals while reducing resource intensity and fossil fuel dependency.

- **SSP 2** -Middle of the road:
  The trends typical of recent decades continue, with some effort towards achieving development goals, historic reduction in resource and energy intensity, and slowly decreasing fossil fuel dependency.

- **SSP 3** Rocky Road- Fragmentation:
  Opposite of sustainability. High challenges to mitigation and adaptation, which come from a general trend among countries to increasingly focus on domestic issues rather than global. A decline in education and technological development investments.

Figure 2.6: Five shared socioeconomic pathways (SSPs) from (Riahi et al., 2017).

- **SSP 4** A road divided - Inequality:
  This pathway describes a highly unequal world, both within and across countries. investments in human capital, combined with increasing disparities in economic opportunity and political power, lead to increasing inequalities and stratification both across and within countries.

- **SSP 5** Fossil fueled development - taking the highway:
  High exploitation of fossil fuel resources and adaptation of energy-intensive lifestyles in order to enhance economic and social development. At the same time, strong investments in health, education and institutions to enhance human capital.

2.3. FLOOD RISK ASSESSMENT

In this research, we will focus on the uncertainty sources for estimating the consequences of a single hazard scenario, a process that will be referred to as flood risk assessment. However, a risk analysis is defined in literature as a quantitative assessment of all (known) undesired events (Jonkman et al., 2016). Our assessment will consider only one scenario and is complementary to a fully probabilistic risk analysis, where all scenarios are integrated.

SPATIAL SCALES IN FLOOD RISK ASSESSMENT

Different spatial scales exist in flood risk analysis. They vary according to the model complexity and purpose of the study. Micro(local)-scale studies focus on single coastal

communities, meso(regional)-scale on a regional level, such as a dike ring in the Netherlands or a coastal sediment cell and macro(national)-scales focus on the national level. Finally, supra-national scale studies assess flood risk at a global level (Merz et al., 2010). Their definition can be based on the resolution that is typically used in the computational model. For example, micro-scale studies have a resolution ranging from 1 to 25 m, whereas for macro-scale studies it ranges from 0,1 to 1 km (de Moel et al., 2015). As the scale changes, the primary uncertainty sources differ. At small scales, they can be identified in the damage calculation (De Moel et al., 2012) and the probability of the hazard event, whereas at supra-national scales the presence of flood defence is the main uncertain input (de Moel et al., 2015), (Vousdoukas et al., 2018a).

2.3.1. PHASES OF A FLOOD RISK ASSESSMENT

Following the definition given before (Section 2.1), the assessment of risk can be divided among the three components.

HAZARD MODELING

Coastal hazard modeling translates boundary conditions into flood characteristics, like flood depths or overtopping rates. Therefore, the first step is to obtain the hydraulic boundary conditions for the model, which can be retrieved, for example, through a statistical analysis of field measurements. Then, an appropriate hydrodynamic model is chosen. Hydrodynamic models can vary according to their level of complexity and purpose. Some models will include more physical mechanisms yielding to higher computational costs, whereas simpler models lose in hydraulic processes detail what gained in computational expense.

Generally, hazard modeling can be divided into two approaches: static and dynamic (Ramirez et al., 2016). The static method is more straightforward and allows for a considerable number of hazard simulations with little computational effort. A static flood model, also called bathtub model, determines flooded locations as those that have a lower elevation than the water level during the storm and that are hydraulically connected to the coastline. This method usually results in a significant overestimation of flooded area, since many important physical processes, like mass conservation and bottom roughness, are not accounted for (Ramirez et al., 2016). Nevertheless, the bathtub model is a rather quick tool for assessing flood impacts at macro-scales, where more complex models would be computationally unfeasible.
Dynamic models overcome the limitations of static models by simulating different physical processes, simplified shallow water equations in particular, for coastal flooding. Dynamic models vary in complexity and thus computational expenses. For example, Delft 3D and XBeach are numerically expensive models focused on coastal hydro and morphodynamic modeling. SFINCS is a less complex model that simulates a simplified version of shallow water equations.

EXPOSURE AND VULNERABILITY ANALYSES

A very important component of assessing the exposure of an area is identifying the damages that the area could experience in the event of a flood. The analysis of flood dam-

ages varies accordingly to their scale and goal. For macro- and meso-scale analyses usually a *land-use approach* is taken. This method consists of aggregating areas with similar land use and assigning them a specific potential damage value (Messner and Meyer, 2005). For example, the standard practice in Europe is to utilise CORINE Land Cover data (Messner and Meyer, 2005),(de Moel, 2012),(Prahl et al., 2016). In contrast, an object-based approach is used for micro-scale analyses, where maximum damages are defined for each type of objects (e.g. houses, vehicles, animals, etc.). Another method that is often used as preliminary assessment is to utilise large-scale population density datasets. In these *population-based approaches*, estimations of the population living in the flooded area are linked to information on Gross Domestic Product (GDP) per capita to compute the total economic activity at risk due to flooding. This work will focus on a micro-scale analysis for coastal communities, hence the uncertainty in the different object-based approaches used in the case study will be analysed.
It needs to be mentioned that most of coastal flood analyses, regardless of the scale of interest, primarily focus on the estimation of direct and tangible damages which can be quantified in monetary terms (see Section 2.1.1). Other types of damages, intangible and indirect are more difficult to estimate and are often not considered, or estimated as percentages of direct damages (Messner and Meyer, 2005).

The last step in risk assessment is to link the flood attributes to the characteristics of the exposed assets, through a vulnerability assessment. Regarding vulnerability, the most commonly used method for the estimation of direct flood damages is the application of depth-damage functions (Jongman et al., 2012), (Cammerer et al., 2013), (Merz et al., 2004). They relate flood depths and the resulting monetary damages. Depth-damage functions (DDFs) have been developed for different areas around the world, although they are still missing for many developing countries and SIDS. While using these functions, uncertainty can arise either from the choice of function (e.g. shape) and from the maximum damage value that is used (Egorova et al., 2008). The use and uncertainty of DDFs will be described in the Section 2.7. For this study, a different range of functions, shapes and assumed maximum damages will be used. We aim to investigate the application and transferability of different flood loss functions to other geographical regions, as well as the impacts of epistemic uncertainty from DDF on damage estimates.

2.4. UNCERTAINTY

From a management perspective, uncertainty can be defined as the lack of exact knowledge, regardless of what is the cause of its deficiency (Regan et al., 2002). It is standard practice to divide uncertainty into three categories according to their nature, from (Merz and Thieken, 2009):

- *Aleatory* uncertainty, inherent to natural randomness of physical variables
- *Epistemic* uncertainty, resulting from imperfect knowledge
- *Linguistic* uncertainty, which arises from language issues

The former one is considered as irreducible and part of the stochastic natural system. The two latter ones, however, can be quantified and reduced. This study will focus on

identifying both aleatory and epistemic uncertainty sources and how to deal with them. Epistemic uncertainty can be further divided in data and model uncertainties (Uusitalo et al., 2015). Models, by attempting to reproduce reality introduce assumptions and simplifications which inevitably result in uncertainties and errors (Uusitalo et al., 2015). Structural inaccuracies in the model can only be dealt with through comparison with other models, which usually requires significant computational efforts. Data uncertainty refers to random or systematic errors owed to measurements imperfection. This kind of uncertainty can be constrained by improving the quality of data collecting instruments and sensing techniques. Input data errors and model uncertainties are not independent of each other but can interact in several ways. The overall outcome is the model output uncertainty. Uncertainty of the model output differs from output error. Prediction error represents how much the output differs from what is considered as ground-truth. On the other hand, output uncertainty refers to how uncertain is our prediction (Loucks and Van Beek, 2017). As an example, a more uncertain output will have a wider range of results by varying one input compared to a more certain output which will vary less. Therefore, an estimate of the model output uncertainty can be drawn from the spread of its distribution.
According to (Loucks and Van Beek, 2017), it is relevant to understand that output uncertainty does not always indicate errors in the prediction due to imprecision in the data and to modelling assumptions (*epistemic uncertainty*), but can also represent the natural randomness of the system (aleatory uncertainty). Including uncertainty analysis in a risk assessment framework can improve decision making by integrating the risk estimate with a description of the model consequences and, as in this study, of the relative importance of different inputs. Indeed, another application of an uncertainty framework could be of driving limited financial resources in collecting new information for the risk analysis.

2.4.1. METHODS OF UNCERTAINTY ANALYSIS

Several methods to identify uncertainty in flood risk have been part of previous studies, including (Uusitalo et al., 2015):

- ***Sensitivity Analyses***, where changes to the input values (e.g. ±10% of the initial values) are made to investigate the sensitivity of the outputs. The corresponding percentage change of the outcome indicates if the risk analysis is robust or sensitive to the specific input. Alternatively, a fully probabilistic approach can be used where the input probability distribution functions (PDFs) are assumed. Samples can be drawn via random sampling (e.g. Monte-Carlo (MC) method (Wagenaar et al., 2016)) and use to test the sensitivity of the outcome.

- ***Comparative Analyses***, which consists of the use of multiple data sources or models to compare the different modeling assumptions and data limitations. This method is appropriate to shed light on model limitations or the trustworthiness of input datasets.

- ***Subjective analytical methods*** such as expert judgement.

This study will mainly focus on identifying the most uncertain types of input data in coastal flood risk, through a sensitivity analysis. Sensitivity analyses can further be distinguished in *local* and *global* analyses. In a *local* analysis, the sensitivity is tested by varying the inputs one at a time and estimating the variation of the model output produced. A local analysis can also be referred to in literature as one at a time (OAT) method (Saltelli et al., 2008). This method has the advantage of being fast and straightforward to set up. On the other hand, it does not take into account inputs combinations, which include non-linear interactions (Saltelli et al., 2008), (Uusitalo et al., 2015). Input combinations are tested while performing a *global* sensitivity analysis, where all the possible combinations of input values are tested. The disadvantage of this approach lies in the substantially higher computational expenses that are required, as the number of model simulations grows exponentially. To minimise the number of model runs, some techniques can be implemented. For example, by making a preliminary sensitivity test and, based on its results, selecting for the primary analysis the variables that have a stronger effect on the output variable. For illustrative purposes, Figure 2.7 depicts the conceptual difference between a local and a global sensitivity analysis. The three axes represent three input and their range of values, at the origin of the axes is the inputs are at nominal values. A local sensitivity entails moving along one axis (X_3 in the figure) of the input space. Contrarily, in a global analysis, the whole input space is investigated (in a three input domain, the whole cube).

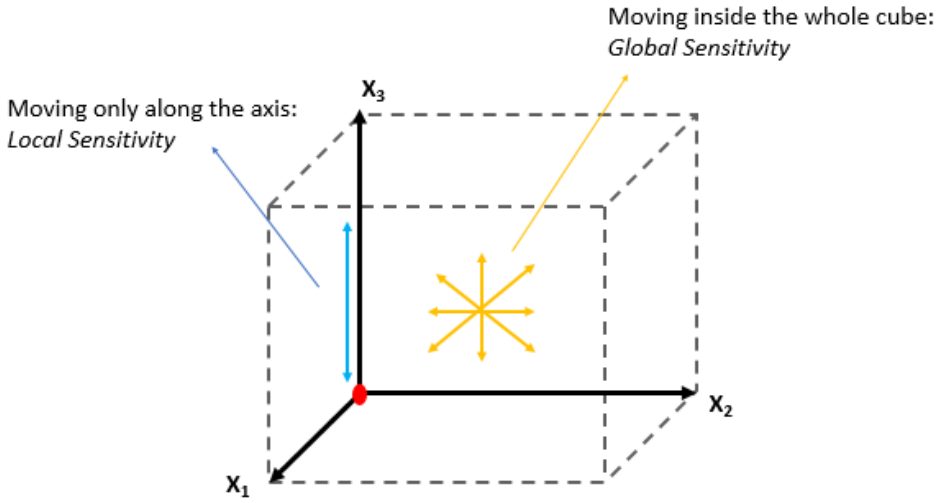

Figure 2.7: Three inputs space domain. The origin represents their nominal values. A local sensitivity is when we 'move' along one axis only. In a global sensitivity, we move inside the whole cube.

The following sections will deal with the uncertainty sources in the different input data that are used in most coastal flood risk analyses. Section 2.5 relates to the data used for hazard modeling, to transform offshore boundary conditions into near-shore flood hazards. Section 2.6 treats elevation models, which are used to model inland flooding

and Section 2.7 with DDFs.

2.5. HAZARD INPUT DATA

OFFSHORE CONDITIONS

Estimated water levels and offshore waves can carry a considerable amount of uncertainty. For example, (Wahl et al., 2017) have proven that uncertainty in retrieving extreme sea level values is comparable, if not larger, than the uncertainty in estimating sea level rise due to climate change. Is common practice to represent offshore conditions with probability distributions(Caires, 2011), (Holthuijsen, 2009). Nevertheless, these distributions are fit to measured data and attempt to reproduce the aleatory nature of waves and water levels. Therefore some uncertainty is already introduced as these distributions cannot reproduce reality perfectly.

BATHYMETRY

Shallow water systems are very sensitive to bathymetry, although little attention is given to errors in the data, especially in relation to what is given to other inputs (Cea and French, 2012). Most studies of nearshore hydrodynamics generate digital seabed elevation models from bathymetry that is measured through discrete sampling of data points, which according to (Plant et al., 2002) and (Hare et al., 2011) introduces different types of uncertainty:

- Terrain variability within each cell's footprint, and between measurements. More complex, rougher terrain will yield to higher uncertainty in the measurement compared to smoother, flatter terrains
- Interpolating distances and techniques used to estimate values between measurements
- Measurement errors
- Naturally occurring morphological changes, which may cause data points measured in the past to not represent accurately the present morphology

Figure 2.8 below shows the different sources of uncertainty: (A) measurement errors, (B) interpolating uncertainty, (C) terrain variability. The grey shaded area is used as an indicator to represent uncertainty. Interpolating uncertainty is a function of the technique used and of the interpolating length. Interpolation over more distant data points will yield more uncertainty than over closer points. Interpolation errors are difficult to estimate and often represent the most prominent source of uncertainty in the model (Amante, 2018).

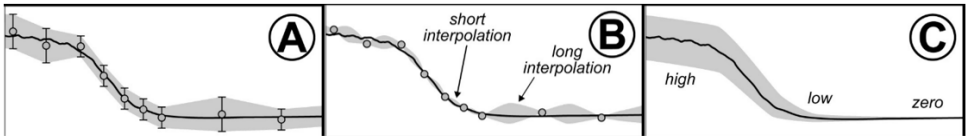

Figure 2.8: Different uncertainties from modeling bathymetry as highlighted from (Hare et al., 2011).

In this study, the consequences of utilising different resolution dataset will be investigated, since for many remote locations in the world only very coarse bathymetry data is available.

2.6. ELEVATION MODELS

Digital Elevation Models (DEMs) are numerical representation of the bare-earth surface. Topographic data are referenced to different horizontal and vertical reference systems. Regarding the vertical datum, a specific topographic point can be referenced to the *ellipsoid*, the *geoid* or to a representation of the *mean sea surface*. For worldwide applications, usually the ellipsoid World Geodetic System 1984 (WGS84) is used.

Many vertical datasets use instead a geoid as reference, an equipotential surface of the earth gravitational field. Infinite surfaces can be defined according to the specific value of the gravity field that is chosen. For this reason, the surface that represents most closely the mean sea level (MSL) is used. Although, a geoid would represent perfectly the ocean surface if there were no land or currents influences on the MSL, which is not the case along the world coastlines and a correction on the geoid surface is usually introduced. Figure 2.9 shows the different reference surfaces in relation to an observation point.

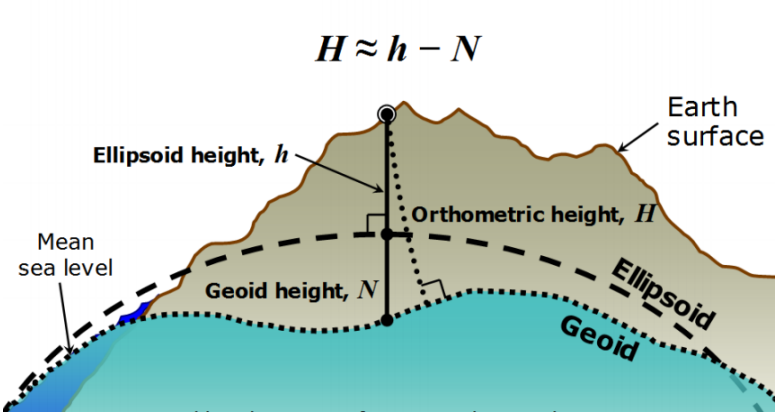

Figure 2.9: Observation point height wrt different vertical datums

The figure shows how the height of an object above the geoid level is referred to as *orthometric height*, whereas the geoid height indicates the undulation of the geoid with reference to (wrt) the ellipsoid. There are different geoid models and the most commonly used for global DEMs is the Earth Gravitational Model from 1996 (EGM96), which is derived from multiple gravity measurements around the globe.

DEMs are derived with different methods, although at the present state the most common can be classified in three groups: satellite-based, air-based and ground-based data. Satellite data have the lowest resolution and include most errors. Air-based (e.g.

UAVs or LiDAR) and ground-based (e.g. GPS surveys) can have much finer resolution but are generally scarce in most areas. Generally, publicly available, satellite-derived global DEMs are used in hazard and risk studies due to the lack of local, high resolution data. Nowadays, UAVs are emerging as new technique to collect high quality DEM(Leitão et al., 2016). One of their interesting features is the ability to collect data from lower elevation and not being conditioned from the presence of clouds. Horizontal resolutions achieved are much finer than with satellites.

In their study, (Hashemi-Beni et al., 2018) compared a UAV-derived DEM with a LiDAR DEM, highlighting a general agreement between the models (less than 30 cm differences). In another study (Tamminga et al., 2015) found in UAV derived DEM a vertical root mean squared error of 9 cm in river zone compared to ground-based surveys.

IMPLICATION OF DEM CHARACTERISTICS FOR CFR MODELING

Both the vertical accuracy and horizontal resolution of a DEM have implications for the accuracy of the risk prediction. Vertical accuracy directly impacts the estimated water depth at each cell of the hydrodynamic model. A DEM with a low vertical accuracy that underestimates the elevation will increase the predicted flooding volume. Differently, the horizontal resolution of the DEM entails the surface variability that is reproduced by the model. A high resolution DEM will reproduce smaller morphological features than a low resolution one. The resolution required varies accordingly to the purposes and needs of the model (de Moel et al., 2015). For example, to model single short waves accurately a small grid cell size is required (Lashley et al., 2018). Nevertheless, if the scale of the model is large (order of kilometers), utilising a small computational grid cell size could be computationally unfeasible and force the use of a lower resolution DEM. Horizontal resolution and vertical accuracy are not necessarily correlated. A high resolution DEM with many measurement errors would be very inaccurate. The following section describes the different sources of uncertainty rising from the use of topographic data in coastal flood risk analyses, also related to their vertical accuracy and horizontal resolution.

(Heritage et al., 2009) suggested that the DEM quality is a function of: (i) the error in the single data points, (ii) the density of the data points and (iii) the distribution of the data points within the surface. Furthermore, according to (Hancock, 2006), also the interpolation method used to produce the DEM may influence its quality, although this was found to have a limited impact (Heritage et al., 2009). In this study we will only consider the error in the dataset as a indicator of the DEM quality. From now on, we will refer to a high quality DEM as a dataset with high vertical accuracy (low vertical error).

2.6.1. UNCERTAINTY IN TOPOGRAPHIC DATA

DEMs have been identified as one of the most critical input data in a flood risk analysis.

Often, global topographic data is used in studies without accounting for the systemic errors that are embedded within them. Many types of errors can be present in an elevation model, including systematic error that stems from a bias in the elevation values or random error that can have multiple causes and different spatial scales. Other kinds of

errors such as those coming from flaws in the measuring equipment are usually identified and removed prior to releasing the DEM. These many errors represent a significant part of the uncertainty in flood risk analyses, which have already been proven to be highly sensitive to the choice of topographic data, (Vousdoukas et al., 2018a), (Paprotny et al., 2019), (Cook and Merwade, 2009), (Van de Sande et al., 2012), (Hawker et al., 2018). (Van de Sande et al., 2012) and (Vousdoukas et al., 2018a) compared flood model simulations using different global satellite-derived DEM and LiDAR-derived DEM (considered as ground-truth) and concluded that publicly available, global DEMs do not meet the accuracy requirement of coastal flood risk assessments. (Hawker et al., 2018) developed a tool to synthetically derive multiple DEMs from single global DEMs. After applying the multiplicity of derived DEMs in their flooding model, they showed how the predictive ability of the model improved, if compared to the application of a single, deterministic elevation model.
Another potential source of uncertainty for coastal flooding lies in the applied DEM resolution. (Saksena and Merwade, 2015) have concluded, after applying different resolution topography maps derived from LiDAR and SRTM datasets, that the predicted flood inundation areas increase with decreasing DEM resolution. Similar findings were also found from (Bouziotas, 2016) and (Hsu et al., 2016). (Hsu et al., 2016) used DEM resolutions ranging from 1 to 40 m to estimate flooding from rainfall events in Tainan City, Taiwan, where the coarser resolution DEMs computed the larger flooding extents. Nevertheless, (Saksena and Merwade, 2015), (Bouziotas, 2016) and (Hsu et al., 2016) focused in areas with relatively flat terrain. It is possible that in more mountainous sites the relation between DEM resolution and flooding extent may differ, as already suggested by (Saksena and Merwade, 2015).

DEMs can be further divided in Digital Terrain Models (DTMs) and Digital Surface Models (DEMs) (Li et al., 2006). DTMs represent the earth bare surface, whereas DSMs represent the surface elevation of objects in the landscape (e.g. building roofs and canopies of trees). Global DEMs are collected as DSM, where different elevation values are measured from the satellite for one pixel and the final value of the pixel elevation is given by the average of the different measurements. Through this averaging process the natural variability of the terrain within the pixel is lost, resulting in a simplified and offset elevation representation, especially for coarse resolution datasets. This offset in global datasets in representing the terrain can be accentuated by the fact that satellite measurements are taken randomly. This means that the values measured for a specific pixel could receive the signal from the roof of a building and not the bare surface. This error in representing the terrain is then more significant in areas with high vegetation or population density(Gorokhovich and Voustianiouk, 2006).

Although created as DSM, these global datasets are often used as DTM for flooding models (Van de Sande et al., 2012). This yields significant errors in the model outputs as the elevation points representing the surface of a specific area will include buildings, trees and other objects heights. For this reason, attempts to convert global DEMs to DSMs have been made including correction for vegetation and buildings. An attempt to reduce the bias from canopies and building height was made in this study and is dis-

cussed in the Appendixes (see Appendix C). Finally, the errors in satellite measurements are also a function of the terrain slope, as they have been proven to be usually larger in steep areas, (Gorokhovich and Voustianiouk, 2006).

In this study, we will focus our attention on understanding the consequences of using local, high quality and high resolution data versus low resolution, publicly available global data. Different DEMs will be tested in the flooding model with different resolutions and accuracy, trying to get some more insights from the model results than by directly applying a single elevation model. At the same time, the implications of using DTMs as DSMs will be shown, together with some possible techniques to reduce the discrepancy in the results between the two types of elevation models.

2.7. DEPTH DAMAGE FUNCTIONS

Depth damage functions contribute significantly to the epistemic uncertainty of damage estimates for riverine floods (Wagenaar et al., 2016), (Merz and Thieken, 2009), as well as for coastal floods (Prahl et al., 2016), (De Moel et al., 2012), (Vousdoukas et al., 2018a). This is mostly due to the little understanding of the processes involved in flood damages. As briefly discussed above, DDFs are commonly used in flood risk analyses to relate flood depths to damage estimations. This is done by first assigning a value to each exposed asset category i (for object-based approaches), representing the maximum damage $D_{max,i}$. These values are usually retrieved from historical floods and insurance claims, complicating vulnerability analysis in countries where damage data is not available. The second step is to express the fraction of maximum damage, $a_i(d_j)$, for each object category as a function of the flood characteristics d_j at a specific location j. When the depth-damage curves are defined for each object category, the total damage D for the area can be calculated from the equation (Jonkman et al., 2008):

$$D = \sum_{i}^{m} \sum_{j}^{n} a_i(d_j) D_{max,i} n_{i,j} \tag{2.1}$$

where m is the number of object categories and n is the number of assets per object category in the area.

DDFs have been developed for many different purposes and conditions, although some general considerations must be mentioned. Most studies and analyses that focus on the development of these functions are based on different type of floodings, such as river floods, rather than coastal floods. Existing flood depth damage curves have been developed using a number of different techniques and assumptions (Schultz et al., 2010). This practice has resulted in the development of functions that are hard to compare and, especially, are difficult to apply in locations that are different from where they were initially developed(Schröter et al., 2014). Moreover, appropriate damage functions are already available only for some countries and areas around the world, typically where

flood risk has thoughtfully been studied. Often DDFs are not available for SIDS, requiring further assumptions for flood risk analyses.

DDFs show many similarity with fragility curves, which relate the probability of failure of a structure to, for example in the case of flooding, water levels. More generally, a fragility curve is a statistical function that describes the performance under a given loading condition (Schultz et al., 2010). There are different methods to derive DDFs, which can typically be grouped in: judgemental, empirical, analytical and hybrid (Schultz et al., 2010). Judgmentally developed curves are based on expert judgement. Empirical methods are based on controlled experiments where different conditions are tested to evaluate the performance of structures. Analytical approaches are based on physical models but require the availability of data and models and are more time consuming to implement. This last method is widespread and often couples real natural disaster damages to physical hazard models that combined can derive a DDF.

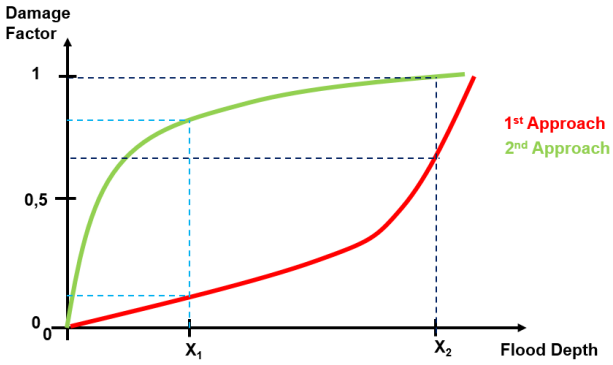

Figure 2.10: Two different approaches in developing a depth damage function.

For flooding-related damage functions, two general philosophies of estimating the increase of the damages under increasing loading conditions have been identified in the literature. These two general approaches are represented in Figure 2.10 and for simplicity will be regarded as *first approach*, which yields to an exponentially shaped DDF and as *second approach*, which yields to a logarithmic shape. The two approaches will be explained for buildings DDF, as this is the focus of our research. The first approach, red in the figure, lies upon the assumption that small flood depths produce minimal damages compared to the total economic value of the building. This is because small flood depths (indicated with X1 in Figure 2.10) are not believed to produce structural damages yet. Therefore, after a certain threshold flood depth is exceeded (X2 in the graph) the damages increase exponentially as finally structural damage to the building occurs, which is illustrated by the second, steeper part, of the red curve.
According to the second approach, heavy economical losses start to occur already at smaller depths and with increasing water levels the rate of damage increase reduces. This is believed to represent buildings where small depths can produce heavy losses by damaging house furniture or the electrical and water systems as well as buildings with

very weak structural strength (e.g. wooden houses). The implementation of one approach over the other is not as straight forward. Considerations regarding the building materials and the house content vary from one area to another. For Small Island Developing States, where building materials are usually not very flood-resistant, the second approach may seem more fit to the case, although this might vary from island to island.

Another relevant point to consider when using DDF, is the geographical origin and the type of flooding from which they were derived. (Cammerer et al., 2013) applied a DDF derived from a riverine flood in Saxony to different case studies in other locations. Their results identified the geographical origin of the flood damage function as the most important parameter to consider when using DDFs. As introduced before, many DDFs are derived combining real damages after a flood event and hazard physical modeling ((Vojinovic et al., 2008), (Tarbotton et al., 2015) and (Messner and Meyer, 2005)). It is crucial, when utilising a specific curve derived from a case study, to acknowledge the particular flooding conditions of the case. For example, riverine floods have usually a longer flood period but smaller flood velocities than tsunamis or coastal floods. As the hazards differ in characteristics, so will the damages that they cause. It is then implicitly assumed that using functions initially derived from riverine flooding for coastal flood damages represents a strong assumption (Jongman et al., 2012). Although the differences are obvious, the lack of local representative damage functions forces the use of DDFs developed for different settings (Schröter et al., 2014). This issue, and the considerable uncertainty that comes with it, is once again exacerbated in data-poor environments such as SIDS. Finally, it has to be mentioned that having the damages related to only one variable that represent the hazard also represents a significantly strong assumption. Indeed, coastal floods with similar water levels may have different inundation periods or flow velocities and thus lead to different impacts. This further increases the amount of epistemic uncertainty embedded in coastal flood risk modeling. In this study we will test several functions developed for different forcing conditions, hoping to represent the epistemic uncertainty within the use of damage functions in flood analyses.

3

METHODOLOGY

CHAPTER SUMMARY

This chapter describes the methodology followed to answer the questions introduced in Chapter 1. Section 3.1 begins with a general description of the methodology and the most important characteristics of the approach chosen. The case study of our analysis is described in Section 3.2. Then we describe the different models, the procedure to set them up and the necessary information to run them in Sections 3.3 and 3.4. Section 3.5 deals with the definition of the uncertainty sources and how their uncertainty is reproduced. Sea level rise predictions and Shared Socioeconomic Pathways are used to represent future conditions in our method and are illustrated in Section 3.6. Finally, an overview on the methodology and the analysis approach is given in Section 3.7, where a list of all the tested inputs and their values is included.

3.1. METHODOLOGY APPROACH

The work is applied to a case study on the islands of São Tomé and Príncipe, where coastal flooding models were already set up from (Giardino et al., 2018). To investigate uncertainty propagation in the model, a similar methodology to (De Moel et al., 2012) and (De Moel et al., 2014) is followed. The conceptual steps, already introduced in Section 1, are described here.

To reach the research objectives, a compromise between methodology, model complexity and the number of inputs included had to be found. The model to assess flood risk needs to include enough processes to provide reliable results, but computational time had to be optimised to respect the project timeline. Initially, the different models implemented to simulate coastal floods were set-up and optimised, also conducting a preliminary sensitivity analysis to identify, from a range of possible parameters, those to be included in the full analysis (see Appendixes A and B).
After having chosen the most important inputs, different datasets were retrieved to be compared with the benchmark simulation (Section 3.5). All the possible combinations for each parameter value were simulated in the model and compared by the computed damages. This approach, despite the significant amount of simulations does not require to fit a probability distribution to each input as in other studies (De Moel et al., 2012), which would have required strong assumptions for some of the selected inputs.

3.2. CASE STUDY

The Democratic Republic of São Tomé and Príncipe is an archipelago comprised of two main islands and several islets located in the Guinea Gulf, see Figure 3.1. The island, member of the SIDS, is under threat from intense rainfall events and coastal flooding, therefore a compound flood risk assessment was commissioned to Deltares by the World Bank (Giardino et al., 2018). Their analysis focuses on different coastal communities over the two main islands that experience compound (rainfall, river and coastal) flooding. During a site visit in December 2018, Deltares was able to collect local bathymetry, topography and exposure data that was used to create coastal flood risk models. The techniques used to collect the data are described in Section 3.5.

Different models have been developed to compute the risk for the coastal communities. For the hydrodynamic modeling, XBeach (Roelvink J.A., 2009) was coupled with SFINCS (Super Fast INundation of CoastS), (Leijnse, 2018) a computationally efficient semi-advanced process-based model that computes flooding in coastal areas. The hydrodynamic model computes the coastal flooding hazards, which is represented by inundation maps. For the exposure and vulnerability analysis, Delft-FIAT (Flood Impact Assessment Tool) was used. In Delft-FIAT, exposure maps containing assets and inundation maps are combined over a specific grid. Using DDFs, damages are calculated for each grid cell.

For this study, four different coastal communities were initially considered: Praia Melao, Pantufo, Micolo and Praia Abade (Figure 3.2). The first three are located on São Tomé, the larger island, whereas Praia Abade is on the island of Príncipe. Of this four

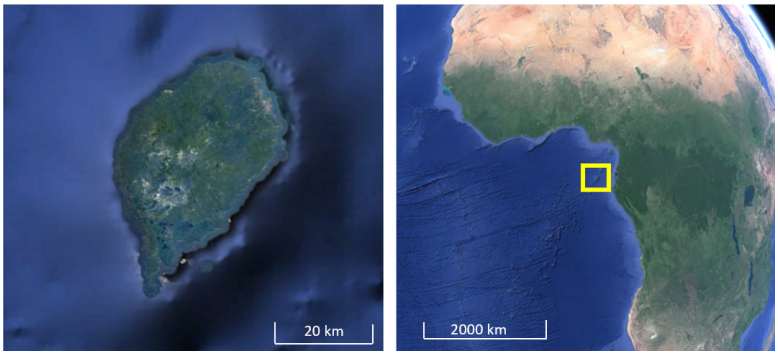

Figure 3.1: (Left) Satellite image of the island of São Tome. (Right) Location of the island in the Gulf of Guinea.

locations, only two, Praia Abade and Pantufo, showed some coastal flooding after the first simulations with the models (see Appendix A) and were therefore the only ones included in the primary analysis.

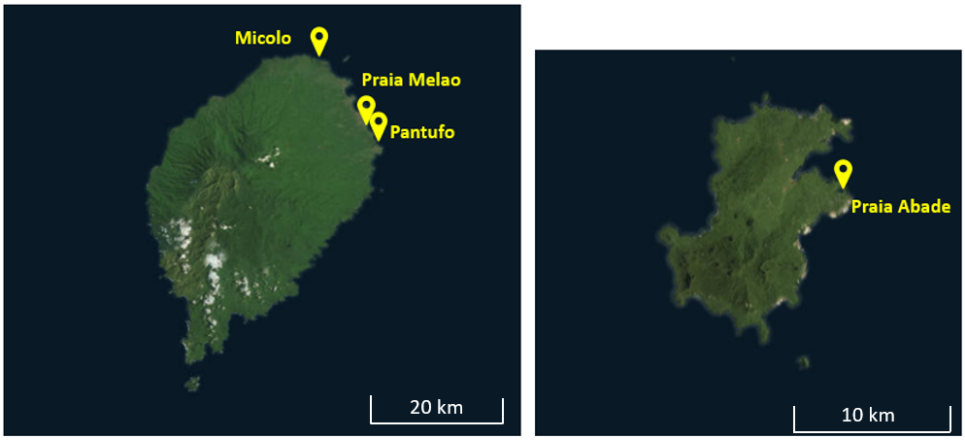

Figure 3.2: The four locations on the island of São Tomé (left) and Príncipe (right).

3.3. HAZARD MODELING

XBEACH MODEL

In this analysis, XBeach functions as a transformation model, which translates offshore boundary conditions to nearshore boundary conditions, which are then inputted in SFINCS, used to compute the inland flooding. XBeach is available in three hydrodynamic options: *stationary wave mode* which solves wave-averaged equations but all infragravity motions are neglected, *Surfbeat mode* where short wave variations on the wave group scale are resolved as well as long waves and the *non-hydrostatic mode*, which is the short-wave resolving mode. For the latter, depth-averaged flow due to waves is computed using the non-linear shallow water equations. A depth-averaged, non-hydrostatic pressure term is included in the equations and is turned off when waves reach a specific steepness

to implement wave-breaking.

The non-hydrostatic mode was used in this study (XBeach-NH) as it has the advantage of including short waves runup, which is particularly important on steep slopes. Indeed, on steep slopes, short wave frequencies can be dominant in the swash zone (see Section 2.2.1), requiring high modeling accuracy. The downside of using XBeach-NH is that is the most computationally expensive mode, thus substantially increasing the computational time required to run multiple scenarios in a sensitivity analysis. In particular, the two-layer version of XBeach was used (NH+), since it allows to set the model offshore boundary point in deeper depths (de Ridder, 2018) with higher model stability.

For the locations considered, multiple 1-D XBeach cross-shore transects were made, going from -20m water depth to a distance inland of roughly 60 m, varying from transect and enough to include all the wave motions. Figure 3.3 below shows a single XBeach transect for the community of Micolo. The ocean bed level was retrieved using the bathymetry measurements collected during the site visit and described in Section 3.5. The offshore slope is 1:100, becoming steeper (~1:20) closer to the shoreline. The 1-D transects are used to transform offshore water level time series to nearshore time series. At a water depth of approximately -2 m, the water level signal from XBeach is given as input to SFINCS, which then computes the inland flooding.

BOUNDARY CONDITIONS

For the hazard assessment, the total storm length is assumed to be 24 hours, as in the work of (Giardino et al., 2018), but only the peak central 6 hours are modeled, since they are expected to give the greatest contribution for the flooding. Both the significant wave height and peak period distributions during the storm are discretized into bins of single hours, during which the offshore forcing is constant. The choice of modeling only 6 hours long storms was made to reduce the computational time and is tested in Appendix A).

Waves are modeled with a shore-normal direction and using a JONSWAP spectrum (Roelvink et al., 2015). The choice of using a unidirectional, unimodal JONSWAP spectrum was based on simplicity. A conservative approach was taken selecting incident wave direction, as this would yield maximum runup for the same wave height and period. At the same time, directional spreading was fixed due to the 1-D profile. The spectral shape peakedness, defined by the peak enhancement parameter ($\gamma_{JONSWAP}$), influences the wave groupiness. In a narrower spectra, the energy is concentrated around a small frequency band, ultimately affecting the formation of wave groups. A primary sensitivity was conducted to test ($\gamma_{JONSWAP}$) and other parameters and to select the most influencing ones for the model. The results are described in Appendix A, together with a complete definition of the model set-up. These results suggested that there is only a weak relationship between the estimated runup and the peakedness of the spectra, hence $\gamma_{JONSWAP}$ was kept at the default value of 3.3 (Roelvink et al., 2015).

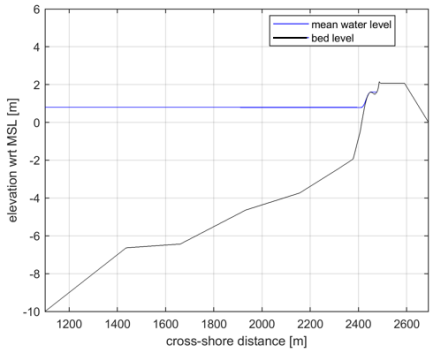

Figure 3.3: Cross-shore XBeach transect at Micolo, with the bed level and mean water level during the storm.

SFINCS MODEL

The SFINCS model is a computationally efficient, process-based model that can be used to model flooding in coastal areas. The model has been developed by Maarten van Oormondt at Deltares. One of the main advantages of SFINCS is represented by its ability to model flooding at small to medium scales in a computationally inexpensive way. The computational efficiency is due, among other reasons, to the neglect of viscosity. Therefore, momentum losses due to horizontal gradients in the velocity profile and turbulent motions are neglected. The model can compute compound flooding by implementing different processes such as rainfall. wind stresses, infiltration and river discharge in a simple manner. Particularly for rainfall and river discharge, their effects are implemented by adding the water level per grid cell due to rainfall and discharge for each time step. Most importantly, offshore water levels and waves can be included in the model, by turning on the advection component (SFINCS-SSWE). The model solves the linear inertial equations, which are obtained from the shallow water equations after neglecting the horizontal viscosity. For a more detailed description of the model, the reader is referred to (Leijnse, 2018).
These models were used in the eight communities of São Tomé and Príncipe commissioned to Deltares, to estimate compound flooding. The results showed a higher risk from rainfall flooding for the majority of the communities (Giardino et al., 2018).

SFINCS computes the inland flooding by using as boundary conditions the water levels from the different XBeach 1-D transects. Each transect represents a boundary point for the 2-D SFINCS grid. The boundary points of SFINCS interpolate between the different XBeach transects to each have a water level time series. This interpolation is based on a weighted distance averaging process. Moving from a 1-D model to a 2-D model in SFINCS to model the inland flooding represents a strong assumption. Indeed, alongshore uniformity of the water level time series is assumed. Nevertheless, this was justified by the results described in Appendix A, where it is shown that the computed runup values are very similar between the different 1-D transects, indicating there is little longshore variability in the water motions. A constant infiltration rate of 5mm/hr was assumed in the absence of infiltration data for all of the communities. The elevation data used for SFINCS was collected locally during a field visit from Deltares, (Giardino et al.,

2018) as described in Section 3.5. A map showing the elevation for the area of Pantufo is in Figure 3.4. The figure shows the area of the SFINCS model with high resolution. On the map, also the five XBeach 1-D transects of Pantufo are drawn with black lines.

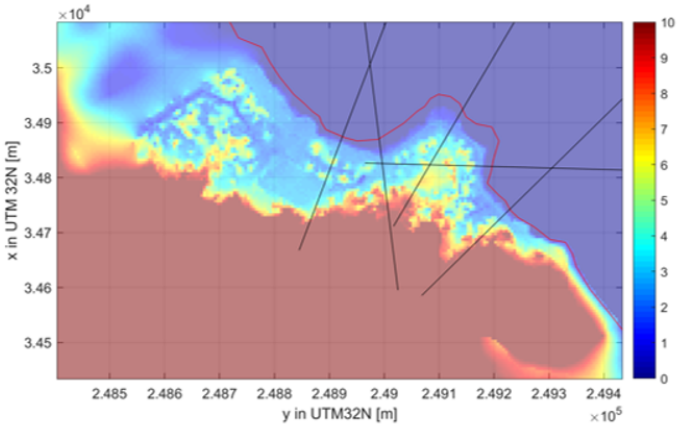

Figure 3.4: Elevation map of the area surrounding Pantufo, derived from the Drone imagery.

In this study, different elevation models will be tested using SFINCS to understand the differences between local, high-quality data and global, low-quality datasets.

3.4. EXPOSURE AND VULNERABILITY MODELING

The damage assessment is finalised through the use of the model Delft-FIAT. FIAT (Flood Impact Assessment Tool) is a flexible Open Source toolset used to run impact assessments and is based on the unit-loss method, which relates flood parameters to damage at the unit level (e.g. a single building or infrastructure). The input data comprises exposure maps, damage functions and maximum damages, which are related through a configuration file. The model approach consists of overlaying an inundation map and an exposure map to determine the flooding depth for each asset. Then, damages are computed using the defined DDFs and the maximum damage values. An explanatory scheme is shown in Figure 3.5.

For the case of São Tomé, detailed exposure maps were derived from the drone imagery and processed using the GIS software ArcGis Pro (ESRI, 2014). Given the location of the roofs of buildings, polygon shapefiles were delineated. Different types of buildings are present and spaced differently. The total asset values per building type have been collected during the Deltares site visit(Giardino et al., 2018) and are shown in Table 3.1 for Pantufo and Praia Abade. The average building area per category was estimated, using statistical tools available in ArcGIS, and used to compute the price per m^2. Using the percentage of each building type in the area and its value, a weighted average of the assets value was computed. This allowed us to model only one building category within FIAT and thus require only one DDF. However, this simplification is acceptable if

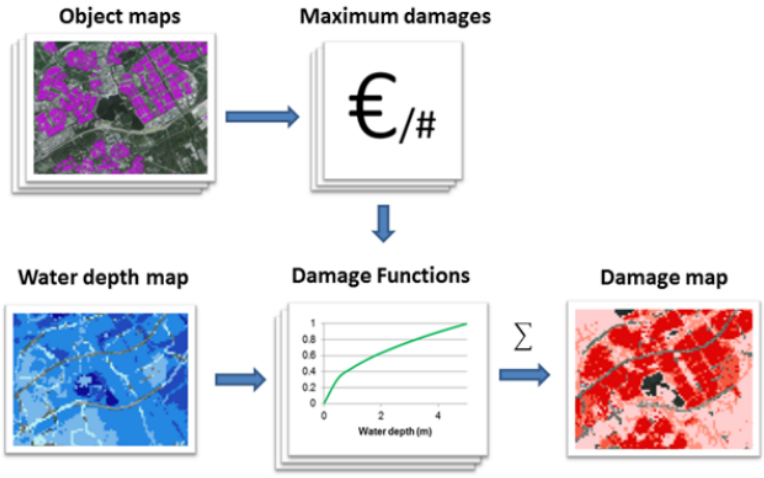

Figure 3.5: Delft-FIAT conceptual methodology, https://publicwiki.deltares.nl/display DFIAT/Delft-FIAT+Home.

the buildings types are homogeneously distributed over the area. This assumption was considered acceptable for the two locations. The drawbacks of this assumption are that if in reality, most of the flooded buildings are less-more valuable than the weighted average, the damages would be over-under estimated. The estimated averaged asset value per m^2 are 55,800 and 81,900 STD for Pantufo and Praia Abade respectively.

Table 3.1: Different building types with their value and averaged area, derived from ArcGIS PRO

	Asset	**number**	**area [m^2]**	**value [STD]**	**value per m^2**
Pantufo	Wooden House 3	713	49	65,000	1,327
	Kitchen-Storage place	214	9	10,000	1,111
	Concrete House	130	112	512,500	4,576
Praia Abade	Wooden House	42	48	120,000	2,500
	Kitchen-Storage place	31	10	10,000	1,000
	Concrete House	8	65	400,000	6,154

Fishing is one of the major economic activities in the island, thus a significant component of the targets at risk is represented by the polyester fishing boats. Usually located on the beach and with not many sheltered areas to protect them from coastal flooding, they represent one of the biggest losses after a storm, (Giardino et al., 2018). For this reason, boats are also included in the damage analysis.

To be used as input in FIAT, both the inundation and assets map need to share the same grid cell size and extent, so that they can be perfectly overlaid. Therefore, the available shape-files representing the buildings and the boats of the coastal communities were transformed into raster files with identical characteristics to the flood map, taken from SFINCS. SFINCS does not output raster files, but these were created in Matlab with the Mapping Toolbox (MATLAB Mapping Toolbox, 2018). A work-flow with the most important pre- and post-processing steps required in the modeling process is shown and explained in Appendix D.

3.5. DATA DESCRIPTION

The selected inputs for the sensitivity analysis, based on the literature review (Section 2) and on preliminary tests (Appendix A and B) are:

- Significant wave height (H_s)
- Storm surge water level
- Bathymetry
- Digital Elevation Model
- Depth Damage Function
- Sea level rise prediction
- Shared Socioeconomic Pathway

The following section treats the collection and description of the fore-mentioned inputs.

3.5.1. OFFSHORE FORCING

PROBABILISTIC CALCULATIONS

To retrieve information on wave and water level characteristics, a statistical analysis was applied. The analysis is based on probability theory and, in particular, extreme value analysis (EVA). Probability theory focuses on random variables, which indicate a random quantity subject to variation and that can be described by a probability distribution function. A probability distribution function (PDF) describes the probability of observing different values of the random variable of interest, whereas the cumulative distribution function (CDF) is the integral, over the random variable domain, of the PDF.

$$\begin{aligned} F_x(x) &= P(X \leq x) \\ f_x(x) &= \frac{\partial F_x(x)}{\partial x} \end{aligned} \tag{3.1}$$

Equation 3.5.1 contains the general expression of a CDF (first line) and of a PDF (second line). A CDF indicates the probability that the variable of interest will be equal or lower than a particular value. In other words, it tells the probability of not exceedence for different values of the random variable. The CDF becomes therefore very important

in EVAs, where the goal is to identify the values of a random variable that are exceeded only with a very low occurrence (e.g. a 1 in 100 year storm water level). EVAs methods for wave heights and water levels has been studied, although there are still some uncertainties around it, both aleatory and epistemic. First of all, natural variables such as wave heights do not behave exactly as their probability distribution describes them. PDFs are a mathematical expression that 'best' defines the variable, but not exactly (*aleatory uncertainty*). Another big inaccuracy is that often the data that is used to extrapolate long return period values is actually shorter than the return period itself (*epistemic uncertainty*) (Wahl et al., 2017). This therefore increases the overall uncertainty that surrounds the boundary conditions that are used to compute hazards in risk analyses.

WATER LEVELS

Offshore water levels are a combination of tidal components and residual effects due to inverse barometric changes and wind stresses, as introduced in Section 2.2.1.

Extreme Sea Levels have been found to be essential for coastal flooding analyses (Wahl et al., 2017). The authors tested different extreme EVA methods to retrieve the 100 year return period water level for different locations around the world. Comparing the different EVA methods, they found the range of possible results to be often greater than the possible results from SLR predictions. Applying EVA methods to observed or modelled extreme water levels allows the quantification of return periods that are longer than the observed records. There is a wide range of techniques and there is no universally accepted standard for risk analyses (Caires, 2011). The most commonly used technique is to fit a Gumbel distribution with two parameters (location and scale) to a time series of annual maxima water levels. Nevertheless, recently more methods have been developed that select more than a single value per year by a peak-over threshold analysis.

This study uses the work of (Muis et al., 2016), who produced a global wave water levels reanalysis based on daily maxima. For this data, a peak over threshold (POT) analysis was applied to obtain extreme values. For the reference scenario of the risk assessment, the return period of the offshore forcing was set to 100 year. The choice was based on the fact that the island, following from the analysis of Deltares, was found to be not highly prone to coastal flooding under conditions with smaller return periods.

A POT consists of generating a cluster of peaks from the sample dataset to which a generalised pareto distribution (GPD) is fit to. GPD is often used in EVA to represent observations that exceed high thresholds. The generalised Pareto indeed is a tail function (a function attribute used to better fit the tails of PDFs), suited for the upper tail of extreme value PDFs (Pickands, 1975). the distribution function of a GPD with threshold u as the following equation:

$$F_u(y) = \begin{cases} 1 - (1 + \xi \frac{y}{\sigma_u})^{-1/\xi} & \text{for } \xi \neq 0 \\ 1 - \exp(-\frac{y}{\sigma_u}) & \text{for } \xi = 0 \end{cases} \tag{3.2}$$

where $0 < y < \infty$, $\sigma_u > 0$ and $-\infty < \xi < \infty$. The two parameters of the GDP are the scale parameter (σ_u) and the shape parameter (ξ). For more information on how the return

values are retrieved, the reader is referred to (Caires, 2011). There are several methods to estimate the parameters of a probability distribution, like the probability of weighted moments, which is chosen for this study, following from the study of (Caires, 2011). This method is considered to perform better than others for the range of distribution tails typically found with wave data. Initially, to identify a threshold value, a similar methodology to (Nicholls et al., 2007) was followed, where different thresholds between the 96th and 99th percentile were considered.

WAVES

Given the location of the two Islands, swell waves coming from storms generated in the southern hemisphere are expected (Short, 2005). For the wave climate, the data was obtained from the ECMWF (European Centre for Medium-Range Weather Forecasts; ERA Interim). The data are 6-hourly and available on a global grid starting from 1979. To transform the offshore wave conditions into shallower depths, transformation matrices were derived from the Delft3D-Wave (SWAN) model (Booij et al., 2015), developed at Deltares. These matrices were developed during the project study, from (Giardino et al., 2018).

The median significant wave height from the offshore wave analysis is 1.5 m and the median peak period is 9.3 seconds. For this study, the median wave steepness of 1.08% has been considered constant for all the wave heights in the different scenarios, in order to retrieve the corresponding wave period.
After translating the offshore wave conditions to a water depth of ±30 m, the time series were used to carry out an EVA following the same methodology described for the water level EVA.

Specifically for the location of Abade in Príncipe, a reduction factor of 50% on the wave condition was applied to take into account the local topography and the location of the community in an enclosed bay. This is a simplification to simulate the diffraction effects of the waves on the headlands next to the community, which would lead to a reduction of the total incoming wave energy. Although the reduction factor may seem very conservative, this choice is based on the limited number of hydrodynamic processes that are modeled in 1D-XBeach. Since processes like wind waves from the North-West, meteotsunamis and other infra-gravity motions are not accounted for, it was decided to be more conservative on the modeled swell waves.

3.5.2. BATHYMYETRY

Bathymetry data also plays a crucial role in modeling coastal hazards. Waves and tides are indeed heavily affected by the ocean bottom in shallow areas, thus giving great importance to the collection of accurate and reliable bathymetry. Bathymetry has been measured globally since many decades and in some countries data sources with small resolutions are available, which are used for ports management and coastal engineering amongst other purposes.
Local bathymetry data was collected along single transects for each community, going from approximately the breaker line to a distance of roughly 1,500 m offshore. Seabed depths were collected from small boats using a hand-held GPS for horizontal position-

ing combined with a hand-held echo sounder to measure the depths. The measurement points are taken every 50-100 m along the profile (Giardino et al., 2018).
In the analysis, the implications of having higher resolution and accurate local data measurements will be compared with using global, low resolution data. This is done by retrieving one dimensional bathymetry profiles for the hazard modeling both from the local measurements and from the GEBCO dataset (Weatherall et al., 2015). GEBCO (General Bathymetric Charts of the Oceans) is a global terrain model for ocean and land at 15 arc-second intervals (~900 m around the equator). It is part of a project to collect, organize and make available to all the whole ocean floor map. Data points were collected for the locations of Praia Abade and Pantufo, using Delft Dashboard (OpenEarthTools, 2013). The collected points were used to derive a surface by interpolating between them. This surface was used to extrapolate water depths along different transects for the two communities. Figure 3.6 shows the transects from where GEBCO bathymetry data was extrapolated for the two locations.

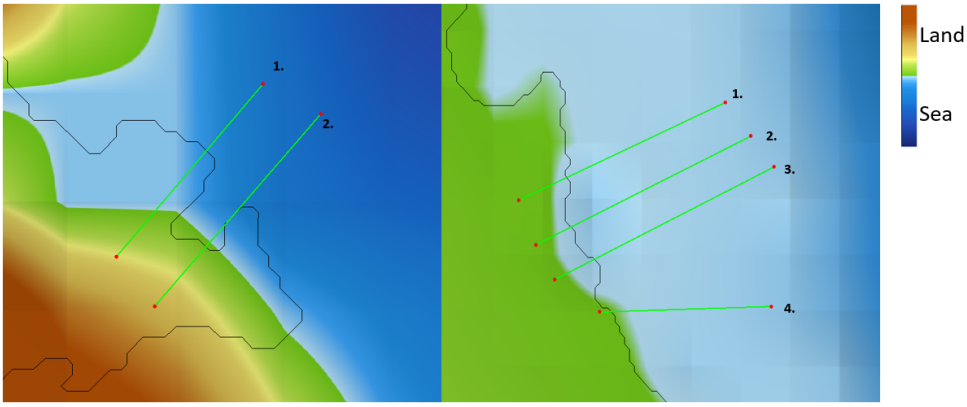

Figure 3.6: Gebco dataset, with coastline position (black line) from OpenStreet Maps and collected bathymetry transects (green lines) for Praia Abade (left) and Pantufo (Pantufo) .

Unfortunately, GEBCO has a very coarse horizontal resolution (approximately 900 m at the equator), which then results in incorrect localization of the bathymetry points. This can be seen in Figure 3.6, where the black line represents the coastline taken from OpenStreetMaps (OpenStreetMap contributors, 2017) and the green and blue colours represent the distinction between land and sea according to GEBCO. For example, some transects were retrieved initially for Pantufo. As can be seen from Figure 3.7, using the geographical coordinate points provided with the dataset results in a most likely erroneous bathymetry profile, suggesting that the data is referenced erroneously as well as that it contains errors. Especially for Pantufo, most of the transects collected described an unrealistic cross-shore profile and were therefore discarded (transect number 1, 2 and 3 in Figure 3.7). Therefore, only transects that did not show spurious data were used (transect 4 for Pantufo and transect 1 and 2 for Abade).

Single transects were collected and an average slope for the offshore and nearshore bed was estimated from the single data-points. After this,the original position of the coastline was retrieved from OpenStreetMap. This was done in order to have a better

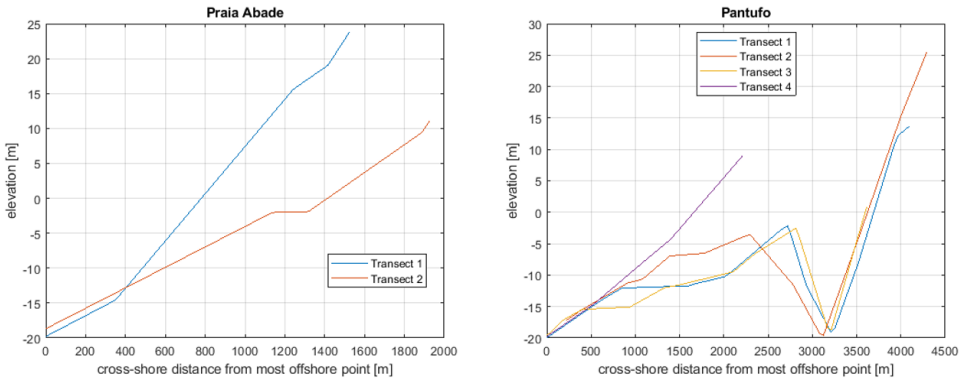

Figure 3.7: GEBCO collected bathymetry transects for Praia Abade (left) and Pantufo (Pantufo) .

horizontal referencing of the coastline. Following that, a single transect was created for each community, using the computed average slopes to model the bathymetry from - 20 m to a beach height of 5 m. The slopes derived for the upper part of the lower part of the profile, from -20 m water depth to -8 m and for the upper part of the profile, from -8 m to the beach. For Pantufo, only one transect was available (number 4 in Figure 3.6), whereas an average between transect 1 and 2 was used. Figure 3.8 shows the comparison between the bathymetry profiles derived using GEBCO and using the more reliable, locally measured data points.

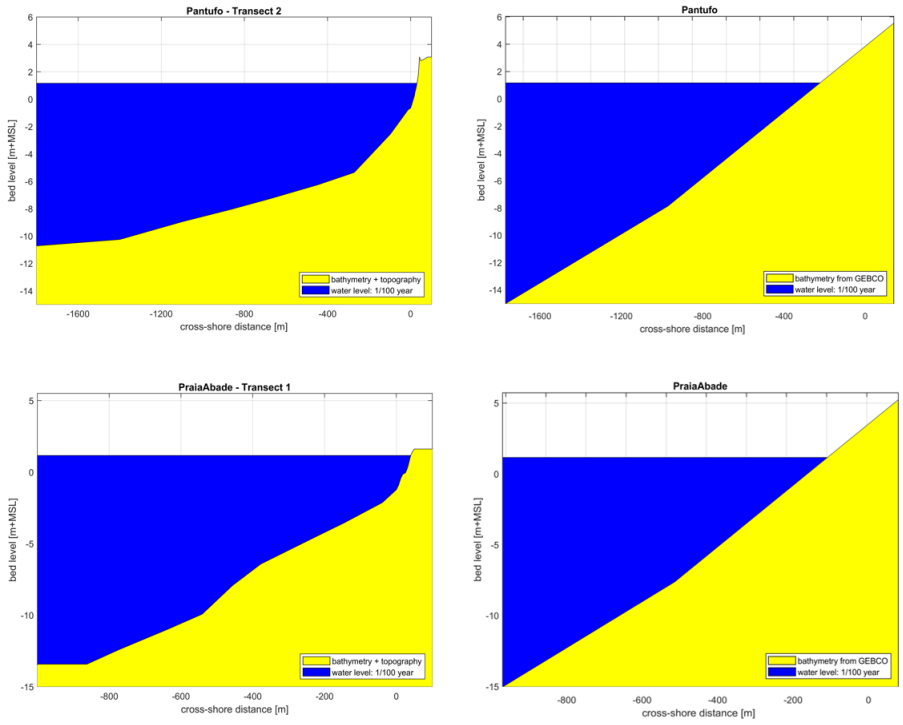

Figure 3.8: Comparison of cross-shore profiles for Pantufo (upper panels) and Praia Abade (lower panels), derived from local measurements (left panels) and GEBCO (right panels).

3.5.3. ELEVATION DATA

Elevation data is both composed of aerial images collected via drone survey and publicly available, global data. For each considered location, the two sources were combined to derive DEMs which were used both for the hazard modeling with SFINCS and for the impact assessment with Delft-FIAT. To create the DEMs, the following data was used:

- A DSM, which represents both the natural and built features on the surface. For São Tomé, the elevation data-set was derived from stereographic TerraSAR-X imagery, produced by GeoVille in 2013. The dataset is in the WGS 84 / UTM Zone 32N coordinate system with a spatial resolution of 10 m and vertical accuracy of 5-10 m. For the location of Praia Abade, this dataset was not available, instead the global Shuttle Radar Topography Mission (SRTM) DEM was used, which has lower accuracy.
- Digital Terrain Models (DTMs), which were retrieved from the drone imagery, that has a horizontal resolution of roughly 10 cm. The DTMs were horizontally and vertically referenced using control points collected using a Trimble R2 real time kinematic survey-grade GPS on a foldable 2 m pole.

The following Figure 3.9 shows the drone image for Praia Abade (left) and the derived elevation map (right). The drone imagery had a limited extension, therefore at its boundary, the drone DEM is merged with the TerraSAR-X DEM for Pantufo and SRTM DEM for Abade.

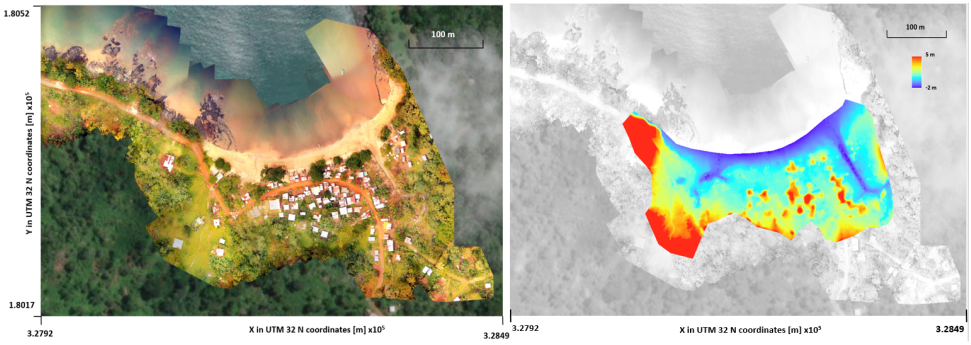

Figure 3.9: Aerial drone image for Praia Abade (left). Derived DTM (right).

In order to investigate the effects of using different DEMs in coastal flooding assessments, we will consider different scenarios using different global DEMs and comparing them to the drone-derived DSM. The drone derived DSM, having the highest resolution and vertical accuracy is considered as ground truth. Different global DEMs were collected for the analysis, referenced to the same vertical datum and used as input for the inland flooding with SFINCS. The sources of the different satellite-based DEMs are briefly described in the next section.

DIFFERENT SATELLITE-BASED DEMS

Satellite-based DEMs differ for the horizontal resolution, vertical accuracy as well as the vertical datum to which they are referenced (see Section 2.6). The following datasets

have been developed globally from different spatial missions and several studies have assessed the errors and differences between each one of them.

TanDEM is an Earth observation radar mission from the German Aerospace centre and Airbus Defence & Space that developed a global DEM in 2015 through radar images from two twin satellites (TanDEM and TerraSAR-X). It is available freely at a resolution of 3 arcseconds (roughly 90 m around the equator). The absolute horizontal and absolute vertical accuracy are estimated at the 90% confidence interval to be below 10 m. The DEM is also available at higher resolution, although only commercially.

SRTM (Shuttle Radar Topography Mission) is a DEM released from NASA. This elevation model has been corrected and a new version with a smaller resolution (1 arcsecond, ~30 m at the equator) was made. Following one of the first release of SRTM, an error-corrected version, ***MERIT DEM*** was developed by (Yamazaki et al., 2017). The error removed include noise as well as tree corrections, based on global vegetation cover maps and building roofs in highly populated areas. The potential issue with the corrected version for this case study is that global vegetation maps may not have been accurate enough for the two islands. However, the SRTM version that was corrected has a coarser resolution (3 arcseconds, ~90m) and the absolute vertical error had been reduced to roughly 12 m.

ASTER DEM (Advanced Spaceborne Thermal Emission and Reflection Radiometer) was developed by a joint program from NASA and the Ministry of Economy, Trade and Industry of Japan, It has a horizontal resolution of 1 arcsecond and a vertical error of 17 m in the 95 percent confidence interval.
ALOS DEM, another global DEM, was unfortunately not available for the location of interest.

In order to use these datasets, they had to be referenced to the same vertical datum. Most importantly, for coastal flooding modeling, it was necessary to have them referenced to the MSL. During the Deltares site visit (Giardino et al., 2018), the elevation difference from the ellipsoid WGS84 and MSL was found to be 20.14 m. Therefore, all the DEMs were first referenced to the WGS84 ellipsoid and after each pixel elevation was reduced of 20.14 m. To reference the DEMs to the ellipsoid, the geoid undulations had to be estimated and added to the pixel elevations, which was done utilising of the Aerospace Toolbox function *geoidheight.m* in Matlab. The geoid height was first calculated for multiple points around the island at a small resolution (10 m). After finding out the little variability of the results for the locations of interest (± 1 cm) a constant value of 16.4 m and 18.5 m were used for São Tomé and Príncipe respectively. Table 3.2 below summarizes the DEMs included in the analysis, alongside with their vertical datum, horizontal resolution and reference system.

Another necessary step was to increase the resolution of the DEMs so to have them with the necessary resolution for the SFINCS model grid of 5 m. The *resampling* tool in ArcGIS was used, with a bilinear interpolation method, which consists of determining the new value of a cell based on a weighted distance average of the four nearest input cell centers. This approach would also result in some smoothing of the data values.

Table 3.2: Different Satellite-based DEMs included in the analysis and specifications.

DEM	Vertical Datum	Horizontal Reference System	Horizontal resolution
TanDEM-X	WGS84 Ellipsoid	WGS84	3 arcseconds (~90m)
SRTM	EGM96	WGS84	1 arcsecond (~30m)
MERIT	EGM96	WGS84	3 arcseconds (~90m)
ASTER	EGM96	WGS84	1 arcsecond (~30m)

Globally available, low resolution DEMs have already proven to not be accurate enough to model coastal floods considering their low vertical accuracy (see Section 2.6). Hence, for this study, they will be regarded as low quality datasets. On the other hand, drone derive DEMs can achieve a much higher level of vertical accuracy (Section 2.6), thus the drone DEM of this study will also be referred to as high quality DEM. The accuracy of the global DEMs was tested in comparison with the drone DEM. The results and methods of comparison are described in Appendix C. Since TanDEM was found to be the most accurate of the global DEMs, it was expected to perform best also at reproducing the flooding.

3.5.4. DAMAGE MODELING- DDFS

In this section the different DDFs that will be used in the analysis and the studies from which they were obtained will be discussed. Our intention was to collect a range of curves that would represent the variety of possible shapes and types used in CFR analyses.

To assess the vulnerability of the assets, local specific DDFs were created, adapting a vulnerability function taken from literature. For the Deltares study, the depth damage function considered comes from a study of the Joint Research Center (JRC) (Huizinga et al., 2017). The study extrapolated information for different countries around the world on already existing DDFs, in order to generalize the results and provide continent-representative vulnerability curves. Figure 3.10 shows some curves developed by the study for different countries in Africa, as well as a generalized, African continent one. The curve for Mozambique was used to create local São Tomé and Príncipe DDFs.

As previously introduced in section 2.7, there is a great variety of possible DDFs that vary accordingly to the flood and exposure characteristics. This study will investigate how the use of different damage functions can yield to different damage estimations and the importance of using data that is as much as possible fit to local characteristics, or if more general information can be sufficient. To reach this goal, different damage functions will be used and compared to the case-specific one. The functions that will be compared are:

- JRC African continent (Huizinga et al., 2017).
- American Samoa curve (Paulik et al., 2015).
- Tsunami derived curve (Tarbotton et al., 2015).
- Coastal flood on a global scale (Hinkel et al., 2014).

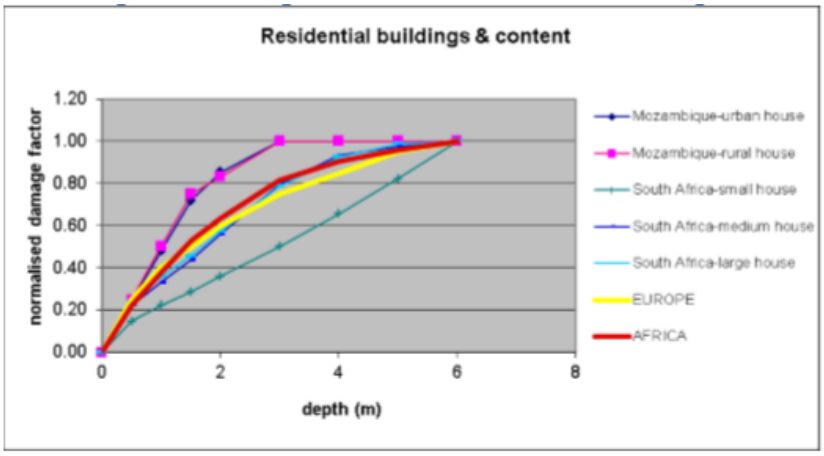

Figure 3.10: Depth-damage functions from JRC report (Huizinga et al., 2017).

- Sint Maarten curve (Vojinovic et al., 2008).
- Damage Scanner Model (DASM) (Kok et al., 2005).

Most of these curves, as it will be shown, were created following the 2nd approach described in Section 2.7, but to include also a curve based on the 1st approach, the American Samoa curve was chosen.
The JRC (Joint Research Centre) African continent curve was developed by (Huizinga et al., 2017) in an attempt to collect information on damage modeling and produce a database of DDFs at a global scale. In their report, they gathered already developed damage curves for riverine and coastal flooding, divided for each continent. There is no distinction between the two types of flooding and according to the authors the proposed DDFs can be used for the damage assessment of a generic inundation event. In their analysis, The maximum damage values taken from literature were corrected for inflation and converted to euros. Also, all the functions were normalised from o to 1 to make them comparable and create continent specific curves. General curves were produced for different category of objects like residential buildings, agriculture and commercial infrastructures. Although it is generalised for the African continent, this curve is expected to give very similar results compared to the São Tomé specific curve, as the latter was derived from it.

The American Samoan curve was taken from (Paulik et al., 2015). This function was chosen as it attempts to model coastal flooding damages on an archipelago with a similar morphology to the case study: American Samoa contains five volcanic islands with very steep slopes of terrain and a similar climate. Although, this island is subject to also different hazard conditions (tropical cyclones are a high threat) and the type of buildings and assets fragility are different. Indeed, American Samoa has a wealthier economy and the houses are expected to be more flood-resistant than in São Tomé since, according to (Reese et al., 2011), the American government has been promoting the construction of hurricane-resistant concrete houses.

Another curve used in this study comes from a review of Tsunami damage functions from (Tarbotton et al., 2015). In their study, existing curves were organized into similar types and damage-state categories. In their article, the importance of classifying the following parameters was underlined: the building damage state (e.g. minor damage, complete damage), the hazard intensity and the building typology (e.g. single-floor wooden house, concrete reinforced masonry, etc.). As the curves were also divided into different damage-states, for our analysis we only considered the worst state, collapse, so that the curve ranging from 0 to 1 would represent no damages at 0 and maximum damage possible at 1. Since multiple functions derived from different locations in the world are proposed in the paper, a range of different functions that could approximately represent the buildings in São Tomé were averaged. For this reason, only wooden and weak concrete house type curves were included. Figure 3.11 shows the different curves taken from (Tarbotton et al., 2015) with the final averaged curve used in this study coloured in red.

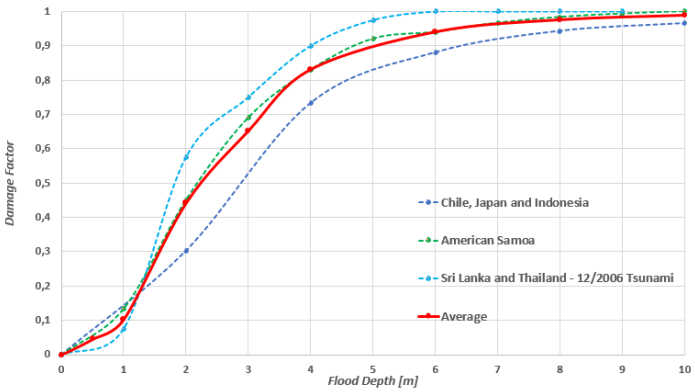

Figure 3.11: Tsunami DDFs for different locations around the world from (Tarbotton et al., 2015).

Nevertheless, particular attention must be paid when using tsunami derived functions for coastal floods. Indeed, tsunamis are very destructive events with significantly more energy and greater inundation extent than coastal floods. Moreover, tsunamis may be linked to earthquakes which could cause further damages.

(Hinkel et al., 2014) assessed coastal flood damage on a global scale for different sea-level rise projections, topographic datasets and mitigation measures. In their work, a logistic damage function with 1 m flood completely damaging 50% of the assets: $Damage(h) = h/(h+1)$, where h is the flood depth. This function was also used in (Prahl et al., 2016) for estimating micro-scale damages for the city of Lisbon. This function, although being very general, has been used for coastal floods in other studies, which thus gives us confidence in its applicability in oceanic islands cases.

The curve used in the assessment of typhoon-induced damages on the Island of Sint Maarten in the Caribbean, (Vojinovic et al., 2008) is also included in the analysis. This

function, as can be seen in Figure 3.13, has the steeper profile and the maximum damages are reached at much smaller depths if compared to other functions. Furthermore, this curve is intended to be used for rainfall flooding. This represents a significant difference to our case of coastal flooding in São Tomé. The reason behind the choice of this function lies in the fact that this study's ultimate goal is to reproduce a substantial variety of damage modeling scenarios and include different buildings behaviour. By implementing this function in the analysis, the case of very fragile buildings is introduced and allows to understand the consequences of selecting a certain DDF with the most conservative approach (the very steep curve).

The DASM is one of the most used flood damage estimation in the Netherlands for riverine flooding (Jongman et al., 2012), (Kok et al., 2005). The model includes a multiplicity of curves to be used for different building types, where house structure and house content are distinguished. For our study, we selected a curve for a single floor residential building, including both the structural and content damage. As can be seen in Figure 3.12, the curve is the sum of the content and structural damage functions, making it a two steps curve. The first step represents the initial, house content damage, reaching 20 percent of the total value at almost 1 m flood depth. The second step begins at a depth of 1.5 m and continues until the maximum damage is reached.
Although this curve is used for riverine flooding in the Netherlands, a much different situation that coastal flooding on oceanic islands, the choice of implementing in the analysis comes from the fact that the damage development is assumed to occur in steps. This approach can be expected to model well both the structural and content damage.

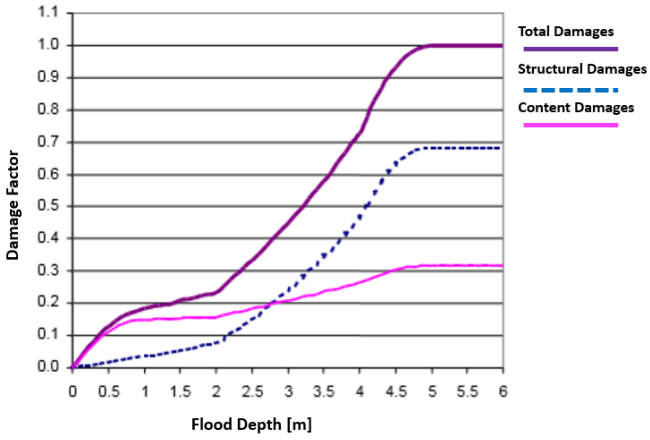

Figure 3.12: Damage Scanner Model residential building damage curve, from (Kok et al., 2005)

A summary of the different curve used in the analysis is shown in Figure 3.13 below. Already this figure can give an idea of the epistemic uncertainty in damage modeling using different DDFs. As can be expected, the JRC African-Continent curve is very similar to the two case specific curves of Praia Abade, developed by Deltares (Giardino et al., 2018), since these two were derived from it. Both these two curves do not introduce damages until a depth of approximately 30 cm is reached (black curve in the figure). This

occurs because some houses in São Tomé, especially in the coastal region, are slightly elevated in order to reduce the risk of coastal flooding. The same step in elevation was applied to all curves included in the analysis. The variety of shapes can also be noticed: the global coastal flood analysis curve and Sint Maarten curve clearly belong to the first approach described in Section 2.7, whereas the American Samoa and the second part of the DASM curves are closer to the second approach.

Already the first two meters of water levels introduce a high uncertainty in the computed damages. A primary sensitivity of the damages to the different curve implemented can already be conducted by merely looking that between the American Samoa and the JRC African Continent curves there is a factor 8 of difference at 1 m flood depth and a factor 3 at 2 m water depths.

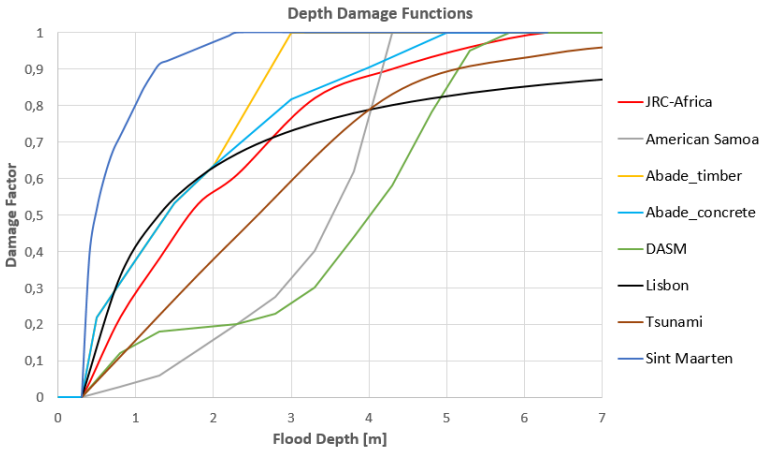

Figure 3.13: Summary of the different damage functions used in this study.

A different approach was used to model damages resulting from boats losses. As already explained, boats represent a valuable asset for the communities of fishermen in São Tomé and Príncipe. Coastal floods are known to destroy and make many fishing boats disappear on the two islands. Therefore, a water depth of 0.5 m was assumed enough to make the boat disappear and lose its total value. Smaller water depths would not result in any damages to the boats. In our work we have not distinguished between structural and content damages to the houses. This ensures a more general approach that can be extended to different cases. Furthermore, we believe that a single curve can be used to represent both damages, if the value of the asset includes both.

UNCERTAINTY IN A DDF SHAPE

Testing the fore-mentioned curves allowed us to assess the importance of many assumptions and characteristics of DDFs. Nevertheless, we also wanted to focus particularly on the effects of changes in shape for the same curve. To achieve these goals, we applied a similar methodology to that implemented by (Egorova et al., 2008) and (de Moel,

2012). This method was run in parallel to the primary analysis and its results are not integrated with the others. To account for the uncertainty in the shape of the damage curve, (Egorova et al., 2008) used a beta distribution with the mean values located on the damage function curve. The choice of the beta distribution is sustained by the fact that the fraction of damage computed are within 0 and 1, which is exactly the domain of the distribution. Another positive aspect of this distribution is that it can be concentrated on narrower interval and have low probability density in the tails, according to the exigence. The PDF of the beta distribution is defined as follows:

$$Be(x|\alpha,\beta) = \frac{\Gamma(\alpha+\beta)}{\Gamma(\alpha)\Gamma(\beta)} x^{\alpha-1}(1-x)^{\beta-1} \tag{3.3}$$

where α and β are two position parameters. The application for the uncertainty of the damage function consists in, for every given value of water depth d, to consider a random variable, R(d) which is beta distributed. The mean value of this random variable is assumed to be equal to the known damage factor value of the damage curve of interest. Based on this assumption, the parameters of the beta distribution are estimated, for each stage of the damage function. For a better description of the mathematical derivation, the user is directed to (Egorova et al., 2008). A peculiarity of this methodology is that the variance is equal to zero when the damage function is equal to zero or one. This means that there is no uncertainty at the points of zero and complete damages and the analysis is only focused on the varying shape. Therefore it is assumed that the moment when the asset reaches complete damage is considered certain. One may argue that the moment at which a building is completely damaged may vary from case to case, although a sensitivity on different building strengths was already performed for the main analysis. The values of the distribution parameters also depend on a constant factor, k, which basically sets the level of uncertainty of the function. The higher the factor, the higher the uncertainty. We adopted the same value of 0.1 as (Egorova et al., 2008) and (de Moel, 2012).

This analysis only included the current time horizon and not future changes. In Figure 3.14 we can see the results from the applied methodology. The green line represents the mean reference curve, whereas the neighbouring dotted curves are the limits of the different 50%, 90% and 98% confidence interval. A significant distance between the 1th and 99th percentile can be seen. Another interesting aspect of this method is that is capable of reproducing a highly convex and a highly concave shape, representing the two most distinct approaches when modeling damages via DDF (see Section 2.7).

The upper bounds of the confidence intervals (75th, 95th and 99th percentiles) have a concave shape and generally have their first part closer to the mean curve compared to the lower bounds, which is particularly visible for the 75th and 25th percentiles. Contrarily, the lower bounds of the confidence intervals have a convex shape. All the curves behaved similarly to the mean one, by having a change of slope at a water depth of approximately 1.75 m.

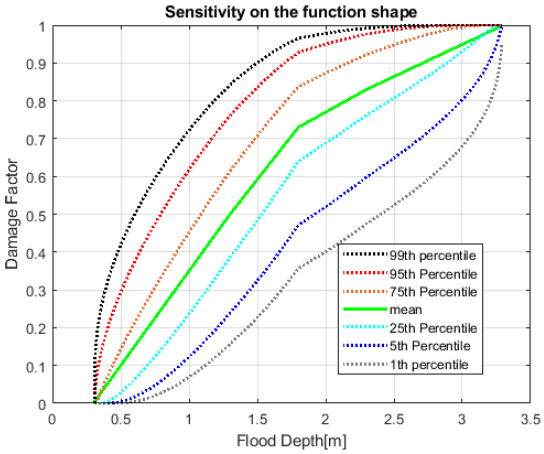

Figure 3.14: Functions shape levels with the 50%, 90% and 98% confidence interval bounds, for k = 0.1.

3.6. FUTURE CONDITIONS

Climate change is expected to increase the exposure and vulnerability of cities to flooding (Nicholls et al., 2007). The growing concern given to the impact of climate change on natural hazard has led to several risk assessments that incorporate scenarios about future climates, to give insight about future coastal flood risk. All the components of risk are subject to changes in time due to both socioeconomic development and climate change, therefore assessing future flood risk challenging. Literature works on future flood risk commonly focus on the inclusion of climatic effects on the physical system.

For the future conditions, three different time horizons are considered in our analysis, the years 2050, 2070 and 2100. To investigate the development of risk for the islands, both climate change impacts and socioeconomic variations were included in the analysis.

3.6.1. CLIMATE CHANGE IMPACT

Regarding flood risk, multiple factors arising from climate change are expected to have a negative consequence for the overall risk. These include wrong thermal expansion of oceans, sea -level rise and variations in storminess. The latter refers, among other things, to the possible increase in storm surge height and storm frequency (Hemer et al., 2013). Estimating the potential future risk of coastal communities to flooding has commonly been based on a deterministic modeling of coastal inundation. According to this approach, specific sea level rise scenarios are used to increase the static water level and the results are compared to the current case. However, projections of sea level rise are subject to numerous uncertainties as a consequence of the many assumptions made concerning future greenhouse gases emission scenarios. These emission scenarios (RCP) vary according to the radiative forcing and the uncertainty over the response of the ice caps and ice sheets. Therefore, the implications when only a single SLR scenario is used, the understanding of the system susceptibility to future flood risk is limited and the un-

certainty in the predictions is hidden. One way to represent the uncertainty in future sea level rise is to include different projections, coming from different RCP scenarios, as well as simulating values within the very likely range (5th-95th percentile) for each scenario. This method partly follows the one of (Purvis et al., 2008). The authors developed a methodology to reproduce the uncertainty in sea level rise predictions and its impact on damage estimates for an event with a return period of 200 year. In their analysis, they fitted a distribution to the predictions of SLR and run a MC simulation. Their results showed that using a single value to estimate damages may lead to a heavy underestimation of the risk, as the sea level increases with lower probability but higher consequences are discarded.

With regards to climate change, many physical factors are influenced. For our case, given the fact that the expected increase of significant wave height due to climate change in the West African region is only expected to be up to 3% (Hemer et al., 2013), we disregarded changes in storminess intensity and frequency. The main impact that we considered on the hydrodynamic forcing from climate change was static sea level rise, which would yield to a higher relative sea level rise on the coastline of the two islands. To represent uncertainty from sea level rise predictions, we considered two different RCP scenario, namely 4.5 and 8.5 and we included the predictions for the lower and upper limits of the 90% confidence interval (the 5th and 95th percentile) and for the 50th percentile. These predictions were taken from (Vousdoukas et al., 2016), where the authors estimated probabilistic projections of extreme sea levels, taking into account contributions of tides, extreme event, glacial isostatic adjustment and other sources, including SLR, both for the *moderate-emission-mitigation-policy* and *business as usual* scenarios (RCP 4.5 and 8.5). Under their results, a large part of the tropics is expected to be exposed annually to the present-day 100-year event from 2050. Predictions were available for a location in the proximity of São Tomé, which was then used and assumed to be very similar. The results of the projections and a better methodology description can be found in (Vousdoukas et al., 2018b). The predictions for SLR for future conditions under the two scenarios are shown in Figure3.15, The two shaded area represent the uncertainty bands given by the 5th and 95th percentiles, whereas the two thick lines represent the 50th percentile values. The 5th percentile for RCP 8.5 and the 50th percentile for RCP 4.5 have very similar values.

Table 3.3 below includes all the values that were simulated for the three time horizons. Since modelling all the 18 different sea level predictions would have not been feasible, only 9 values were computed, trying to select them to be very close to the ones in the table. The computed values were: 0.12, 0.2, 0.26, 0.3, 0.47, 0.54, 0.87, 1 and 2 m.

Table 3.3: Sea level rise values included in the analysis for the two Islands of São Tomé and Príncipe

	RCP 4.5			**RCP 8.5**		
Year	5th	50th	95th	5th	50th	95th
2050	0.124	0.205	0.31	0.189	0.3	0.475
2070	0.196	0.32	0.49	0.307	0.486	0.98
2100	0.262	0.538	0.862	0.531	0.878	2.05

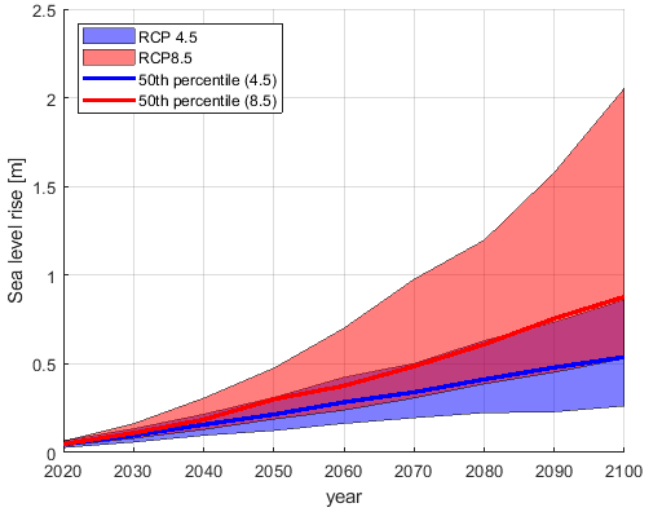

Figure 3.15: Projected sea level rise for the Islands of São Tomé and Príncipe, for the scenarios RCP 4.5 and RCP 8.5, from (Vousdoukas et al., 2016)

3.6.2. SOCIOECONOMIC CHANGES

Socioeconomic changes have already demonstrated to have a great impact on the possible outcome of future flood risk assessments (Bouwer et al., 2010), (Vousdoukas et al., 2018a). For our analysis, it was decided to represent the possible uncertainty of socioeconomic changes by applying different SSP scenarios to estimate future assets value for the two islands. Indeed, the future assets values were assumed to increase proportionally to the local GDP and population growths. One of the variables that are considered in the SSP scenarios is projected GDP growth. The local GDP growth for decadal time steps was available from (Riahi et al., 2017) and population growth data was taken from (INE, 2012). To regard the uncertainty that comes from selecting one SSP scenario or another, we modeled future damages for the years 2050, 2070 and 2100 using different GDP projections, according to different SSPs. These GDP projections are used as a proxy to estimate the asset value growth and the increase in population (and thus of assets number). Figure 3.16 shows the time development of GDP growth factor with reference to the year 2018, whereas Table 3.4 summarises the values considered for the analysis and the population growth factors. The 2018 GDP value was taken from (Fund, 2018).

Table 3.4: Projected GDP growth values included in the analysis, values taken from. Population growth factors are taken from (INE, 2012)

Year	SSP2	SSP 3	SSP 4	Population growth factor
2050	6.3	10.5	19.3	1.19
2070	5.8	9.2	15.3	1.31
2100	4.3	6.0	9.4	1.48

The factors indicate significant increases in capital value, with assets being up to 11

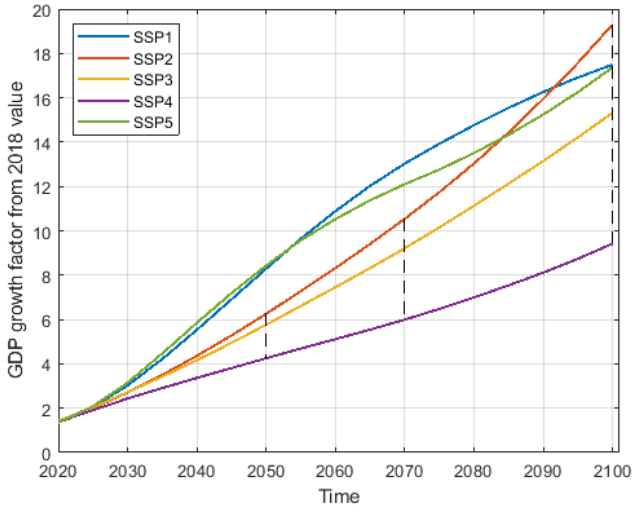

Figure 3.16: Projected GDP growth factor from the year 2018, values taken from (Riahi et al., 2017)

times more valuable in 2050 and 25 times more valuable in 2100, depending on the scenario assumed. We based our choice to include SSP 2. 3 and 4 both because of the indications from (Hongbo, 2014), as well as the three scenarios selected, capture the widest possible range of predictions for the island for the year 2100. According to (Hongbo, 2014), one of the limiting factor for the economic growth of SIDS is their smallness. This feature gives rise to economic disadvantages, such as limited natural resources, high import dependence, and constrained possibilities to achieve economies of scale. Moreover, tourism, one of the main national income sources in SIDS, is often impacted by natural disasters (Moore, 2010). Therefore, SSP3 and SSP4 scenarios are likely most representative of what could happen in São Tomé and Príncipe.

Summarizing, the methodology will include GDP growth modeling for SSP 2, SSP 3 and SSP 4.
The relative increase in asset value is calculated as follows:

$$Asset_{Factor} = \frac{GDP_{t,s}}{GDP_{2018}} x \frac{Population_t}{Population_{2018}} \tag{3.4}$$

where t represents the future time horizons (2050, 2070, 2100) and s the SSP scenarios.

Ultimately, including a change in the maximum asset value further allows us to test the sensitivity to the maximum damage value parameter, as previously done in multiple studies on flood risk ((de Moel, 2012),(De Moel et al., 2014), (Prahl et al., 2016), (Merz and Thieken, 2009), (Egorova et al., 2008)). Since in our modelling approach, the value of the asset, is used as multiplying factor for the ratio of damage (see Section 3.4), we are not expecting any non-linear behaviour of the model outputs from varying this input.

3.7. SUMMARY

Figure 3.17 shows the conceptual methodology for this study, indicating the model and which part of the risk definition they simulate. The different types of inputs varied in the analysis are also shown. The table below represents a summary of the different inputs of data and scenario considered in our sensitivity analysis. As it has been mentioned in Section 2, our objective is to conduct a global sensitivity analysis, which differs from a local sensitivity analysis by testing every single combination of the inputs. The added value of a global analysis is that it allows investigating different dependencies between the inputs and not merely the influence of a single output on the results. A summary table with the different inputs used for each variable in the risk assessment module is shown below (Table 3.5). In the table the second input is called storm surge and not water level. This is because the tidal forcing, which is also part of the water level, is kept constant. Only the storm surge parameter is varied. When considering parameters that represent future time horizons, it becomes challenging to select a single value to use as reference. Nevertheless, the SSP 3 and the median sea level rise prediction for the 50th percentile under RCP 8.5 were considered as reference. The reason for choosing the predictions following RCP 8.5 lies in the fact that it represents the worst case scenario and it has the most significant uncertainties.

In red are highlighted the reference value for each input.

Table 3.5: Summary of the different inputs used in the analysis, the nominal values are highlighted in red

	Different values/dataset used	Modeling module
Offshore Waves	The mean and both the low and high extremes of the 99 percent confidence interval of the 100 year return period value	Hazard modeling (XBeach)
Water levels	The mean and both the low and high extremes of the 99 percent confidence interval of the 100 year return period value	Hazard modeling (XBeach)
Bathymetry	• Gebco (900 m resolution) • local (50-100 m resolution)	Hazard modeling (XBeach)
Topography	• Drone at 1 m resolution • Drone at 5 m resolution • TerraSAR-X at 10 m resolution (Pantufo only) • SRTM at 30 m resolution • ASTER at 30 m resolution • MERIT at 90 m resolution • TanDEM at 90 m resolution	Hazard modeling (SFINCS) & Exposure modeling
Depth Damage Curves	• Local fit • American Samoa • DASM • Tsunami derived • Global coastal flooding • JRC African-continent • Sint Maarten	Vulnerability modeling (FIAT)
Sea Level Rise	The 5th, 50th and 95th percentiles of local sea level rise predictions according to the RCP 8.5 scenario	Hazard modeling (XBeach)
Shared Socioeconomic Pathways	• SSP2 • SSP 3 • SSP 4	Vulnerability Modeling (FIAT)

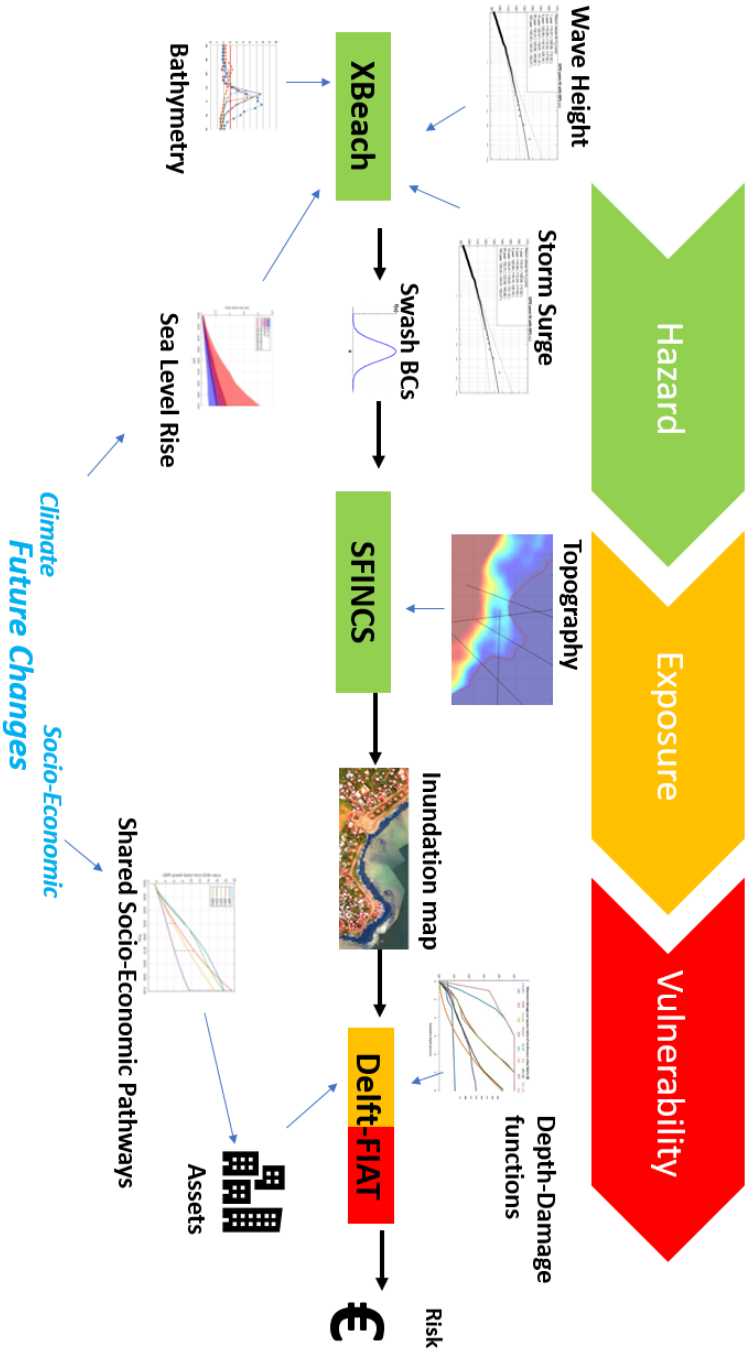

Figure 3.17: Systematic methodology for the study

3.7.1. ANALYSIS METHODOLOGY

The following Figure 3.18 will help explain the methodology applied to analyse the results. As previously mentioned, local and global sensitivity analyses are both possible with the batch of simulations made. However, it is not possible to exactly quantify the impact of one input onto the others, which is one of the advantages of global sensitivity analyses (Saltelli et al., 2008), (Uusitalo et al., 2015). Nevertheless, we developed a simple methodology to investigate first-order impacts of one input on the output, when the whole input domain is explored.

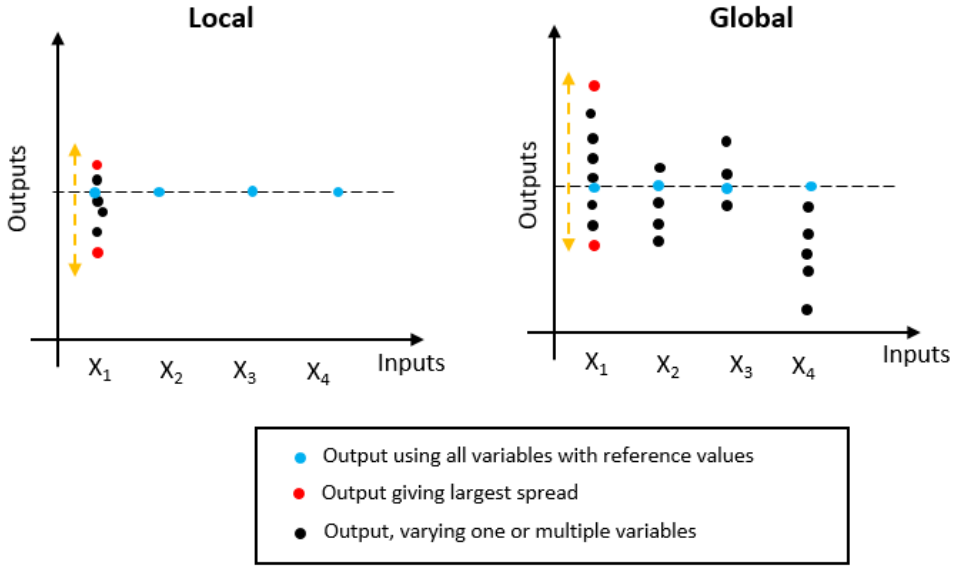

Figure 3.18: Methodology for the analysis of results

Local sensitivity analysis will be performed by looking at the largest spread of results possible when a single input is varied, and the rest are kept at their nominal value. This excludes relationships between variables and multi-linear behaviours. In Figure 3.18, the red dots represent the greatest spread of results varying the first input.

The global sensitivity analysis is made through means of examining the effects of changes in a single input value but without keeping the other variables at baseline. For the global analysis, the red dots in the figure still represent the results giving the widest spread possible by varying a single variable, but now all the possible combinations of other variables are also included. For each simulation with a change in input value, the computed damages are scaled to the value of estimated damages computed using the reference value for the same input. Therefore a value close to 1 indicates a small change in the model output, whereas a value far from 1 indicates a significant difference in the results. Moreover, overestimation of the results is shown by values higherr than one, whereas underestimation of the results is given by values smaller than one. To help us in the visualisation of results, box and whisker plots were selected to represent the ratio of

damages to the reference case, see Figure 3.19 for reference. The results are plotted with a box, which sides represent the 25 and 75th percentiles, the red line inside represents the median value (50th percentile). Whisker plots are drawn together, where the end indicates the 5th and 95th percentiles. Data points that fall outside these range of values are considered outliers.

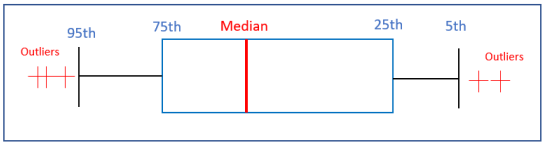

Figure 3.19: Explanation of box and whisker plot.

Often we will refer to statistical confidence intervals as *likely* and *very likely* range of results. For a clear definition, the 50% confidence interval (c.i.) and the 90% c.i. will be also addressed as *likely range* and *very likely range* respectively. More specifically, a c.i. is an interval estimate, that refers to a statistically predicted interval of parameter values. The 50% c.i., for example, will tell us between what range of values our parameter will fall in 50% of the cases. Its interval limits are the 25th and 75th percentiles. Similarly, for the 90% c.i. the limits are given by the 5th and 95th percentiles.

INPUTS INTERACTIONS

Furthermore, the interaction of pairs of inputs was also investigated in the analysis. It comprises of looking at the distribution of results given by varying one input while holding another input (the one which influence is being tested) constant at different values. With this approach, the impact of a particular value or dataset of the second input on the sensitivity of the first input can be assessed. Figure 3.20 depicts the concept of the approach. If we refer to the same example as for Figure 2.7, investigating two inputs interaction (X_1 and X_2 in the figure), consists of moving along one face of the cube. Therefore, the difference between this method, a local and a global sensitivity analysis can be understood.

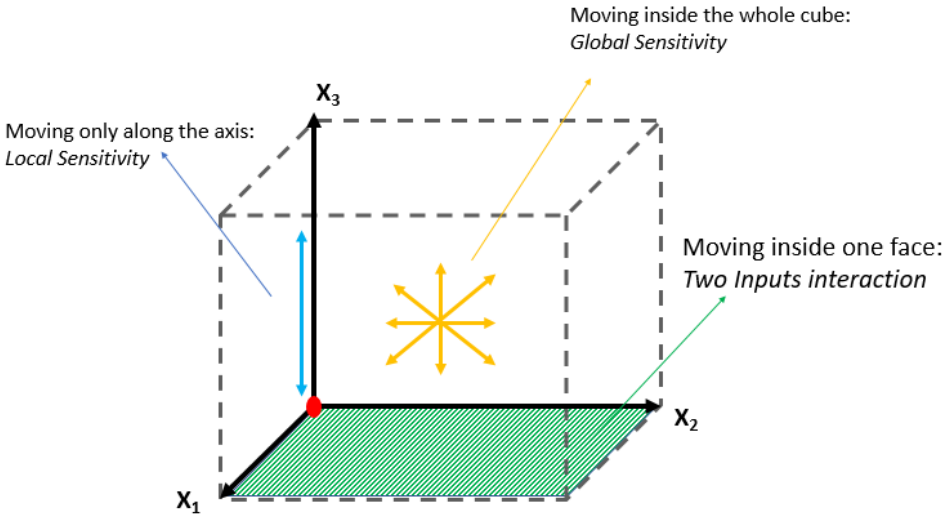

Figure 3.20: Three inputs space domain. The origin represents their nominal values. A local sensitivity is when we 'move' along one axis only. In a global sensitivity, we 'move' inside the whole cube. To test a pair of input interaction, we 'move' inside one face of the cube

4

RESULTS

CHAPTER SUMMARY

Initially, the results of the statistical analysis on offshore conditions are presented. We then assess the model validation based on the local community perception of risk. Following that, we first describe the general results of our analysis for the current situation. The sensitivity to single inputs on the estimated damages is then addressed. Then we include and compare the results for the future time horizons, highlighting differences and common trends. Finally, having identified Digital Elevation Models and Depth Damage Functions as critical input for output uncertainty, we describe the results of some extra steps that were taken to further investigate their sensitivity.

4.1. STATISTICAL ANALYSIS ON HYDRODYNAMIC FORCING

The methodology explained in Section 3.5.1, of applying a peak over threshold analysis to the data was used to derive extreme values for offshore significant wave height and storm surge level, together with their 99% confidence interval. The results showed very little variability to the different threshold values, leading to the decision of merely using the 98th percentile as threshold for the POT analysis, as recommended in (Wahl et al., 2017). The sample points that are used for the GPD have to be extracted in such a way that they can be considered independent. To achieve that, only the exceeding values in the time series that are sufficiently far apart are retained, so that they can be thought to belong to different storms. In our case, we have clustered peaks at a distance of less than 48 hours apart. Figure 4.1 on the left shows the clustering of peaks in the time series of water levels.

The GPD cumulative distribution function (CDF) was compared with the empirical CDF to estimate the goodness of the fit (see Figure 4.1, on the left). The fit is particularly accurate, especially if compared to a fit using the Gumbell distribution, which, as can be seen in the figure, has some discrepancy from the middle and upper part of the empirical CDF.

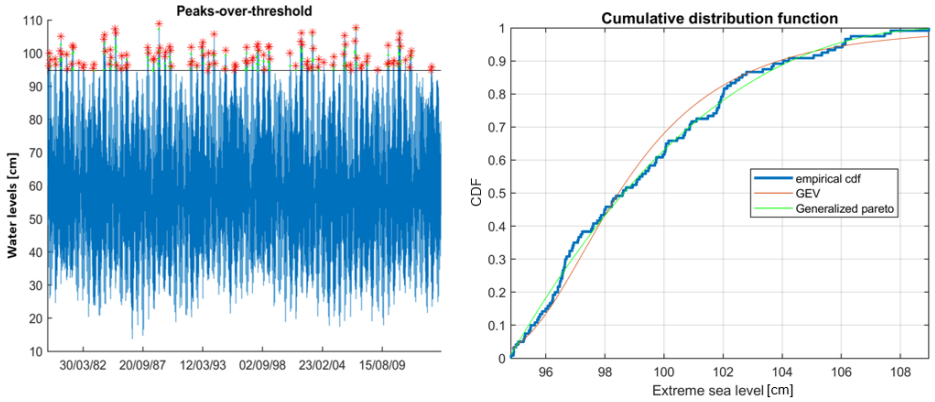

Figure 4.1: (Left) POT results for the water level time series. (Right) Comparison between estimated GPD, GEV and empirical CDF

The return values for multiple time intervals were then also computed, yielding to the results shown in Figure 4.2, which also include the 99 percent confidence interval. For the reference case, we will consider the 100 year return period value of approximately 110 cm. From here forward, we will refer to water level as storm surge.

For H_s, values were retrieved following the same approach. Although in this case, values were retrieved separately for the location of Praia Abade and Pantufo, since data was available for both locations after the transformation matrix of SWAN. From the results, return values were used as hydrodynamic forcing. Here below, the GPD for the location of Pantufo is depicted (Figure 4.3). Generally, there is higher uncertainty in these values compared to the water level analysis. This can be seen from the wider spread of the 99% confidence interval for longer return periods.

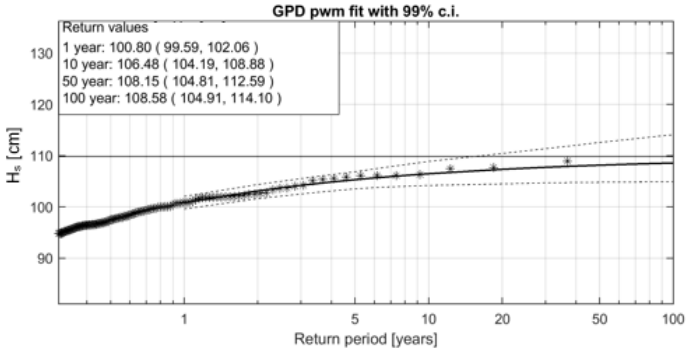

Figure 4.2: Extreme water levels return values for Sao Tome and Principe.

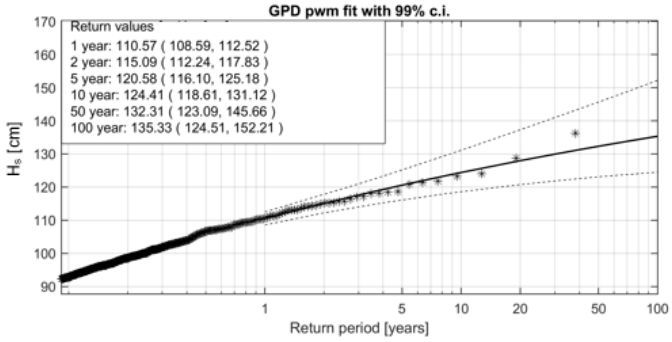

Figure 4.3: Extreme significant wave height with return periods for Pantufo.

Table 4.1 summarises the return values retrieved from the statistical analysis.

Table 4.1: Range of values used for H_s and storm surge in meters in Praia Abade and Pantufo.

Value	H_s Pantufo	H_s Praia Abade	Storm surge
Low	1.24	1.05	1.05
Mean	1.35	1.18	1.08
High	1.53	1.38	1.15

4.2. MODEL VALIDATION

Model validation is an essential step in flood risk analyses. Risk models need to be validated to gain trust and understand what can be concluded from them as well as what are the efforts required to improve them. Validation is usually based on the outcomes of the model that are of interest for the risk assessment. As an example, flow velocities may be of more importance in flash floods (very fast floods) than in slow-rising fluvial floods studies, which usually focus more on flood extents and depths (Merz et al., 2010). In flood risk analyses, multiple validation techniques have been developed that vary accordingly to the different characteristics of the flood event modeled. These techniques also vary accordingly to the different risk component(hazard, damage, etc.). The authors of (Molinari et al., 2019) have analysed the state of implementation of validation techniques, grouping them under: comparison with observed data, comparison with other models and expert judgement. Comparison with observed data usually gives the highest reliability in the model outputs, although it is the one most affected by the paucity of data. Indeed, it is often difficult to measure damages or flow velocities during a storm. New developing methods include using satellite data, measurements with drones and studying high water marks on buildings. At the same time, crowd sourcing is growing in popularity as a validation approach in data-poor environments (Frigerio et al., 2017). Although, such non-traditional methods are subject to sources of errors like incorrect information and wrong geolocalization, which negatively affect their reliability and accuracy. Given their lower reliability, new data sources are mainly integrated with traditional approaches to provide additional information (Schnebele et al., 2014). A successful example of fusing crowdsourced data with authoritative data is provided in (Schnebele et al., 2014), where the authors highlighted the useful insights and alternative information provided by the analysis of posts on the social media Twitter to estimate damages from Hurricane Sandy in New York.

In this study, to validate the model results, perceived flooding maps developed by the interested communities were used (Giardino et al., 2018). These maps indicate the area that local inhabitants have considered as main natural hazards from sea storms. Since there is no measured data, the models could only be validated qualitatively in such way. The hazard described by the locals is assumed to refer to hydrodynamic forcing conditions with small return periods. Therefore, the hazard model-train was first run with the one year return period conditions to compare the results with the local perception.

PRAIA ABADE

The model results for the 1 year return period storm are shown in Figure 4.4 on the left, whereas the local perceived risk map is on the right. The dark grey lines represent the rectangular grid of SFINCS. The local community has identified coastal flooding as the main issue, which occurs for approximately 3 days per month around spring tide (Giardino et al., 2018). Boats and the houses between the beach and the coastal road are the most impacted by runup (as indicated by the red box in the figure), with occasional runup reaching also the first line of houses behind the road. Comparing the modeled water depths, to the local perception risk map, we see that the hazards are qualitatively reproduced. In general, the water levels for this community are higher than other ones as the mean topography of the area is lower.

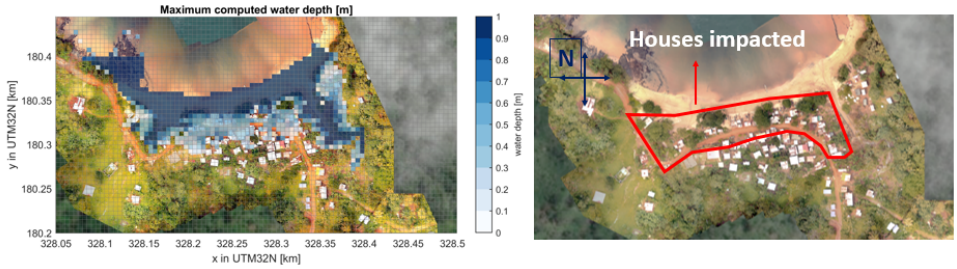

Figure 4.4: Model results for a 1 year return period storm (right) and locally perceived risk (left) in Praia Abade.

PANTUFO

Results for Pantufo are illustrated in Figure 4.5. The risk in the area is mainly related to the damages caused by storms to the fishermen boats (yellow boxes in the figure). At the same time, there are a few houses exposed to coastal flooding, located on the southern rocky headland (red box). The perceived hazards are reproduced quite well from the model, especially for the damaging of the boats.

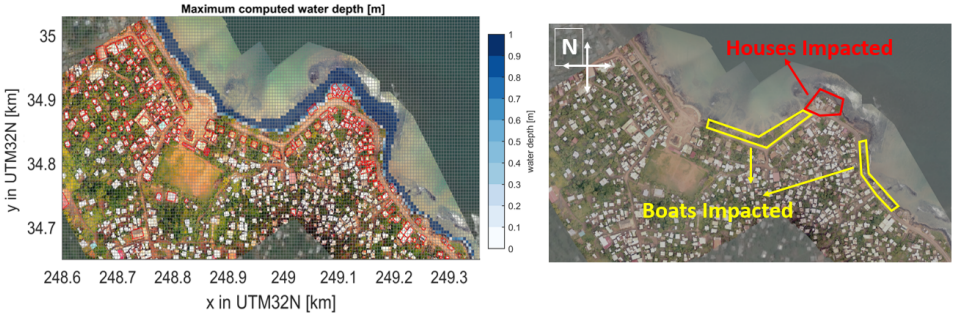

Figure 4.5: Model results for a 1 year return period storm (right) and locally perceived risk (left) in Pantufo.

At the same time, as the sensitivity benchmark analysis on XBeach showed, the hazard model shows what is referred to as *face validity*. A model can be said to have face

validity if it seems like it is going to measure what is supposed to measure. For example, the model is expected to show larger values of overtopping or runup for increasing values of water levels (see Section A).

Regardless of the results of coastal flooding, it has to be mentioned that during the project work conducted by Deltares, it has been found that for the other discarded communities of Micolo and Praia Melao, as well as partly for Pantufo, most flood risk comes from rainfall events. Indeed, in their study, (Giardino et al., 2018) have highlighted how rainfall water is responsible for most of the damages in the above mentioned three communities.

4.3. GLOBAL SENSITIVITY FOR THE CURRENT TIME HORIZON

PRELIMINARY TESTS

Preliminary sensitivity tests were conducted with XBeach and SFINCS to narrow down the number of parameters included in the main analysis. The following parameters were tested:

- Significant wave height, H_s (m)
- Storm surge level, wl (m)
- Bed friction
- Spectrum peakedness
- Storm Length
- Grid resolution

The results of the preliminary sensitivity tests have shown a much larger sensitivity on the predicted runup from H_s and storm surge level, compared to the other parameters. The smallest sensitivity was found from bed friction and the JONSWAP spectrum peakedness. A better description of the assessment is illustrated in Appendix A. Following these results, only H_s and storm surge level were included in the main analysis.

4.3.1. MAIN RESULTS

The results of the reference run for both location are plotted in Figure 4.6, where the upper panels show the maximum computed water depths and the lower panels the damages computed from FIAT. Both results come from the simulations with the highest resolution of 1 m. The damages are expressed in Sao Tomean Dobras (STD) per m^2. These results show how much more flood-prone is Abade than Pantufo, although significant damages to boats occur in both locations. Larger damages concentration (red colours) is found where the boats are located, closer to the coastline, whereas lighter concentrated damages (yellow in the figure) are usually found where buildings are. For Pantufo, a larger number of boats is at risk than for Abade, whereas fewer buildings are damaged. Looking at the maps of Pantufo, we can mainly identify two hotspots for risk regarding buildings, one on the headland and the other one more to the east of the town. Still in Pantufo, a rather wide flow of water is modeled at the top-left boundary (top right panel in the Figure). This boundary is where the drone-derived DEM finishes and is merged with Terra-SAR DEM, which is generally lower (see Section 3.5.3 and Appendix C). The

merging of the two DEMs is necessary to have a continuous topography at the boundary of the drone DEM. It needs to be reminded that this high resolution is only possible with the drone and for a microscale study. Larger scale modeling would most likely not allow for such a high computational resolution (see Section 2.3).

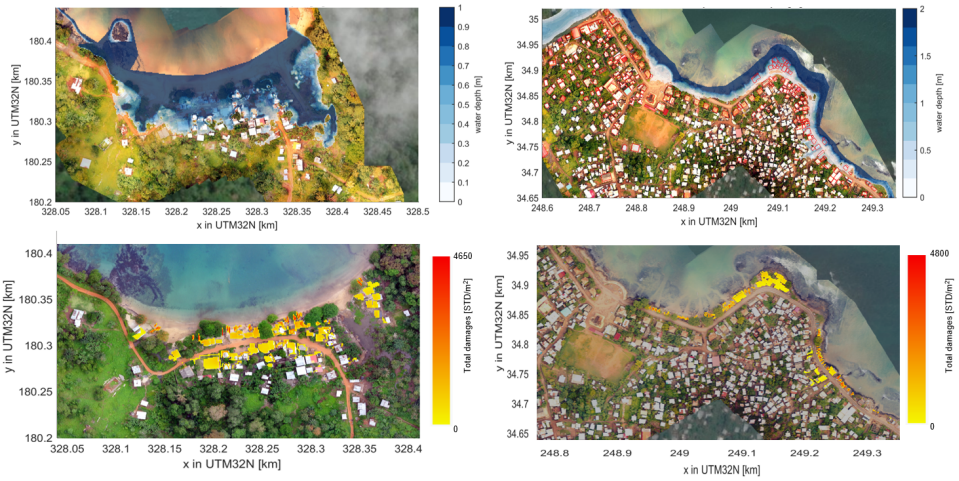

Figure 4.6: Maximum computed water depths (top) and total damages (bottom) for Praia Abade and Pantufo.

The following results were computed for expected hazards with a return period of 100 years. To compute the Expected Annual Damage, EAD, the output damages, expressed in the local currency of Sao Tomean Dobras (STD) were simply divided by 100 (see Section 2.1.1). The whole distribution of results for the current time horizon, combining all possible simulations is shown in a histogram in Figure 4.7. The left panel shows the occurrences of different damage ranges combining the simulations for both locations, whereas in the right panel they are separated. The red dots indicate the damages estimates for the reference simulation. Both communities seem to have a similar distribution of damages,with a positive skew and a long right tail, especially for Pantufo. The red dots in the left panel indicate the results from the "best practice" run, made by using the reference value for each input (see Section 3.7.

The following sections will include the results focusing on a single input at a time, for their global sensitivity.

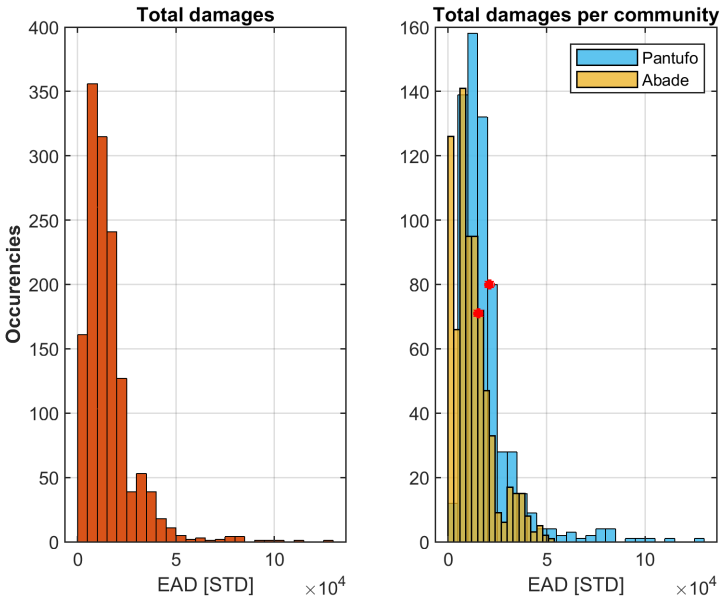

Figure 4.7: Histograms for the total computed damages for the 100 years return period, both for the two communities combined (left panel) and for the single community (right panel).

4.3.2. HYDRODYNAMIC FORCING

In this case, hydrodynamic forcing refers to the sensitivity to significant wave height and storm surge. The analysis is made by comparing the results from a scenario with higher/lower wave height/storm surge to the results from the scenario with the reference parameter value. In this case, the reference is represented by the mean value of the fitted GDP (Generalised Pareto Distribution) discussed in Section 4.1.
Figure 4.8 below includes the comparison for both Significant wave height and storm surge height of the two communities combined. As can be seen, significant wave height has a more substantial impact on the model outputs, yielding to both lower and higher damages than the water level. Indeed, the very likely range of results is 0.8-1.2 and 0.85 - 1.15 for the two parameters respectively. These results are in accordance with the output of the statistical analysis illustrated previously, which showed a wider 99% confidence interval for the 100 year return period value for H_s compared to storm surge. The difference of range of results even increases if we include the outlier values.

We can also notice how for both the parameters there are long upper and lower tails. Although, these results are not consistent for both locations. If the two communities are analysed separately and for each single parameters, we notice different behaviours. The following plot (Figure 4.9) depicts the results looking only at H_s (bottom panels) and at storm surge (top panels) . Left panels are for Praia Abade, whereas right panels are for Pantufo. The long tails are mainly present in Pantufo, whereas the range of results for Praia Abade is much narrower. This is partially due to the higher range of values for H_s

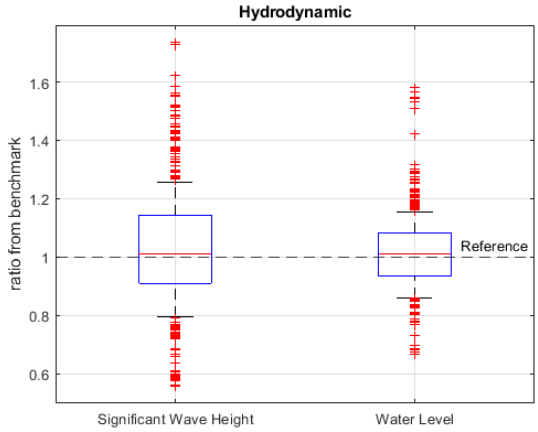

Figure 4.8: Hydrodynamic parameters sensitivity for both locations.

used in Pantufo compared to Praia Abade (see Section 4.1 and Table 4.1) that leads to a higher sensitivity.

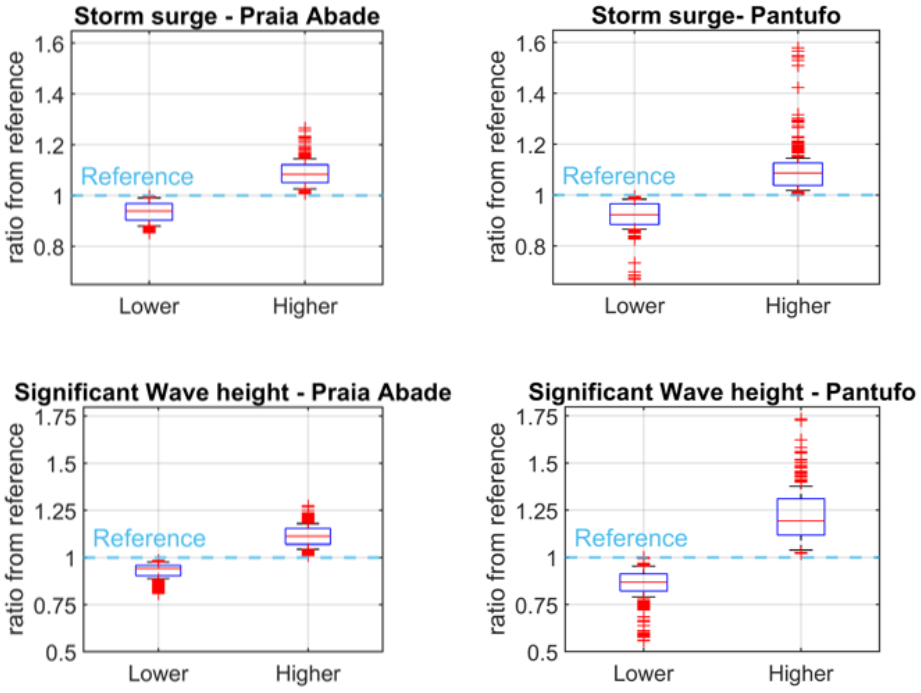

Figure 4.9: Significant wave height (bottom) and storm surge level (top) sensitivity for both locations.

4.3.3. BATHYMETRY DATA

To test the impact of using different bathymetry data, it was only possible to compare the simulations with cross-shore transects derived from GEBCO and from the local measurements. In this case, modeling wave transformation with the GEBCO bathymetry always gives larger damages, with a median increase of computed damages of 15% for Praia Abade and 27% for Pantufo (see Figure 4.10). Once again, the results of Pantufo have a larger spread than Abade, both for the very likely range but especially when looking at the whole distribution of results. Also, the likely range of results in Pantufo is twice as large than in Praia Abade (0.2 width compared to 0.1).

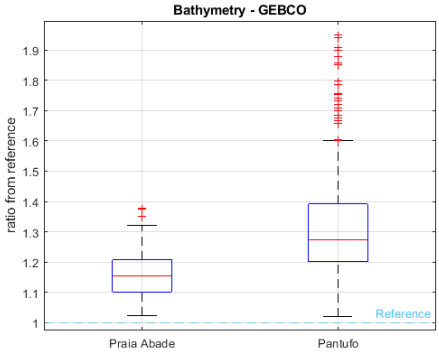

Figure 4.10: Sensitivity to different bathymetry datasets for the two locations.

4.3.4. DEM SENSITIVITY

This sensitivity refers to the comparison between globally available DEMs and the drone-derived DEM with a resolution of 1m. A quantification of the errors in the estimated elevation between the drone DEM and globally available DEMs was conducted and the results are described in Appendix C. TanDEM was found to be the closest to the drone, with a mean error of 3.23 and 2.9 m in Praia Abade and Pantufo respectively. Both SRTM and MERIT showed very similar mean errors, although larger in Praia Abade than in Pantufo. ASTER had the biggest mean error of 6.9 m in Praia Abade and 5.8 m in Pantufo.
Since for both locations, some building roofs and tree canopies were still included in the Drone DEM, it was corrected (see Appendix C for an explanation of the methodology) and the 1 m resolution used as reference value. First, the large discrepancy in representing elevation between the different DEMs can be visualised through graphs of cross-shore distribution of wave height and bed elevation, computed by SFINCS. For each location, a representative transect was used to collect water level signals from single point locations, with a 1m spacing, every second. From this data it was then possible to compute the distribution of H_s. The transects location is shown in Figure 4.11.

The results are shown (Figure 4.13 and 4.12) for each DEM with the respective bed level elevation, to evaluate the differences. For both locations, the peak water level is drawn as a black line. The drone DEM with a 5m resolution is included for comparison.

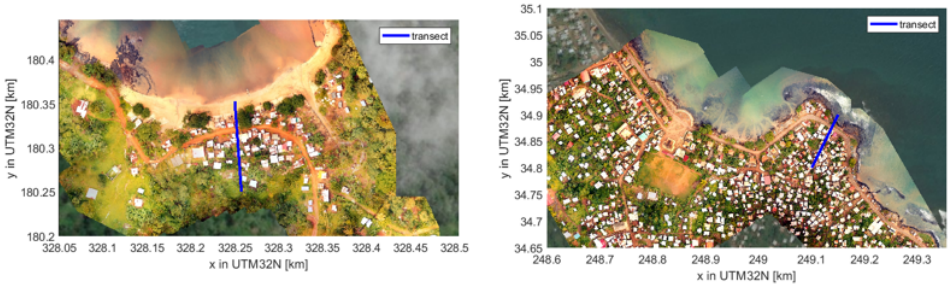

Figure 4.11: Location of the transects in the two communities.

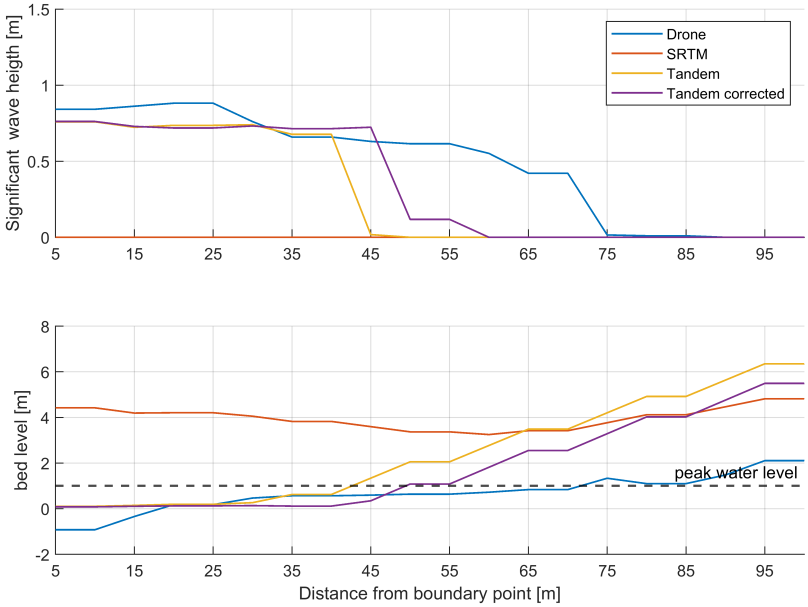

Figure 4.12: Praia Abade cross-shore distribution of the significant wave height (top) and bed elevation (bottom) for different DEMs.

For Praia Abade, also the bed elevation of SRTM is plotted (Figure 4.12), in order to show the large overestimation and the consequences for the computed significant wave height. Generally, the drone elevation is much lower than the others, but we can already see the improvement of correcting TanDEM, both for the bed elevation and the significant wave height. This alone proves the drastic consequences of using data collected on a global scale, with low quality, for CFR assessments.

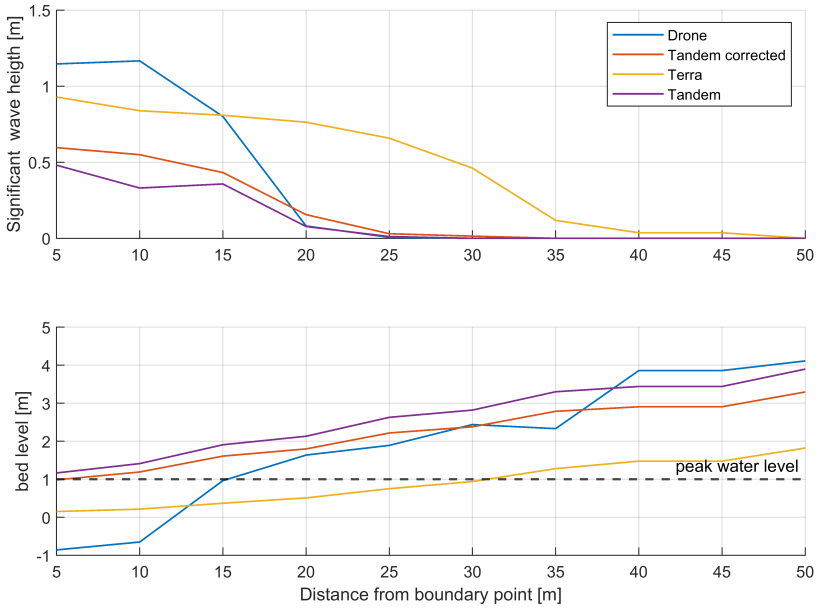

Figure 4.13: Pantufo cross-shore distribution of the significant wave height (top) and bed elevation (bottom) for different DEMs.

In Pantufo, the reason why TerraSAR-X yields larger damages is clearly noticeable in the graph (Figure 4.13, yellow line), where the bed elevation stays lower than the other DEMs further inland. Also the improvement made by correcting the TanDEM DEM is visible. Indeed, the modeled bed elevation (red line) is closer to the drone one and the benefits of this improvement are reflected in the simulation of the significant wave height, which more similar to the one computed with the drone-derived topography.

Following this, the results from the simulations with different DEMs, plotted in a similar fashion as for the previous sections, are shown in Figure 4.14. The results with the ASTER, MERIT and SRTM are to show how modeling the topography using these DEMs produces the most significant error. These DEMs significantly over estimate the elevation for the two communities, resulting in no flooding (See Appendix C). In the comparison the results using the drone DEM with a 1m resolution is considered as ground-truth and the other simulations are referenced to them.

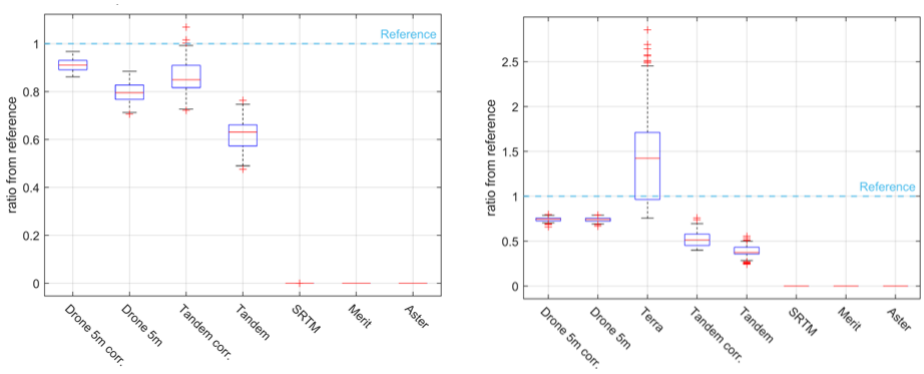

Figure 4.14: DEMs sensitivity for Praia Abade (left) and Pantufo (right).

For Pantufo (right panel), Terra-SarX DEM gives the largest computed damages (more than 2.5 times larger than when using the reference DEM) and with a significantly wide spread in the results, if compared to the other DEMs. The other DEMs have a much narrower spread of results, with TanDEM giving the largest mean error from the reference run (approximately 60%). Correcting for building and trees does improve the results for TanDEM, with a decrease of the median error of 10%. As it could have been expected, the simulations with the drone at 5m give the best median error of approximately 25%, but not much improvement is gained when the Drone is corrected for buildings and canopies. Moreover, the simulations with the drone give the smallest range in the output, with a very narrow interval of results.
Similar results can be found for Praia Abade (left panel). Again, SRTM, MERIT and ASTER give totally unrealistic results and compute no damages, highlighting the negative consequences of using such models for coastal flood risk assessments, where they could heavily underestimate flooding. Furthermore, even in this location we notice an improvement in the prediction if we correct the TanDEM DEM. Indeed, the median error changes from 35% without the correction to 15%, with the correction. Praia Abade is more sensitive to the removal of spurious points in the drone DEM than Pantufo. In fact, the median error improves of 10%, if simulations are made with the corrected drone. Moreover, both batches of simulations with the drone have a smaller spread in the very likely range of results than with TanDEM. The very likely range of results with TanDEM is more than twice as large than with the corrected Drone DEM (0.71 - 1.05 compared to 0.86 - 0.98). The range of results is smaller in Praia Abade than in Pantufo. This is due to the fact that TerraSAR-X, which has a lower elevation than the Drone-DEM, was not available for Praia Abade.

4.3.5. DDF SENSITIVITY

In this section the sensitivity to the different damage functions is investigated. An important remark is that in this case only the damages to buildings were used for comparison,

since the damages to boats were computed using the same damage curve for all the scenarios, introduced in Section 3.5.4.

The sensitivity to DDF for the community of Praia Abade (Figure 4.15) shows much variety between the various curves. American Samoa, Tsunami and JRC have a small spread of results although the reasons for such behaviour are different. American Samoa and Tsunami have a milder slope, therefore are less sensitive to changes in water depths (see Section 2.7), whereas JRC is a curve with a very similar shape to the reference and thus when compared, the results have small variations. American Samoa and Tsunami curves substantially underestimate the damages, with a very likely range of computed damages that is approximately 75% smaller than reference. The curve Sint Maarten gives the largest spread and highest damages (265% increase of the median damage and), due to its very steep slope and to the fact that it represents weaker buildings, where the maximum damages are already reached around a water depth of 2m. It is worth noticing that the DASM curve performs better than American Samoa, despite the fact that the former is derived for riverine flooding in the Netherlands and the latter for coastal flooding in a Pacific Island, thus with more similar environmental conditions and type of hazard to this case study. Finally, the curve used for coastal flooding in the city of Lisbon is among the most accurate to reproduce similar results to the reference scenarios, with a median error of approximately 25%.

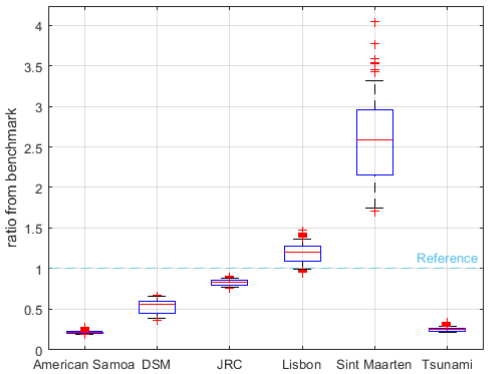

Figure 4.15: Sensitivity to DDFs for Praia Abade.

If we analyse the results for Pantufo (Figure 4.16) we can identify very similar trends to Praia Abade. One of the main difference with the other location is that the maximum ratio from the reference run reaches a value of approximately 3.25 (325% increase in the computed damages), with Sint Maarten curve, compared to a value of 4 in Praia Abade. Even in this location we can notice that American Samoa and Tsunami both yield to the largest underestimation of the damages, with a median ratio to the reference scenario of approximately 0.25, (4 times smaller). A shared result from both locations is that generally a milder curve results in a smaller spread of results (American Samoa, Tsunami) compared to steeper curves (Lisbon or Sint Maarten). In general, very similar results are

found between the two communities.

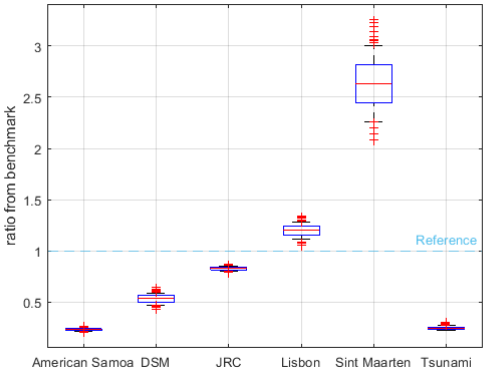

Figure 4.16: Sensitivity to DDFs for Pantufo.

4.3.6. OVERALL COMPARISON FOR CURRENT SCENARIO

We will now compare the possible ranges of results that each input gives in the global analysis, showed in Figure 4.17. Here all the results given from the different values were grouped for each input. This allows us to directly compare the inputs and to identify the most sensitive ones. The results are first shown for the two locations (Figure 4.17), and then combined in a single graph (Figure 4.18).

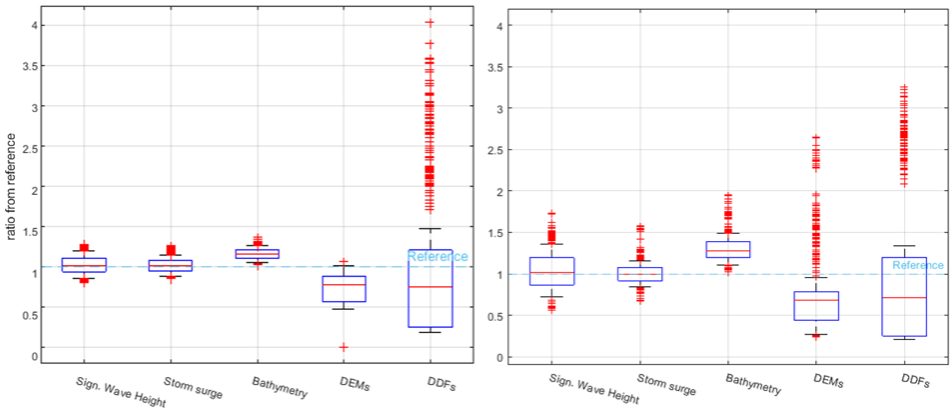

Figure 4.17: Sensitivity to the different inputs for Praia Abade (left) and Pantufo (right).

In the following figure 4.17, the inputs are compared for the two locations. Pantufo has a wider spread of results for the hydrodynamic components and the bathymetry, as already illustrated. Nevertheless, the contrast between the two locations is found mainly for DEMs, with Praia Abade having a smaller range of uncertainty. It is important to know that these results do not include the simulation with all the publicly available DEMs

which computed zero damages. On the other hand the DDF input shows a larger difference in results for Abade, reaching values of computed damages up to 4 times larger than the reference simulation. The lower and higher tails in Pantufo suggest the presence of certain thresholds that are exceed, as the community becomes suddenly more flooded. Although some differences are present, a common pattern of smaller uncertainty in the hydrodynamic and bathymetry inputs and larger uncertainty in the damage curves can be recognised for both locations. This becomes even clearer when the results of the two locations are merged together, as illustrated in Figure 4.18. The box plot of DEM in the plot reaches 0 as this time it includes the simulations of SRTM, ASTER and MERIT.

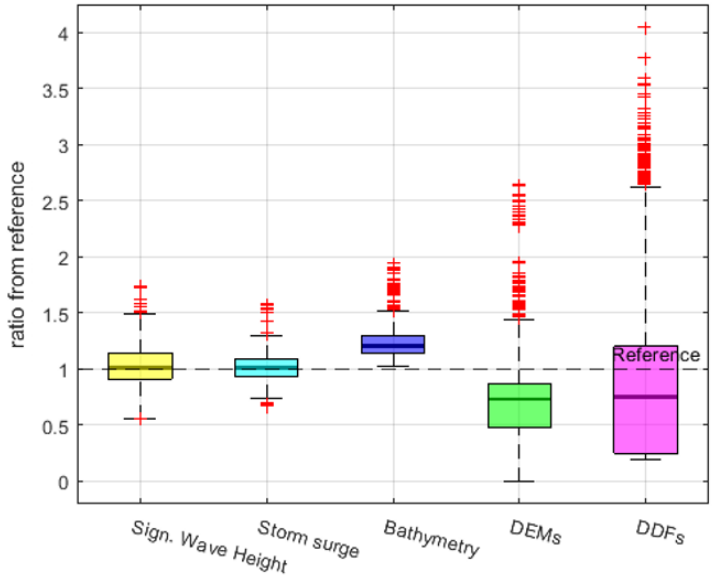

Figure 4.18: Overall inputs sensitivity.

4.4. RESULTS FOR FUTURE SCENARIOS

For the future time horizons, the complete batch of simulations combining all the seven inputs and their respective values was run. Although resulting in a large amount of computational time, this was considered necessary to apply the same methodology for all the possible scenarios.

As it was previously mentioned in Section 3.6, for future scenarios, not only climate change induced sea level rise was included, but also socioeconomic changes and their inherent uncertainty. The importance of including socioeconomic changes comes from the assumption that asset value and numbers will most likely change in future years. The assets value were then increased, using GDP and population growth factors as a proxy (see Section 3.6). In Figure 4.19 we show the computed damages for the different time horizons considered, always for the 100 year event. The results are divided using three possible flood risk assessments: including only climate change, including only socioeconomic changes and including both climate and socioeconomic changes to estimate

future damages. For this comparison, the sea level rise value and SSP scenario used to compute the damages are the reference ones (see Section 3.7).

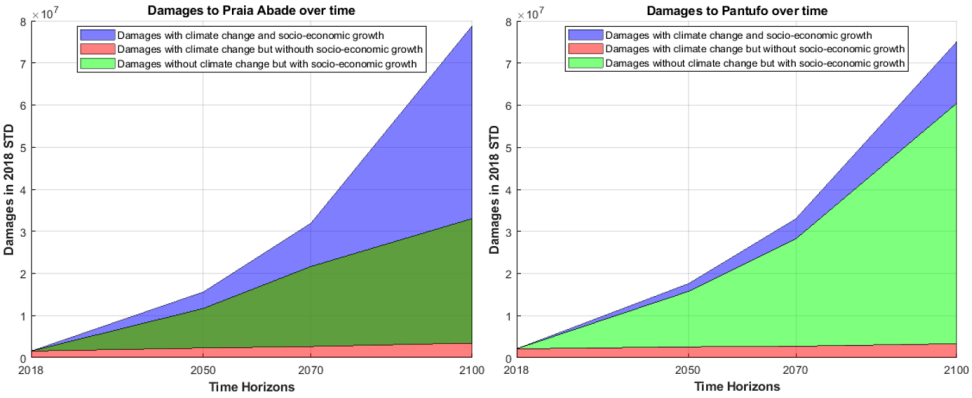

Figure 4.19: Damages to Praia Abade (left) and Pantufo (right) over time, differentiated by contributing factors.

For both locations, including only climate change (red in the figure) yields to a significant underestimation of possible future damages. For the different horizons, including only socioeconomic changes can already have a large impact on the computed damages. For Praia Abade and Pantufo, the damages increase of a factor 10 and 11 respectively for the year 2050 and of a factor 50 and 35 for the year 2100, when both changes are included. The results are summarised in Table 4.2 below, with damages expressed in the local currency. The largest damages are obviously estimated when both socioeconomic and climate changes are included in the analysis. Differently from Pantufo, Praia Abade seems to be more sensitive to climate changes, since the damages computed when both socioeconomic and climatic changes are combined differ substantially from when only the socioeconomic changes are considered.

Table 4.2: Computed EAD in local currency for the three possible scenarios

	Time Horizon	Scenario 1	Scenario 2	Scenario 3
Praia Abade	current	15,680	15,680	15,680
	2050	116,700	2,3020	156,010
	2070	216,400	26,490	319,410
	2100	330,240	3,4850	788,440
Pantufo	current	21,170	21,170	21,170
	2050	25,960	157,540	176,090
	2070	27,350	282,120	330,160
	2100	33,160	604,640	751,020

The effect of combined physical forcing and economic variations on future risk estimates can also be seen in Figure 4.20, where for the two locations, the damages distributions are plotted with semi-logarithmic axes, In the same manner as for the previous

graph, the 50th percentile value for sea level rise under RCP 8.5 and the reference SSP 3 scenario are used to compute the damages. Both for Pantufo (left) and for Praia Abade (right), the distribution of damages is similar, although the median value of estimated damages increases exponentially. The red dots highlight the position of the reference simulations results for each time horizon.

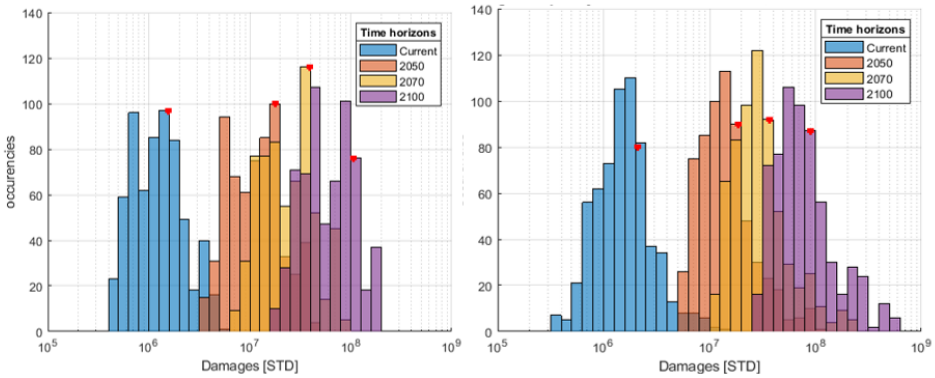

Figure 4.20: Total damages distributions for Praia Abade (left) and Pantufo (right) for different time horizons.

4.4.1. GLOBAL SENSITIVITY FOR FUTURE CONDITIONS

In this section, we show how the different input's global sensitivities change through the four time horizons. For the simulations of future time horizons, the results from SRTM, MERIT and ASTER are not included. The results of Pantufo and Praia Abade are combined in the following analysis. It was decided to include the uncertainty coming from sea level rise by including only the range of values using the 5th,50th and 95th predicted values for the 8.5 RCP scenario. Moreover, the 5th percentiles of RCP 8.5 are very close to the 50th percentiles of RCP 4.5. Therefore it can be said that the included values also take into account the highest 50% of predictions under RCP 4.5 (see Section 3.6.2. For comparison, the spread of results obtained by applying the values for one scenario or the other is shown in Figure 4.21, for the year 2070, where it can be seen that the uncertainty using RCP 8.5 is more considerable than when RCP 4.5 is used.

In Figure 4.22 we can see how the inputs global influence on the model outputs changes with increasing climate change and socioeconomic changes. First, we can notice how the spread of results from the hydrodynamic (H_s and Storm surge), as well as from the bathymetry slightly decreases in magnitude and we find results with a narrower range. Moreover, we can also identify that the spread of results from DEM and DDFs have opposing trends. The former one increases, going from 0 to 2.75 in the current time horizon, to a maximum of almost 3.5 in 2100. The latter one reduces, starting with a 0.25-4 range in the current year, to 0.25-3 in 2100. Despite these fluctuations, these two inputs are always among the most impactful on output variability

The influence of using different SSP scenarios stays pretty constant, although it slightly increases through time. This is because the general spread of GDP growth estimated

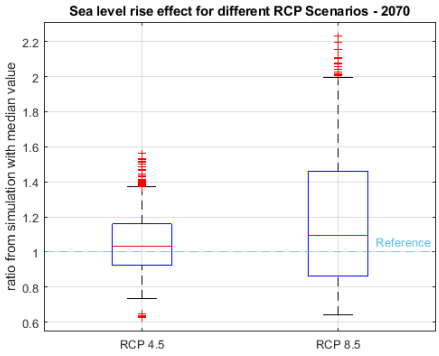

Figure 4.21: Sensitivity to the two RCP scenarios.

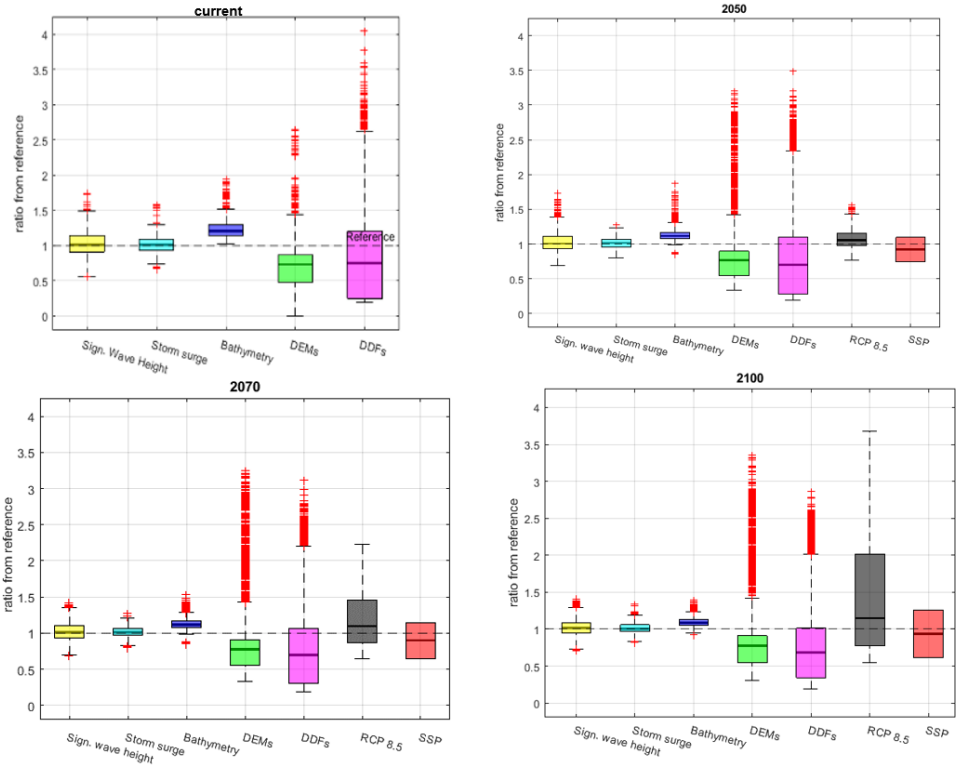

Figure 4.22: Overall input sensitivity through time.

by the different scenarios grows wider for more distant time horizons, which is being reflected in the results. Therefore, although the relevance of including socioeconomic changes is extremely important as highlighted in the previous section, it seems that choosing one or another scenario yields to a maximum difference of results of roughly a factor 2 (the lower limit of SSP box is 0.6 and the upper limit is 1.25). This indicates that the uncertainty coming from different SSP scenario is smaller than that coming from other inputs like DEMs or SLR. This limited uncertainty is partially due to the limited knowledge available on socioeconomic developments and their implementation in risk analyses. If we consider RCP 8.5, we can clearly see how the likely range of the results becomes more significant with time. This had to be expected, as it reproduced the uncertainty coming from the very likely range of sea level rise predictions, which does increase in magnitude and width as the time horizon increases (see Section 3.6). Indeed, the spread of results from applying different sea level rise predictions for the RCP 8.5 scenario undergoes the largest change among the 4 time horizons compared to the other inputs. For the year 2100, sea level rise predictions are, together with DEMs and DDFs, the most influencing inputs for the risk estimate.

4.4.2. LOCAL SENSITIVITY OF THE INPUTS

Another way to test the influence of the different inputs is to look at their local sensitivity. For this type of analysis, only the impact of varying one input on the results of the reference simulation are investigated, which means that all the other possible simulations are discarded (see Section 3.7.1).

Figure 4.23 shows the relative contribution of each input to uncertainty in the estimated EAD. The results are presented for all the 4 time horizons and separated for the two communities of Pantufo (blue in the figure) and Praia Abade (red in the figure). This graph allows us to look at the local sensitivity of each variable. The hydrodynamic components, together with the bathymetry, have always the smallest impact on the model outputs, throughout all the time horizons. In particular, their range of change on the EAD stays always well below 30%. Furthermore, their relative weight compared to the other variable also diminishes with time. The results for the DEMs and DDFs vary more between one community and the other. For Pantufo, the DEM always has a larger impact than the damage curves and the difference between the two inputs increases with time, with the DEM continuing to have a larger impact. Exactly the opposite happens in Abade, where the DDFs have a larger impact on the damages, although their impact stays almost constant for the four time horizons. The different impact that the choice of DEM has on the two communities can partially be explained by the availability of the TerraSAR-X only for Pantufo. TerraSAR-X is the dataset estimating the lowest elevation in Pantufo, at least in the proximity of the coastline (see Figure 4.13). The same dataset is not available for Praia Abade, where the lowest DEM is the drone-derived one (see Figure 4.12). The fact that the sensitivity to DDF grows in Pantufo and not in Praia Abade can be found in the fact that the water depths computed for more distant time horizons in Praia Abade are within a range to which the DDFs are less sensitive.

Worth noting is the growing importance of the SSP and RCP 8.5 for both communi-

ties. Especially RCP 8.5 relative weight grows faster through time, particularly in Pantufo. A possible explanation of the faster rate of growth of the importance of this parameter in Pantufo is that, exceeded a certain elevation threshold, a large part of the community suddenly becomes prone to flooding. It is likely that the 2m of increase in sea level would expose most of the community. The same pattern is not visible in Praia Abade, potentially due to the fact that the community is already highly exposed to flood risk at much lower water levels and that in the occurrence of an even smaller sea level rise, the community is already almost completely damaged. This finding suggests the presence of thresholds and different risk evolution trends through time for the two locations.

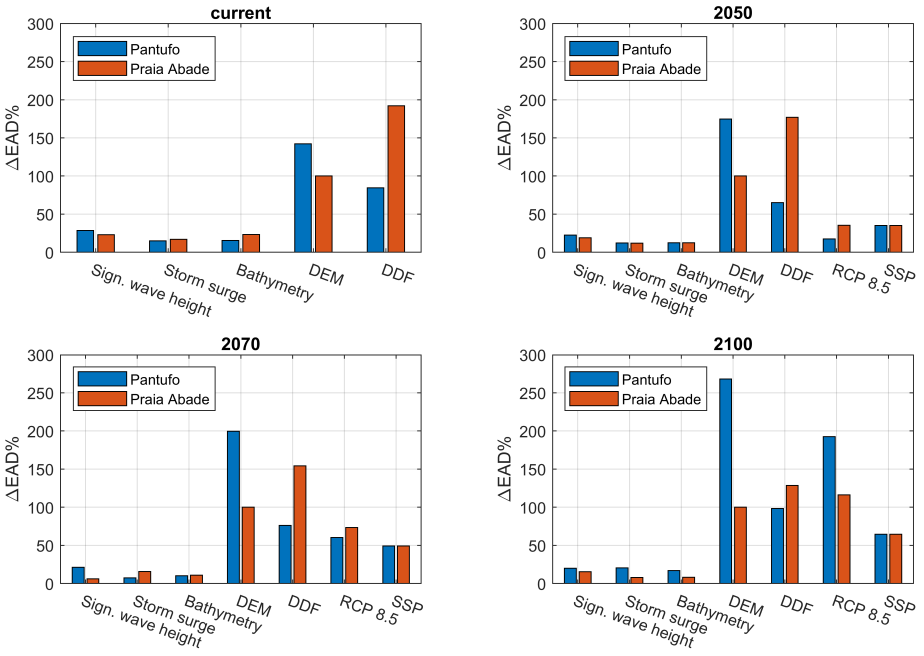

Figure 4.23: Contributions to uncertainty in estimated EAD for the two locations from a local sensitivity.

4.5. SECONDARY TESTS

4.5.1. SENSITIVITY TO FUNCTION SHAPE

The previous results have highlighted the presence of significant uncertainty coming from the damage function and damage analysis. Although, the sensitivity of the model was only tested applying several functions taken from literature. Therefore, it was decided to investigate the damage function uncertainty by adopting a different approach, which could focus more on the possible variation of a single function's shape. The approach is described at the end of Section 3.5.4.

The methodology investigated thoroughly reproduces the overall spread of results obtained from the simulations with different functions from literature, although the up-

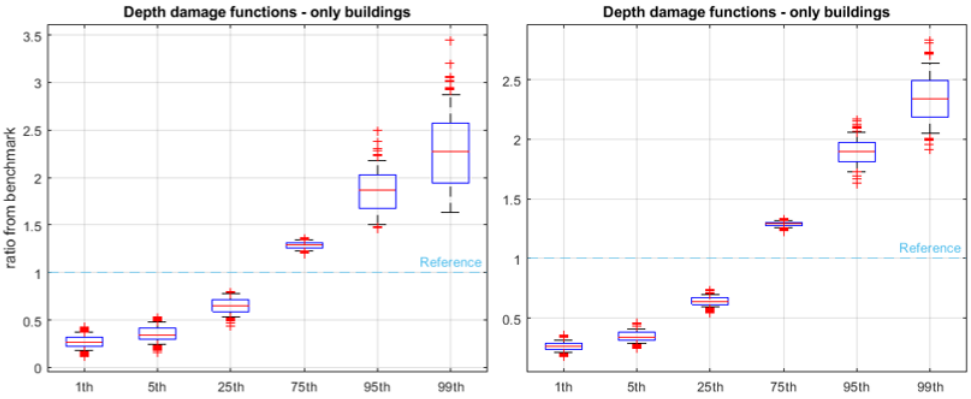

Figure 4.24: Sensitivity to function shape for Praia Abaḍe (left) and Pantufo (right).

per limit of the range of values is slightly smaller. This is because the highest value of damages for the other DDF analysis come from the Sint Maarten curve, which already computes maximum damage at approximately 2m water depth, whereas the curves in this analysis only compute maximum damages at a depth of 3.25 m.

4.5.2. SENSITIVITY TO GRID RESOLUTION FOR SFINCS

The DEM seems to play an essential role on the output for our flood risk analysis. To further investigate the effect of different resolutions, for both the communities we created a set of DEMs using the same data from the drone. According to (Leijnse, 2018), the necessary grid resolution to reach a good level of accuracy in predicting the $R_{2\%}$ is also a function of the slope, with steeper slopes requiring smaller grid resolution. On coasts with high incident wave presence a higher grid resolution is therefore recommended.
The resolutions are tested under 9 hydrodynamic conditions, combining the three values for H_s and the three values for storm surge (see Section 4.1). The different DEM cell sizes in our analysis are shown in Table 4.3, together with the number of computational grid cells required, for the two communities.

An higher computational grid resolution results in larger computational time. This is clearly visible in Figure 4.25 where the computational times are plotted in a logarithmic scale with reference to the run of 0.5m resolution, with longest run time. The run time and number of grid cells exponentially increase.

The maps in Figure 4.26 and 4.27 below compare the extents of flooding measured, for Praia Abade. The red map represent the simulation with decreasing resolution (from 1 to 30m), whereas, in all the panels, the blue area below represents the computed flooding extent from the 0.5m resolution simulation. For both figures, the top left panel always shows the comparison with the 1m resolution. The difference in colour intensity for the red maps qualitatively indicates the flooding depths. The darkest red represent water depths higher than 1m.

In Praia Abade, as the cell size increases, the flooding extent reduces. Particularly

Table 4.3: Drone resolutions, required grid cells and average run times for the two locations

	Pantufo		Praia Abade	
Resolution	**Average run time [s]**	**grid cells**	**Average run time [s]**	**grid cells**
0.5	8,254.5	812,528	4,674.6	371,560
1	596.3	211,667	301.3	93,264
2	77.5	51,194	56.9	23,505
5	4.6	8,680	3.0	3,851
10	1.4	2,137	0.8	1,003
15	0.9	971	0.4	462
20	0.5	562	0.3	263
30	0.2	259	0.1	128

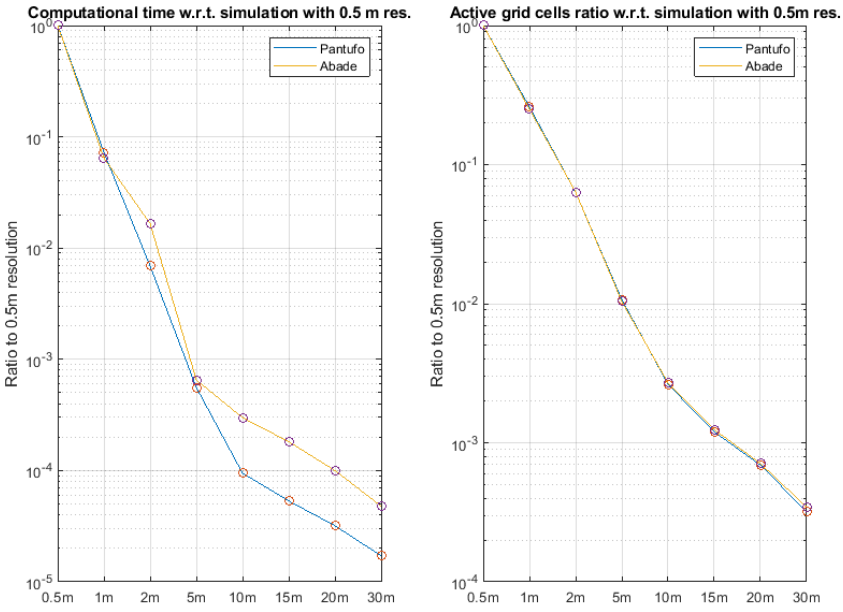

Figure 4.25: Computational time (left) and grid cells number (right) with varying cell size.

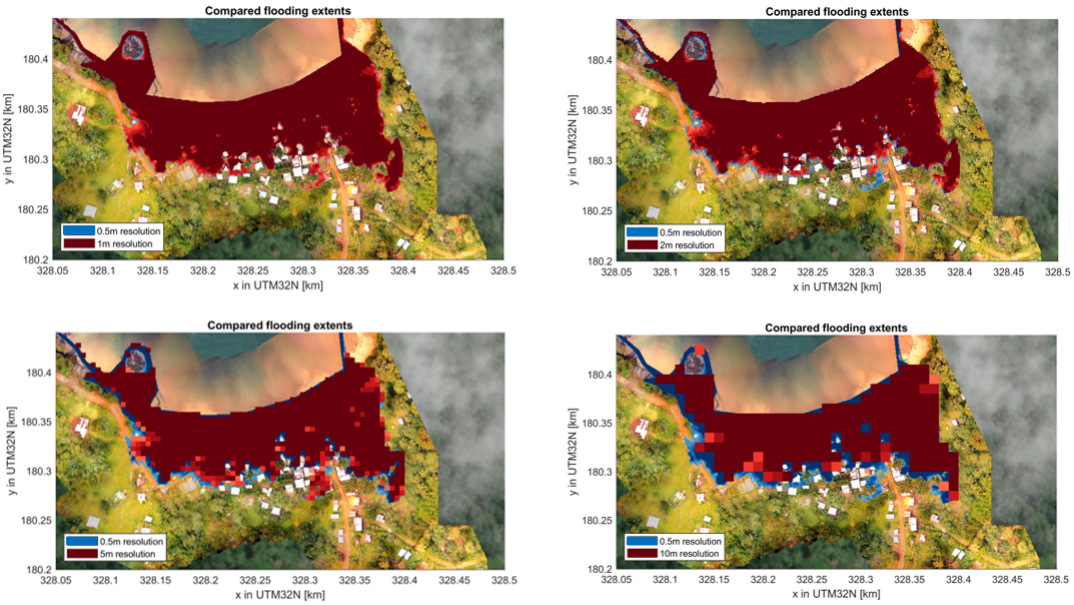

Figure 4.26: Comparison of flooding extents for different resolutions in Praia Abade (1).

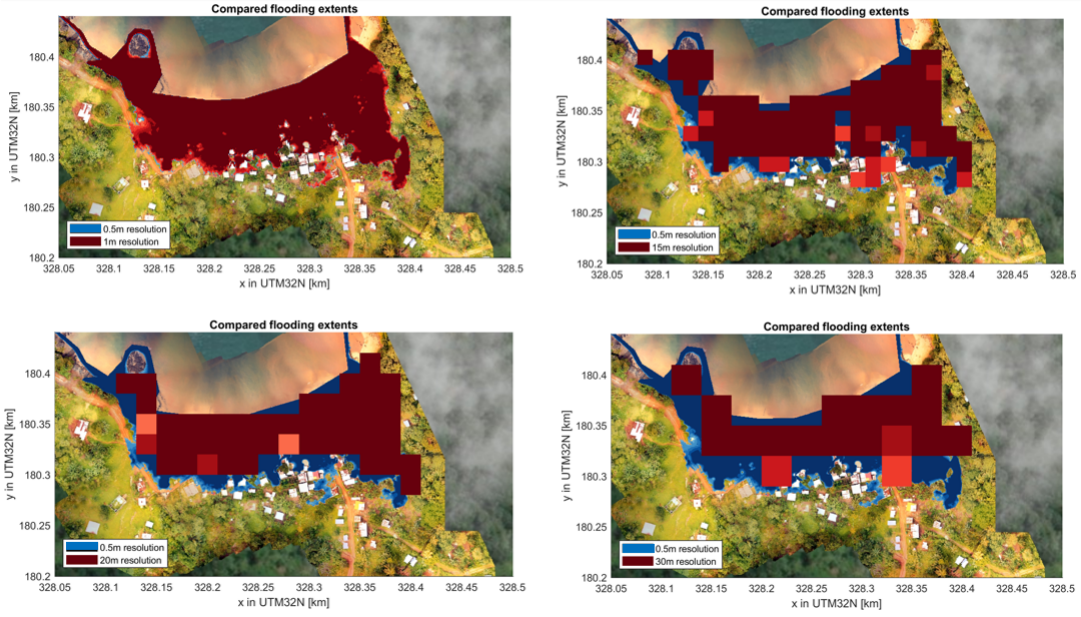

Figure 4.27: Comparison of flooding extents for different resolutions in Praia Abade (2).

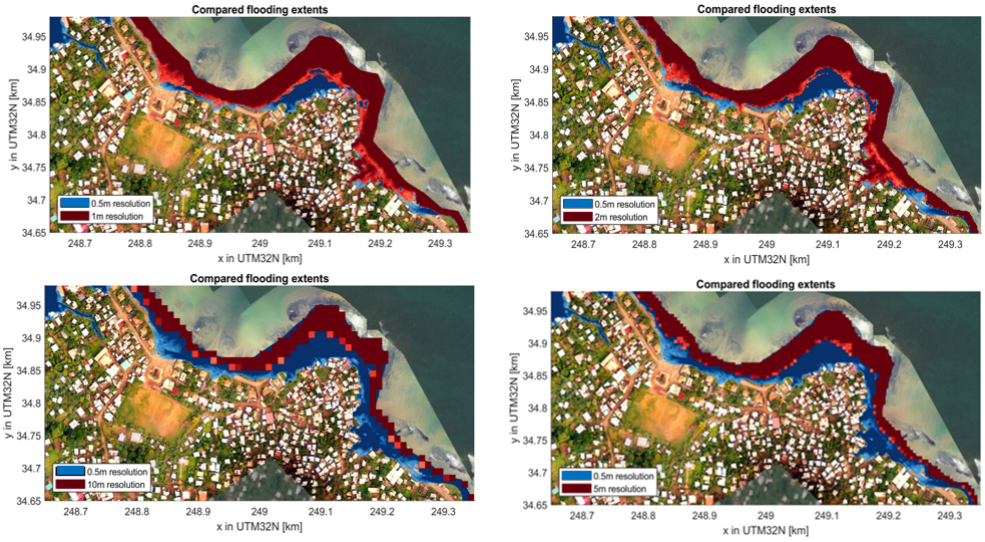

Figure 4.28: Comparison of flooding extents for different resolutions in Pantufo (1).

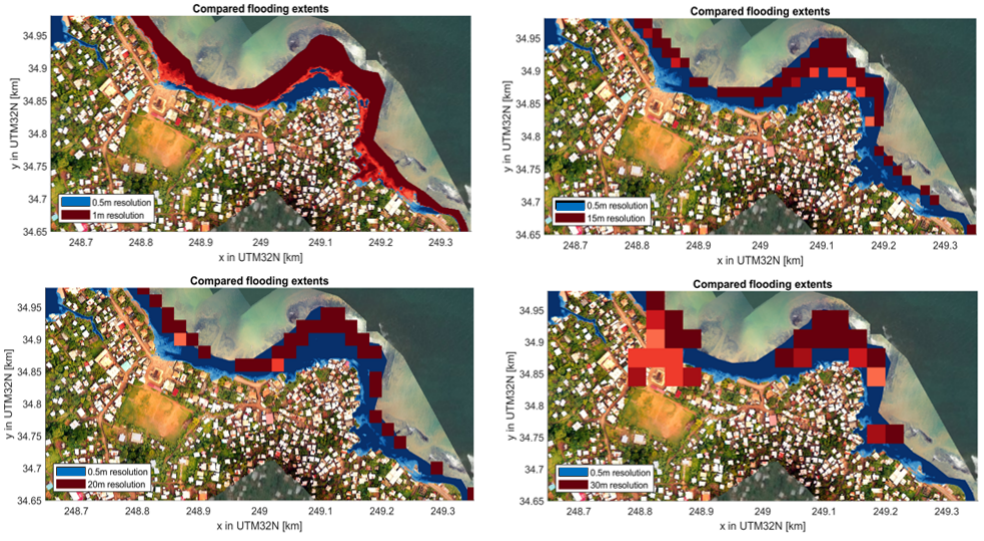

Figure 4.29: Comparison of flooding extents for different resolutions in Pantufo (2).

we can see a substantial decrease in accuracy as we move to a resolution of 5 and 10 m. In Pantufo we find already large differences with the results using a 1m resolution. Indeed, a part of the headland that is flooded using the 0.5m resolution, is not captured by the other resolutions. In Pantufo (Figure 4.28 and 4.29, some issues where found at the boundary of the drone DEMs due to the merging with the other DEM TerraSAR-X, as previously mentioned. These issues are significant for the resolution at 0.5m where on the top left boundary, a stream of water is computed which comes from grid cells that have a lower elevation from the TerraSAR-X DEM. For this location, already a much smaller flooding extent is computed with a resolution of 1m. Further decreasing the resolution reduces the flooding extent. Although Some anomalies are found when a resolution of 30m is used (bottom right panel in Figure 4.29)

By multiplying the averaged water depth between all wet cells and the total area flooded, given as results from the model, it was possible to measure the volume of inland flooding from the coastline position. For each flood volume, the error to the reference resolution was computed. Since the comparison was made, for each resolution, on a total of 9 simulations, it was also possible to estimate the mean of the errors, as well as the maximum and minimum errors.

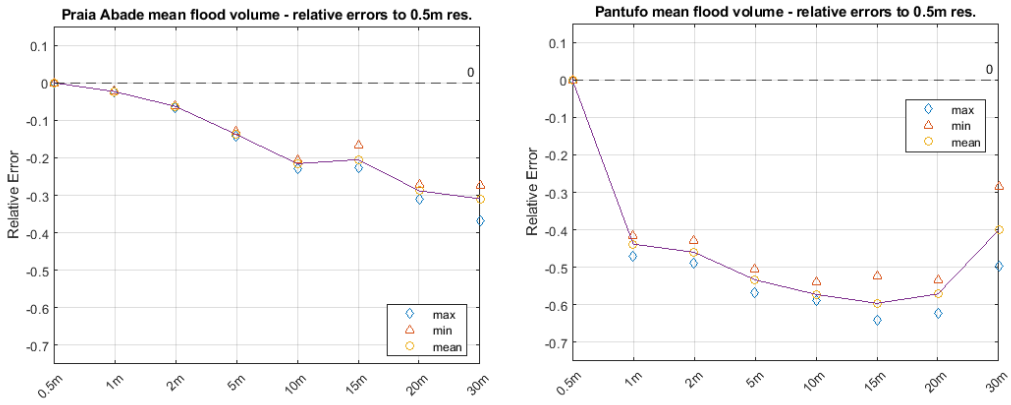

Figure 4.30: Computed flood volume errors from the reference simulation, for Praia Abade (left) and Pantufo (right).

Figure 4.30 shows the relative errors in the computed flood volume. The fact that we only have negative numbers tells us that all the other resolutions underestimate flooding volumes. For Praia Abade (left of the figure) we see a decreasing accuracy in reproducing the flooding extent as we increase cell size. The simulations with 1 and 2m resolution still achieve a good level of accuracy in modeling the flooding volume to the reference case, with a mean error well below 10%. The mean relative error increases up to 20% with a resolution of 10 and 15m, as well as the range of results, since for the 15m resolution we have a min and a max relative error of 16% and 23%, respectively. The mean error and the difference between min and max are most significant for the largest resolution of 30m. The model becomes therefore more sensitive under to the hydrodynamic forcing at larger resolutions.

In the location of Pantufo we find partially different results. As the plots in Figure 4.28 and 4.29 already showed us, we have a considerable underestimation of the flooding when using a resolution larger than 0.5m. Indeed, for this location, already a resolution of 1 m gives a mean error of 45%. It has been said already that part of the flooding computed by the 0.5m simulation, close to the north-western boundary, is indeed unrealistic and arises from the merging with the TerraSAR-X DEM. At the same time, much of the discrepancy in the results come from the area flooded on the headland. From a resolution of 1 m to one of 20m, We see a similar trend to Praia Abade, where the flooding volume mean errors increase together with the spread between the min and max errors. Surprisingly, the 30 m resolution gives the best mean estimate of the volume, although its spread of errors is the largest of all, indicating that the model with that resolution is much more sensitive to variations in wave height and storm surge.

In this Chapter the results of the analysis have been presented. Next chapter 5 contains the discussion and the findings that arose from these results.

5

DISCUSSION

CHAPTER SUMMARY

First, an overview of the methodology is given comparing it with other studies, focusing on its advantages and disadvantages. This section also includes a review of the most important assumptions of our approach, highlighted to understand the limits of our findings. The uncertainty in the inputs considered and their impacts on the predicted risk are assessed for both the current and future time horizons, in Section 5.2. In the same section, also the implications of a local and global analysis and multiple inputs uncertainty interaction are highlighted. We then stress the importance of Digital Elevation Models and damage modeling for accurate and reliable risk assessments. Finally, some implications for risk management, regarding the collection of input data and the communication of model results, are given in Section 5.5. Some pathways where future research efforts could be directed to are suggested in the last section.

5.1. OVERVIEW OF THE METHODOLOGY

The results of the analysis allow for the quantification of uncertainty from multiple sources: (i) the offshore water levels, (ii) the significant wave height of the storm, (iii) the local bathymetry data, (iv) the Digital Elevation model applied to represent the topography, (v) the damage curve used to compute buildings damages, (vi) future sea level rise predictions and the choice of (vii) the Shared Socioeconomic Pathway selected to estimate future growth of assets value. The selection of the inputs was based both on literature review (see Chapter 2), which helped to identify the most significant uncertainty sources highlighted by previous studies, and on preliminary sensitivity tests (see Appendix A and B), which provided a quantitative comparison used to rule out the least sensitive inputs. In Section 4.3 we followed a similar approach to (Vousdoukas et al., 2018a), where the different uncertainty factors are assessed separately. Some points of novelty of this research include the assessment of uncertainty propagation from input data for all the steps of a flood risk analysis. In coastal studies, this has previously been done by (De Moel et al., 2012) and (Vousdoukas et al., 2018a), although their studies focused on a larger spatial scale, which did not allow for the use of highly complex hydrodynamic models like XBeach. Focusing on a smaller scale, we were able to test our inputs using models that include a substantial number of physical processes. Furthermore, we applied this method to a SIDS, a developing country typically characterised by the paucity of local data. Our methodology is the result of combining different needs such as project time, computational expenses of the models, including a sufficient range of values for each input and having a considerable number of simulations to be able to assess the sensitivity and uncertainty of the model outputs. This methodology has proven to be relatively fast to set up and to include new inputs or values. The speed of the methodology comes at the expense of its complexity. Many uncertainty analyses are conducted using a fully probabilistic framework, where each input is fit to a probability distribution and different values are sampled and tested in the model. The advantage of such methodology is that it allows to compute the covariances of the inputs, from which global sensitivity indices that quantify inputs contribution can be derived (Sobol, 2001), (Saltelli et al., 2008). Nevertheless, we are confident that the presented method could be integrated into a probabilistic framework to improve both its computational effort and applicability of its findings, as previously done in similar studies (De Moel et al., 2012), (Wagenaar et al., 2016). This could be achieved by fitting probability distributions to the different inputs. A possible approach is described in Section 5.6.1.

5.1.1. LIMITATIONS OF THE STUDY

The current research is focused on a case study and carried out within a short timeline. Therefore as a consequence of the many assumptions made in the process of developing this study, its findings and results may not apply directly elsewhere. Before drawing conclusions is important to mention the most important underlying assumptions and limitations inherent to the study, which are listed below:

1. **Focused on a case study**
   The findings of this analysis may largely differ from another site. Specific spatial

characteristics of the area of interest could be substantially different on another SIDS, such as the low-lying coral atolls of Kiribati. The geographical differences would most likely affect the estimated damages even under similar external forcing conditions. The high sensitivity of the analysis to the location of interest is already visible when comparing the results for the two communities of São Tomé and Príncipe, which are not identical.

2. **A simplistic storm is modeled**
   The modeled storms represent the peak 6 hours of a 24 hours storm, with a Gaussian distributed storm surge. If all the storm length was to be modeled, or with a different distribution, the computed hazards may have differed.
3. **1-D wave transformation model**
   The wave transformation model (XBeach) is in a 1-D domain, thus excluding 2-D phenomena, and assuming that waves are coming at a shore-normal angle. Processes like edge waves and long-shore currents are not considered. Moreover, we are only considering remotely generated swell waves and not locally generated wind waves. Other hydrodynamic processes, such as meteotsunamis are also discarded.
4. **Assumed hydrodynamic long shore uniformity**
   Water levels from XBeach are interpolated to the whole 2-D offshore boundary of SFINCS, thus assuming alongshore uniformity in the water levels. Although this choice was based on the results illustrated in Appendix A, a more accurate assessment would include multiple transects from XBeach for each location, or a full 2-D model grid.
5. **Little hydrodynamic variability**
   We acknowledge that the hydrodynamic variability, both for the significant wave height and storm surge is somewhat small if compared to other coastal areas of the world. Indeed, the extreme events modeled have a rather narrow 99% confidence interval of expected values, even for long return period (e.g. 100 year). It can be expected that the local sensitivity of these parameters may well be more substantial for another site. Nevertheless, it is not known precisely how much the increased range of values of these two parameters would affect the other sources of uncertainty considered in this study.
6. **A single type of building considered**
   Only one representative type of building is included in the analysis, using a weighted averaging approach based on the distribution of buildings present. This assumption disregards the spatial distribution of different buildings, which may affect the overall risk. Such assumption would yield to an underestimation of flood damages in the case that the large majority of the more valuable buildings is located in the most hazard-prone area. Nevertheless, this assumption was supported by the heterogeneous spatial distribution of buildings in Pantufo and Praia Abade.
7. **Only direct and tangible damages are included**
   Only direct damages to physical assets are considered, although flood risk includes further types of consequences. The quantification of other damage categories, such as indirect and intangible damages (loss of tourism activities, emergency measures expenses, psychological disturbance, fatalities, etc.) may also be rele-

vant.

8. **Absence of spatial planning for new housing development**
   The spatial distribution of houses built in the future was assumed to be identical to the current one. Since people might relocate in areas with lower flood risk, this assumption could result in an overestimation of the damages. Furthermore, the possibility of exceeding the level of available land for new constructions is not considered, which may have lead to estimating an unrealistic population growth in the communities.
9. **No adoption of safer standards for housing materials**
   Despite the economic growth, we have assumed a constant vulnerability of the assets, which could lead to an overestimation of the damages, since possibly new assets would be constructed in a more flood-resistant manner.
10. **Limited choice of inputs**
    The selection of inputs was not exhaustive and was limited by the project timeline. As an example, the tidal spring-neap cycle and its possible combinations with storm surge are not considered exhaustively, as only the worst case scenario is considered.
11. **Disregarded model uncertainty**
    The analysis does not include model uncertainty, which is embedded in the model chosen and its assumptions. If a different model was applied, the results would have not been identical. Model uncertainty could be tested by comparing the several models under the same conditions.

Addressing the methodology limitations is important to understand the applicability boundaries of our findings. At the same time, it demonstrates the many assumptions and choices that are to be faced when modeling coastal flood risk. Dealing with uncertainty also means to understand the implications of such assumptions and provide decision-makers with more insightful information on the model results.

5.2. UNCERTAINTY IN INPUT DATA

5.2.1. GENERAL FINDINGS

CURRENT TIME HORIZON

From the results presented in the previous chapter, we have identified, for the present time horizon, DDFs and DEMs to be the main source of uncertainty for coastal flood damage estimates. Our findings are largely in accordance with (De Moel et al., 2012), who identified damage curves to represent the critical input for three coastal communities in the Netherlands. (Wagenaar et al., 2016), (De Moel et al., 2014), (Merz et al., 2004) and (Merz and Thieken, 2009) have all highlighted how damage curves and in general damage modeling as one of the main sources for epistemic uncertainty. Although not being the most important for both locations in our study, varying the DDF yielded an average very likely range of results from 0.25 to 1.25 times the reference simulation. The aleatory uncertainty of H_s and storm surge, as well as the epistemic uncertainty of bathymetry data are found to have a smaller influence on the estimated damages uncertainty.

FUTURE TIME HORIZONS

When future temporal changes are included, the results indicate DDFs, DEMs, and SLR predictions as those inputs contributing the most to increase the uncertainty in the model outputs. Nevertheless, this is also because SSP scenarios have a smaller inherent uncertainty, which is not amplified when combined with other inputs. Some inputs impacts on the output change when moving from the current scenario, to future scenarios. SLR undergoes the largest increase, which can also be expected since its 90% confidence interval increases in width through time (see Figure 3.15). The hydrodynamic boundary conditions variables slightly decrease their effect on output uncertainty.
In general, we see an exponential growth of the damages through time, due to the large growth of the asset values under socioeconomic changes. Disregarding socioeconomic changes would lead to under-estimating future risk, hence they should always be implemented in risk analyses. The Figure below 5.1 depicts the relative weights from the global analysis, averaged for the two locations.

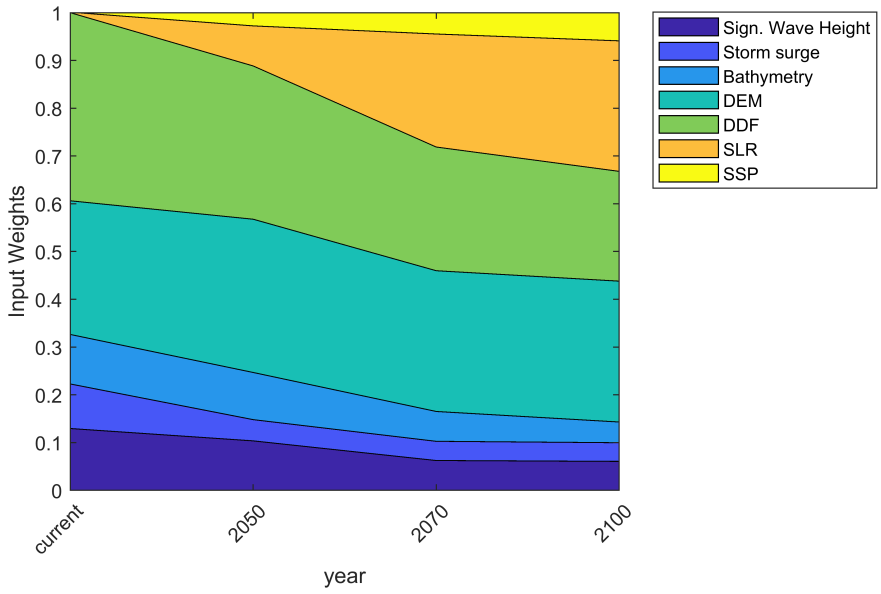

Figure 5.1: Relative weights from the global analysis, averaged for the two locations.

5.2.2. DIFFERENCES BETWEEN LOCAL AND GLOBAL ANALYSIS

The method applied allowed us to conduct a local and a global sensitivity analysis and find preliminary implications of the two. Indeed, if we compare the results of the two analyses we notice some contrasting points. In the following plots, the relative weight of each input is measured for both methods and for all time horizons. The weight of a single input is given by the largest range of damages estimated varying that input.
Figure 5.2, shows the weights for the location of Praia Abade. The weights in the upper pies are from the local sensitivity, the ones at the bottom are from the global analysis.

First, we can notice how the relative importance of the damage curves largely grows for the current time horizon when interactions between input conditions are included increasing from 54 to 61% . This occurs also for bathymetry, significant wave height and storm surge, whereas the relative impact of the DEM decreases and its weight is almost halved when considered globally. This behaviour is also present for the three future conditions, where the relative impact of DEM always decreases, although staying rather considerable. The impact of the hydrodynamics and bathymetry almost doubles in weight for the last time horizon. It is possible that the DEM strongly influences the sensitivity of other inputs, which could be assessed with global sensitivity indices like the method of (Sobol, 2001). Another input that loses weight in the global analysis is the SSP scenario, which has a constant uncertainty range between the two analyses and is not influenced by other inputs (see Section 4.4). Clearly, the uncertainty coming from RCP and SLR grows with time, as the uncertainty in the exact values of these inputs is also larger.

With the Figure 5.3 of Pantufo, we notice similar trends. First of all, the effect of the DEM, as already highlighted in Section 4.3.6, is much larger, but even in this case, its relative importance decreases when inputs uncertainties are considered globally. Moreover the influence of the damage curves seems to increase with time. This could be explained by the increased intensity of the hazard as sea level rise predictions become larger. In the furthest time horizon, a larger part of the city experiences flooding and at larger depths, which ultimately increases the importance of which DDF is chosen for modeling buildings damage. Even in this location we see that the hydrodynamic parameters and bathymetry increase their relative weight in the global analysis.

It can be concluded that, addressing a sensitivity analysis with a local assessment of the inputs may only give an idea of the relative importance of each input. It is shown that, when inputs are considered together, their sensitivity can largely vary. Although this is largely acknowledged in literature (Saltelli et al., 2008), (Uusitalo et al., 2015), (Sobol, 2001), (Loucks and Van Beek, 2017), (de Moel, 2012), often local sensitivity analyses are preferred for their simplicity and computational demand. It is recommended that, if possible, a global sensitivity analysis should always be preferred over a local analysis. The need for global analysis is even strengthened in data-poor environments like SIDS. In a situation with limited resources to collect data and highly uncertain inputs, knowing which input matters the most to improve the quality of the assessment is crucial. An optimal choice can only be based on a global analysis. For example, in the present time horizon, a project manager would invest more efforts in collecting highly accurate DEM data, if his/her choice is based on a local sensitivity (see top left pie, Figure 5.3). However, his/her choice may move towards the improvement of damage modeling, if the choice is based on a global sensitivity (see bottom left pie, Figure 5.3).

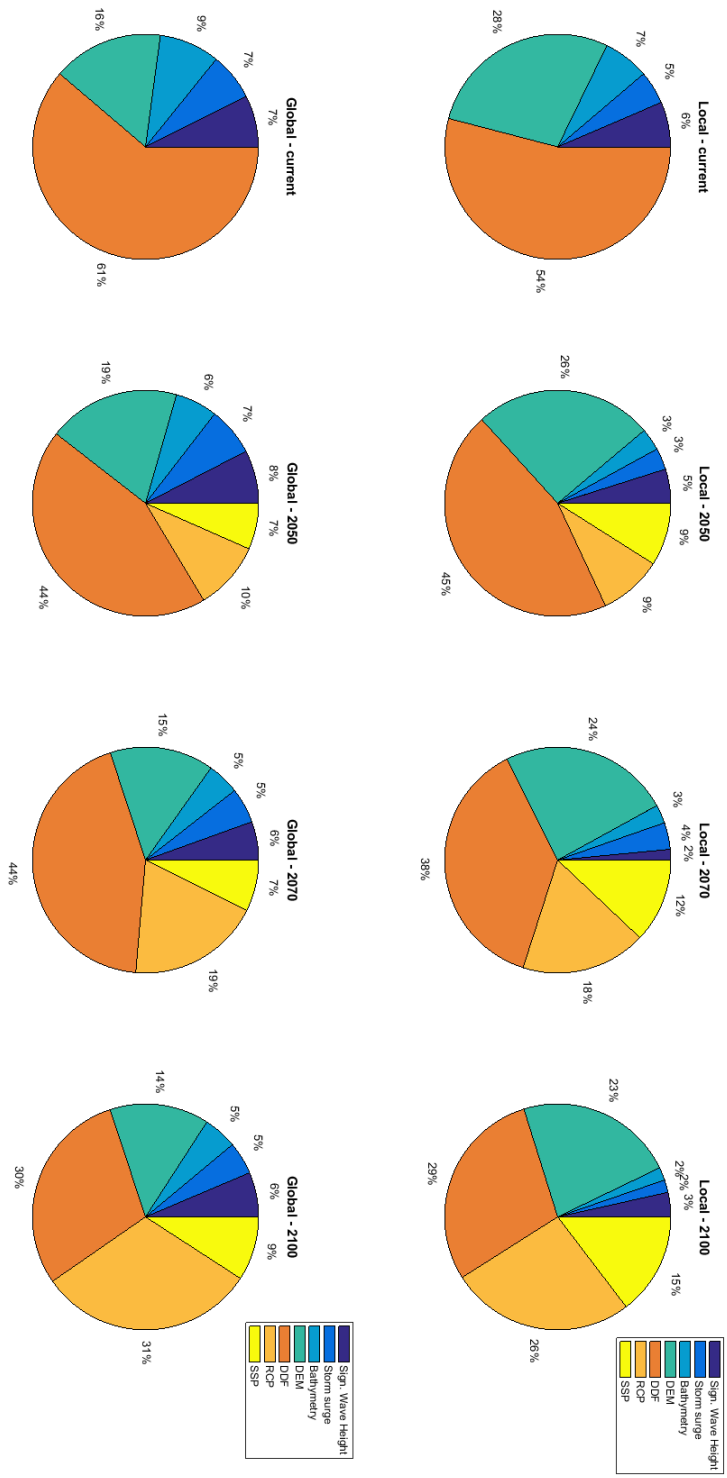

Figure 5.2: Local vs global sensitivity analysis in Praia Abade. The top pies represent the weights for the different input based on a local analysis, whereas the bottom pies are based on a global analysis. The four time horizons are included.

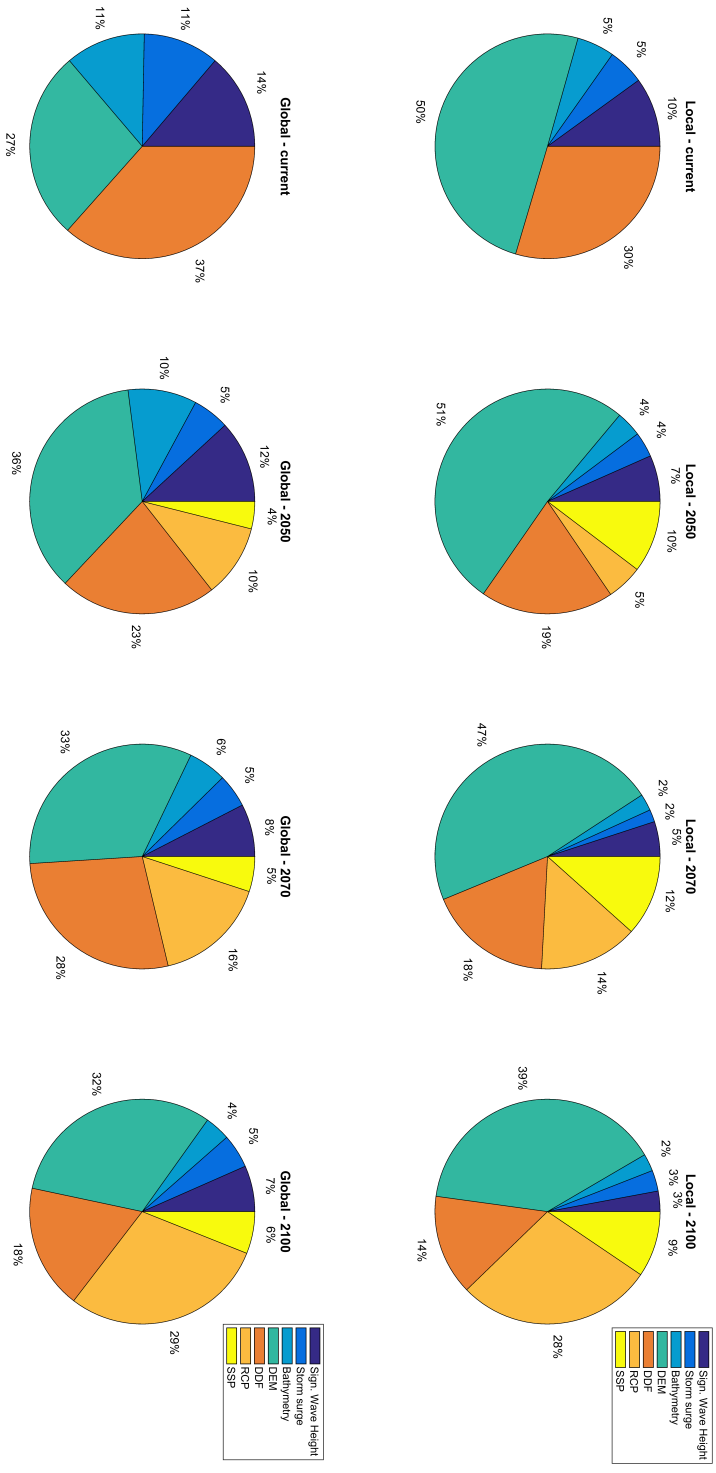

Figure 5.3: Local vs global sensitivity analysis in Pantufo. The top pies represent the weights for the different input based on a local analysis, whereas the bottom pies are based on a global analysis. The four time horizons are included.

5.2.3. INPUTS INTERACTIONS

In this section, we will try to highlight some of the most identifiable inputs interactions in our results. The approach is described in Section 3.7.1 and Figure 3.20. This approach represents a point of originality of our research. Indeed, even though many studies have already focused on global sensitivity analyses for flood risk, not much information was given on inputs influence on each other (de Moel, 2012), (Apel et al., 2004), (Wagenaar et al., 2016). The analysis was assessed for H_s and storm surge, only considering the current time horizon. Since larger sensitivity to these parameters was found in Pantufo, the analysis was applied to this location.

The following Figure 5.4, shows the distribution of results varying the two hydrodynamic parameters, when the bathymetry (left panel), the DEM (right panel) and DDF (bottom panel) inputs are fixed at a specific value. The two boxplots for each x-axis variable are the distributions of H_s (left) and storm surge (right).

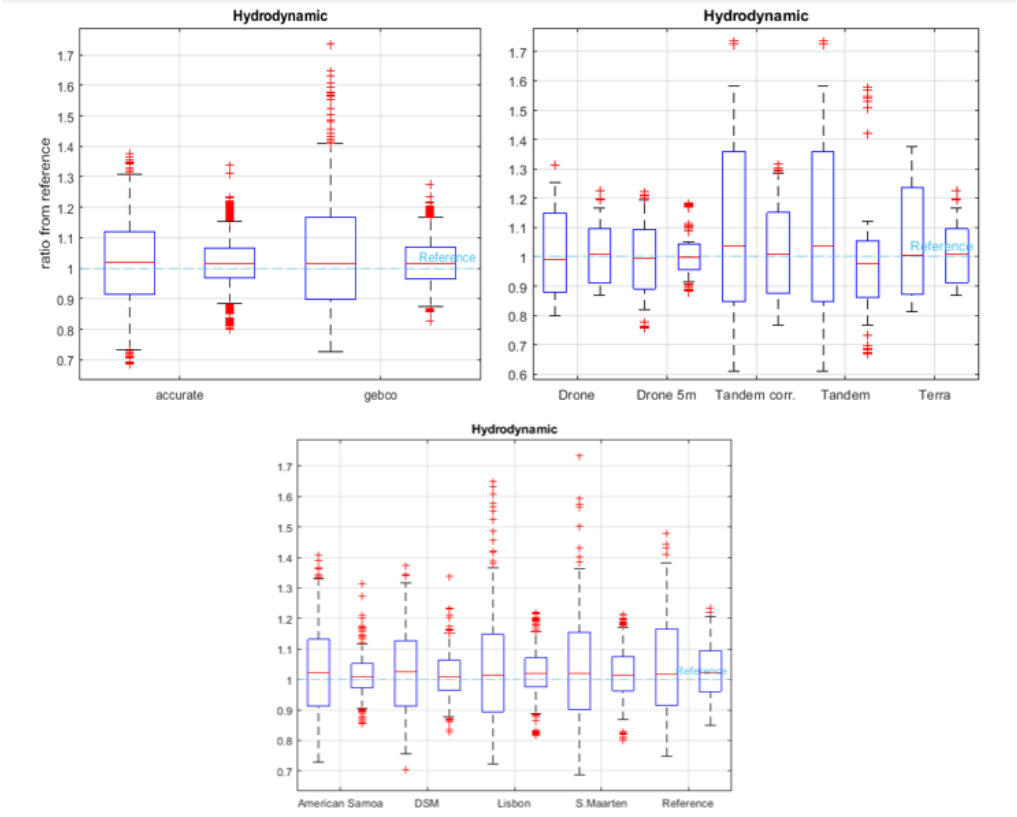

Figure 5.4: inputs influence on each other, in Pantufo. The plots show the spread of results varying H_s and Storm surge level while keeping the inputs bathymetry (top left), DEM (top right) and DDF (bottom) at a specific value. The boxplots for each variable are H_s (left) and storm surge (right).

The spread of results almost doubles for wave height, when the bathymetry from GEBCO is used instead of the accurate dataset (top left panel, first and third boxplots).

GEBCO therefore increases the sensitivity of significant wave height, although the same cannot be said for storm surge level. Furthermore, different DEMs can amplify or diminish the impact of significant wave height and therefore increase or reduce the amount of overall uncertainty. This occurs primarily for the two TanDEM DEMs, which give a very likely range of results from 0.85 to 1.35 for H_s. The corrected version of TANDEM has the most significant influence on storm surge (top right panel, third boxplot from the right). The two drone DEMs give the smallest range of results, around 20% for wave height and 10-20% for the storm surge level. The more substantial influence given from TanDEM may be explained by its lower resolution and subsequent smaller surface variability. With a resolution of 90m, the DEM creates a topography model with tiles of 90 by 90 m^2 where the 5m computational grid cells have the same elevation. Therefore, when water levels exceed a certain threshold, a large part of the community becomes flooded. This suggested threshold exceedance behaviour is further investigated in Section 5.2.4 Regarding the damage curves, the steeper curves amplify the interval of results for H_s, being more sensitive to changes in water depths. Indeed, a higher significant wave height results in a higher water level setup at the coastline. This occurs for the curves Specific, Lisbon and Sint Maarten. Somewhat surprisingly, this does not occur much similarly for storm surge level, where the results are not influenced significantly by the choice of damage curves. This may suggest that water level variations yield smaller variations in flood depths, if compared to H_s.

These results show us how one input can largely influence the impact of another, H_s in this case. Regarding the bathymetry and DEM choice, is important to highlight that the most considerable differences are given by the publicly available, low-resolution (GEBCO) and low quality datasets (TanDEM). This empathises the importance of having a high quality DEM and the impact that it can have on damage estimates in data-poor environments.

Therefore, careful attention should be paid in the collection of these variables, as they can negatively influence other parameter's sensitivity. The proposed approach does not allow for a thorough quantification of the different inputs influences and is only limited to two inputs interactions. Other tools may provide a better assessment of such relations, like a Bayesian Network (BN). BNs combine probability theory with graph theory. Graph theory consists of the mathematical representation of a network, where the relationships between lines and nodes are described. BNs depict probabilistic dependence relations in a graph. The interest surrounding them is growing in the coastal engineering field, (Plant and Holland, 2011a), (Plant and Holland, 2011b), (Pearson et al., 2017). Some authors have also highlighted the unexplored potential of BNs for assessing uncertainty in natural hazards risk analyses (Vogel et al., 2014), (Vojinovic et al., 2008). Being a graphical tool that can handle large quantities of data, a BN could be useful in shedding light on relations between different variables in uncertainty propagation.

5.2.4. EXCEEDANCE OF THRESHOLDS

In flood risk modeling, multiple parameters interact in a multi-variate space. In such systems, nonlinear relationships between the processes is an expectable behaviour, and a small parameter change can yield to a transition from a stable state to a new equilib-

rium state (Groffman et al., 2006). Ultimately, this new state can be drastically different from the initial one. Some of the main drivers of non-linearity and system instability are thresholds and system self limitation (Phillips, 2003).

A threshold is a point past which a disturbance in external conditions causes rapid changes in the system behaviour (Horan et al., 2011). Different variables can represent a threshold, for example the change of slope in the terrain, or the height of the beach crest. After such thresholds are exceeded, damages increase non-linearly and make the system response to the forcing more complex. However, recognizing a threshold is not straightforward (Voice et al., 2006). Threshold behaviour, for coastal flooding, can arise from a change in external factors or from reaching an internal tipping point(Phillips, 2003). For example, sea level rise has proven to induce the exceedence of tipping points for flood risk in complex coastal systems (Sweet and Park, 2014). Self limitation, on the other hand, means that the system behaviour is limited by the system itself.

Considering coastal flood risk, a self limiting behaviour can be identified in our case study, for the location of Praia Abade. Estimating the damages of a given flood event, the maximum value that can be reached is limited by the number of assets that are "available" to the hazard. In this location, under the largest sea level rise, the damage increase is rather small, as most damages already occur with lower water levels and, in simple terms, there are no more houses to flood.

Some possible thresholds that have been identified in Praia Abade and Pantufo include:

- Change in elevation that yields a much larger amount of damages (Terra-Sar X in Pantufo)
- Water levels exceeding the 30cm buildings elevation
- Water levels exceeding the 50cm threshold to fully damage boats
- Sudden change in slope of DDF

Some of the identified thresholds come from modeling assumptions and can determine whether a certain asset will be damaged or not. The 50cm water level that needs to be exceeded for the boats to be taken away from the flood determines whether the whole value will be lost or not (see Section 3.5.4). Such assumed threshold is necessary for the analysis but its value is arbitrary. In reality some boats would be heavier than others and 'survive' larger depths. Such model thresholds simplify reality and introduce epistemic uncertainty. Since perfect model do not exists, knowing the implications of the many assumptions introduced in the analysis is fundamental to improve the understanding and application of the model predictions.

5.3. IMPORTANCE OF DEM

We investigated the consequences of having high-quality topographic mapping, using drone-derived DEM , against using lower quality, globally available DEMs (Section 4.3.4). Moreover, we could also analyse the effect of adopting different resolutions for the model

grid of SFINCS (Section 4.5.2).

Our results clearly showed that having a high quality dataset is much needed for topography. Particularly, the publicly available DEMs investigated (SRTM, ASTER, MERIT and TanDEM) highly overestimate the land elevation and consequently underestimate the risk of flooding. ASTER, MERIT and SRTM all have shown to nullify the overall risk for both locations, as their computed flooding extent are minimal and the estimated damages to the assets zero. The error metrics shown in Appendix C highlight the large difference between these topographic datasets and the drone-derived DEM. Despite the fact that ASTER and SRTM had a smaller resolution (~30m) than TanDEM (~90m), yet the latter performed best at reproducing a similar elevation to the drone DEM, with a mean error of 2.9m in Pantufo and 3.23m in Praia Abade. Generally, our findings are in accordance with (Vousdoukas et al., 2018a), (Van de Sande et al., 2012), (Paprotny et al., 2019), (Cook and Merwade, 2009), (Colby and Dobson, 2010) who identified high quality DEM to be of high importance for an accurate flood risk assessment. More particularly, our results align together with those of (Van de Sande et al., 2012), who compared the SRTM and ASTER DEM for the coastal community of Lagos, Nigeria. Their research also underlined the effect of different spatial scales. Indeed, at an higher geographical detail, the error found applying the publicly available DEMs increased. This comes in agreement with our results, which indicate that for micro-scale studies (see Section 2.3) the bias can be relatively higher than at larger scales. (Vousdoukas et al., 2018a) and (Paprotny et al., 2019) assessed the sensitivity to DEM at regional to continental scales, therefore the results may not be directly linked to those of our study. On the other hand, our results differ from those of (Cook and Merwade, 2009) and (Colby and Dobson, 2010), who found that the estimated flooding extent reduced when using a DEM with higher resolution and vertical accuracy for two locations in USA.
A possible explanation of the very low reliability of satellite based DEMs for our case study might be the negative correlation between their vertical accuracy and terrain slope. Indeed, in their study (Gorokhovich and Voustianiouk, 2006) have highlighted an increase in the prediction error given by SRTM on steep slopes and mountainous areas, compared to flatter terrains. The fact that the TerraSAR-X (~10m horizontal resolution) DEM overestimated damages is most likely due to the over-correction of buildings and trees and smoothing that was previously applied to the DEM. This further underlines how smaller resolution does not necessarily relate to better vertical accuracy and that comparison between different DEMs can help to identify many artefacts and spurious points.

Furthermore, we have underlined the potential improvement when publicly available DEMs, which are originally produced as DSM, are corrected from buildings and vegetation. Indeed, by applying a very simple correction method (Appendix C) we were able to improve the prediction using TanDEM of 10% in Pantufo and 20% in Praia Abade. Correcting for buildings and vegetation is a commonly practised technique that increases the reliability of the DEM to be used as a DTM. Nevertheless, a conservative correction should be preferable over large correction, as indicated by the large over-estimation of damages when using TerraSAR-X.

Another source of uncertainty that was investigated is the effect of DEM resolution using the same dataset. We have shown that increasing the DEM resolution yields a smaller extent of flooding and a consequently smaller volume (Section 4.5.2). This is particularly clear for Praia Abade, where already increasing the grid size from 0.5m to 10m gives a mean error of 20%. Results in Pantufo partially differed, with an already large inaccuracy given from the 1 m resolution (40% mean error). This large difference at low resolutions may be linked to the higher terrain slope and variability of Pantufo compared to Abade. At the same time, the error is partly explained from the merging with other dems at the boundary of the drone DEM (see Section 4.5.2). Despite the differences between the findings from Pantufo and Praia Abade, we can conclude that generally a larger grid cell size relates to smaller flooding volumes. A possible explanation is that at larger resolutions, less processes are correctly modeled and that hydraulic connectivity between grid cells is more limited due to the smaller terrain variability reproduced.
This comes in disagreement with (Saksena and Merwade, 2015), (Hsu et al., 2016) and (Bouziotas, 2016) who found that increasing DEM resolution resulted in larger flooding estimates. Again, a possible explanation may be found in the different topography of the areas investigated. Our study focused on a relatively steeper, more mountainous area compared to the ones of the fore-mentioned studies. Linking this findings with the computational times of the model can help coastal modelers in choosing a grid resolution for a specific case. A 2m resolution gives an error smaller than 5% compared to a resolution of 0.5m with still a 2 order of magnitude decrease in model computational time.

Finally, we want to emphasise the growing applicability of unmanned aerial vehicles (UAVs) in remote-sensing for environmental variables. Nowadays, commercial satellite imagery can achieve high horizontal resolution and remains the best-suited option for large-scale monitoring of the coastal environment. At the same time, still some significant limitations, like cloud coverage, hinder the application of these systems. In such circumstances, the application of smaller UAVs, could be beneficial. They can collect information at finer scales (mm to cm) and serve several purposes. In the coastal engineering field, they have proven themselves successful at identifying rip currents (Benassai et al., 2017), at measuring surface flow velocities (Tauro et al., 2016), topography (Tamminga et al., 2015), (Leitão et al., 2016), sediment distribution and coral health (Parsons et al., 2018).

5.4. DAMAGE MODELING

Depth damage functions stood out as one of the most sensitive inputs in our analysis. Most of the uncertainty arising from their application is of *epistemic* origin, thus due to limited knowledge. (De Moel et al., 2012), (Merz and Thieken, 2009), (Wagenaar et al., 2016), (Prahl et al., 2016), (Jongman et al., 2012), (Egorova et al., 2008) all highlighted the large amount of uncertainty surrounding damage modeling, although mostly for European case studies. Their analysis investigated the sensitivity of damage estimates to DDFs that were originally developed for the locations of their study. In this research we

dealt with the issue of applying DDFs that had been initially derived for other locations, basing our choice on the type of flooding or on the environment. This process requires further assumptions in the methodology and increases the overall uncertainty in the results. Despite this, often damage curves are directly taken from literature or previous studies and applied in different areas making little, if any, corrections and adjustments ((Wagenaar et al., 2016), (de Moel, 2012), (Schröter et al., 2014)). From our results, we can acknowledge that the selection of a curve, based on the type of flooding or on the type of building may yield to incorrect results. Indeed, choosing a curve for a similar setting, like the one for American Samoa, gave us an underestimation of results by a factor 4. Contrarily, using the DASM curve, which is based on riverine flooding for the Netherlands gives much more similar results to the case of São Tomé and Príncipe. We are therefore confident in affirming that a proper understanding of the underlying assumptions (see Section 2.7) is a more robust approach when selecting a depth damage curve, than basing the choice on curves derived for similar flood types or building strengths.

The method of (Egorova et al., 2008) was used to test DDF shape sensitivity (Section 3.5.4). Varying the shape of the same function allows for including weaker or stronger building in the assessment. The set of functions developed, from the 1st to the 99th percentile (see Section 4.5.1), reproduces almost the same uncertainty coming from the different curves applied (Section 4.3.5. This methodology could be used in a project to reproduce building strength uncertainty. Indeed, a concave and convex shape represent two opposite methods in modeling the physics of damage. A convex shape assumes the majority of damages to occur only at relatively high water depths, which could appropriately represent a strong building. Alternatively, a concave shape would yield large damages already at lower water depths. This other approach may be more representative for developing countries where buildings are generally weak (like São Tomé and Príncipe, (Giardino et al., 2018)) or for buildings where valuable assets are exposed at low water depths (expensive floor, electricity sockets, etc.).

5.5. IMPLICATIONS FOR RISK MANAGEMENT

5.5.1. QUALITY IN INPUT DATA

xcs fscs

High quality input data is often scarce in SIDS. Awareness on the implications of having good data can drive investments in better data collecting techniques, if they are proven to bring a substantial improvement in the risk assessment. For our case, this distinction is applicable to bathymetry and DEM, where GEBCO and TanDEM represent the low-quality datasets (see Section 3.5.3). The bathymetry measured with the echosounder during the site visit is regarded as high quality, (Giardino et al., 2018) as well as the DEM derived from the drone imagery. GEBCO is considered of lower quality due to the many spurious points and unrealistic transects found for São Tomé and Príncipe (see Section 3.5.2). We compared the damage distributions obtained using datasets with good and bad quality, for the two inputs. The distribution of damages plotted include all the simulations from the global analysis, for the current time horizon only. The results are presented in Figure 5.5 and 5.6. The top panel shows the distribution of damages

including all possible scenarios, whereas the middle and bottom ones depict the distributions of damages including all possible scenarios but using only a specific dataset for bathymetry and DEM respectively. The mean and the 50% confidence interval are used as comparison metrics to estimate the mean error introduced with the different dataset, as well as the change in output uncertainty. The red lines illustrate the width of the confidence interval.

In Praia Abade (Figure 5.5), the bathymetry dataset of GEBCO gives an increase in the mean damage of approximately 15%, together with a larger confidence interval, meaning larger uncertainty on the model outputs. Similarly, a lower quality dataset for the DEM produces a variation of 20% in the predicted mean damages, although in this case they are underestimated. Using the TanDEM DEM also yields a reduction of the width of the likely range of results.

The results for Pantufo (Figure 5.6) are rather similar to those in Praia Abade, though the impact of the low-quality dataset is larger. Even in this location the low-quality bathymetry dataset yields an increase in the mean damages, from approximately 1.6 to 2.1×10^6 and a widening of the confidence interval. The publicly available TanDEM DEM reduces the accuracy in the prediction of 0.73×10^6 (nearly 50%) and gives a smaller uncertainty range for the outputs.

From these two figures it can be concluded that having lower quality of data can contribute to a significant error in the prediction in these two locations, both for underestimating or overestimating the risk. Moreover, using a different dataset can yield to a variation of the width of the distribution, ultimately indicating a variation on the level of uncertainty reproduced by the model. The consequences of this are twofold and highlight the importance of properly estimating a model's uncertainty. In the case of bad quality bathymetry we see a large increase in the model outputs which could ultimately lead to assume that the model itself gives uncertain results. On the other hand, the TanDEM DEM leads to a smaller confidence interval, which could lead the risk analyst to a false high estimate of the model robustness.

More generally, the results from our sensitivity analysis indicate that bad quality in input data can largely affect the predictions of the model. Considering their very likely range of results, DEMs and DDFs can have an impact on damage estimates of a factor that ranges, through the four time horizons, from 4 to 6 and from 8 to 10, respectively. For coastal flood risk assessments in SIDS a large variety of reliable hydrodynamic models that include complex processes and can achieve a high level of accuracy in the prediction is already available. Unfortunately, the efforts made in developing such models can be useless if the provided input data is not reliable. Therefore, more efforts should be aimed at improving and developing new data collection techniques for environmental variables that are necessary for such studies. Decision makers called to manage the coastal zone in SIDS, where often data is limited, may need to choose where to direct their economical resources, and if possible, to select which type of data should be prioritised. Applying uncertainty analysis in a project, could help practitioners in choosing where to direct their economical sources to improve coastal flood risk predictions.

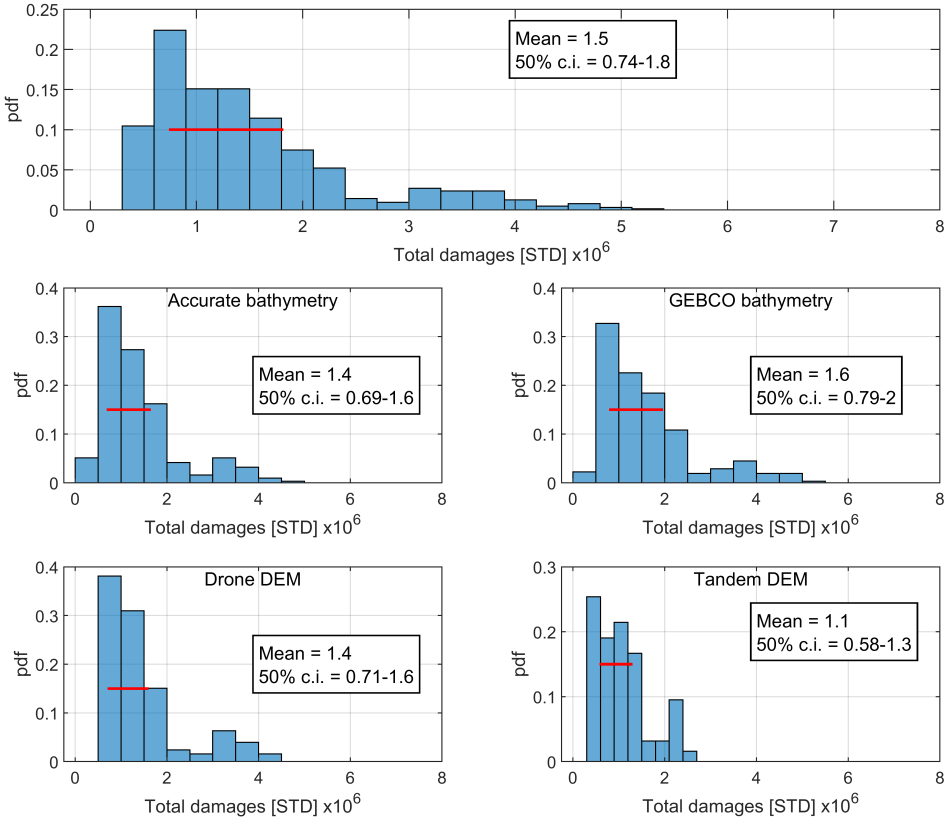

Figure 5.5: Damages distributions for Praia Abade using different datasets for bathymetry (middle panels) and DEM (bottom panels).The top panel shows the distribution of damages with all possible combinations

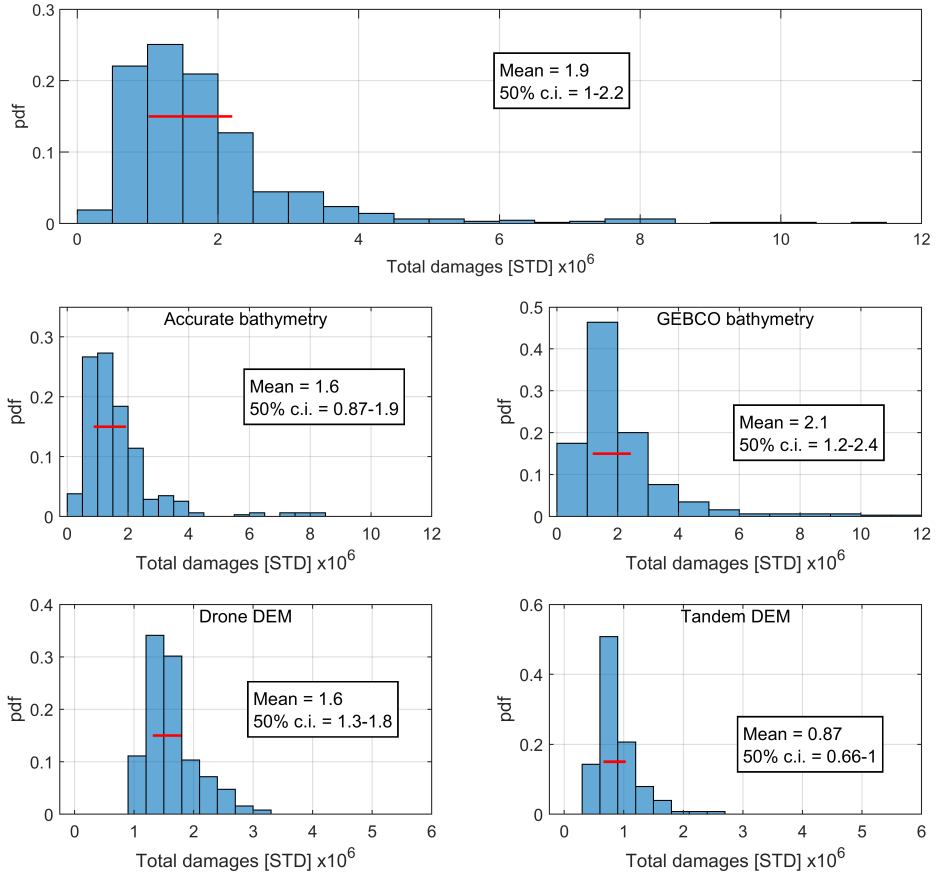

Figure 5.6: Damages distributions for Pantufo using different datasets for bathymetry (middle panels) and DEM (bottom panels).The top panel shows the distribution of damages with all possible combinations

5.5.2. COMMUNICATING RISK UNDER UNCERTAINTIES

Underlying assumptions and the consequences that they bring are often not communicated to the end user of a risk analysis. These include stakeholders and decision makers in the context of natural hazards and environmental management. A very important aspect, that comes alongside with an uncertainty analysis is the risk communication. Risk, as introduced in Section 2.1, can be perceived differently by people. Therefore communicating risk in an comprehensible way to a specific receptor can represent a challenging task. It could be beneficial to increase the application of uncertainty analyses, alongside with improving its communication to the practitioners. Uncertainty information is important especially in the light of the need for future predictions. Often models are calibrated according to existing conditions that may largely differ from future ones, which means that the model may not be able to deliver accurate future predictions. Therefore, communicating the uncertainty in the model output and the model limitations is a recommended step to improve decision making for future scenarios(Loucks and Van Beek, 2017).

Policy makers and stakeholders often operate under political and institutional constraints, which prompts them to not prioritise the improvement of the scientific information on flood risk (Morss et al., 2005). Most importantly flood risk managers are also to face *decision uncertainty*, which differs from the *scientific uncertainty* that has been investigated in this study.
Decision uncertainty refers to the different implications for cost and liability of a certain strategy or flood management policy and often include variables that are complex to account for (Morss et al., 2005)).

The task of communicating risk under uncertainties is further complicated by another type of uncertainty, which has quickly been mentioned in Section 2.4, *linguistic uncertainty*. Language uncertainty is often overlooked (Carey and Burgman, 2008), as well as the task of communicating the uncertain scientific information to stakeholders (Pidgeon and Fischhoff, 2011). Indeed, scientists communicate in a highly technical language that practitioners working in the public sector may initially struggle to comprehend. Therefore, according to (Thompson, 2002), model outputs with uncertainty call for further translation of the science to be useful for successful policy planning. We recommend that the study of risk communication, especially under uncertainty, should be addressed in order to develop new tools and guidelines.

5.6. FUTURE STEPS

In the course of our project, some steps that would have improved the methodology were left out, due to time constraints and complexity. Building on this method and adding new steps and components is although highly recommendable, if this research is to go further. Some potential future developments are highlighted in this section.

5.6.1. IMPROVING THE CURRENT METHODOLOGY

The presented method has proven to be robust and allow for the assessment of different uncertainty sources. Nevertheless, improving on its speed and probabilistic assessment is desirable, particularly if such uncertainty analyses are to be included in future flood risk assessments. Here are some steps that should be included in future research.

PROBABILISTIC ANALYSIS

One of the biggest drawback of our methodology is the absence of a full probabilistic assessment. Often in uncertainty analyses, probability distributions are fit to each input and are then sampled through, for example, a Monte Carlo analysis (Wagenaar et al., 2016), (de Moel, 2012). The benefits of such assessments are that inputs impact on the outcome of the model can be directly quantified, including the effects of inter-inputs relations, through the use of methods such as (Saltelli et al., 2008) and (Sobol, 2001) which are based on the estimation of parameters variances and covariances.

One of the most adopted techniques to reduce the computational burden of uncertainty analyses is to implement a sampling method for the variable space. The implementation of a MC sampling methodology may also be limited by the large number of simulations required. Indeed, to provide reliable results, many model iterations need to be performed. One way to overcome this is to adopt the Latin Hypercube Sampling (LHS) method (McKay et al., 1979). LHS aims at reducing the number of sampling required by dividing the range of values of each uncertain input variable into n equi-probable intervals, and sampling at the same frequency in each one of them. Its application in uncertainty analysis has been studied and is widely implemented, (Helton and Davis, 2003). Figure 5.7 shows a comparison of the two sampling approaches for a two variables space.

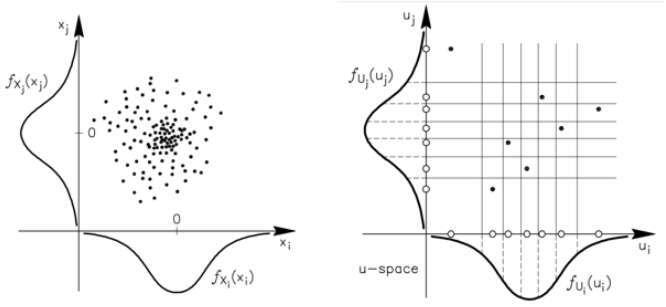

Figure 5.7: Example of simple random sampling (crude Monte Carlo) on the left and Latin Hypercube Sampling on the right, from (Hurtado and Barbat, 1998)

One of the biggest challenges of adopting such approach is to fit a PDF to each input. For variables like H_s and storm surge, it is rather simple, providing that enough data is available to perform a statistical analysis as in Section 4.1. For DDFs, a possible suggestion is to use the methodology of (Egorova et al., 2008), which has proven to be capable of reproducing most of the uncertainty coming from DDFs (see Section 4.5.1). Regarding SSP scenarios and SLR predictions, a PDF could be fit based on the possible spread

of values for different time horizons. The fitting of PDFs becomes trickier when considering bathymetry and DEM. Given the paucity of data in SIDS, it is already difficult to have a single dataset for such inputs, let alone to have enough to fit a probability distribution. Then, expert knowledge could be exploited to select the distribution to be used, based on typical shapes, for each input. Otherwise, for simplicity, a normal distribution could be fit to each data point, taking the measured value as mean. The issue then becomes how to define the variability of each sample point, in other words the standard deviation of the normal distribution. One possible solution is to use the values given for the publicly available DEM such as ASTER, where for each tile, the standard deviation of all the measured points within the tile is given. Given the large inaccuracy of satellite based DEMs found for our case study, this approach may be too unreliable and thus a simpler approach based on assuming a standard deviation value based on literature may be preferable.

ACCOUNT FOR MITIGATION

The impact of risk mitigation measures on uncertainty analyses for coastal flood risk has been already addressed in (Vousdoukas et al., 2018a), where it was shown to have a substantial impact on damage estimate. The effect of Disaster Risk Reduction (DRR) measures may largely reduce the overall uncertainty, as well as guide the selection of which option would be more beneficial. Possible mitigating measures include:

- Raising the elevation of the buildings
- Relocate houses in safer areas
- Construct a seawall or a breakwater (hard solution)
- Nature-based flood defences (soft solution)

Natural-based solutions entail a large variety of engineering measures that aim at exploiting ecosystems services for the benefit of both the human and natural environment. The creation or restoration of large coastal ecosystems like mangroves, coral reefs and seagrass are some of the possible natural flood defences.
Some of the fore-mentioned options could be easily tested in the current model setup. The elevation of buildings could be modeled by simply shifting to the right the DDF. The building's strength would not change, but damages would start occurring at larger depths. Other DRR options, like building a seawall or a breakwater or nature-based solutions would demand more efforts as they would need to be included in the hydrodynamic modeling. Indeed, the implementation of vegetation on the foreshore and the consequential wave energy dampening involves an appropriate calibration in the hydrodynamic model.

EXTEND THE METHODOLOGY TO OTHER LOCATIONS

The findings of this study may be largely impacted by the local variability in the system studied. To extend our findings beyond São Tomé and Príncipe, and improve the confidence in their applicability, more locations should be included in the framework. The hydrodynamic models are relatively easy to set up, given that the necessary information is available. Their simplicity is mainly due to the 1D -2D interpolation at the boundary between XBeach and SFINCS, which assumes long-shore uniformity of the

water lvel timeserie and may not be applicable elsewhere. To provide better guidance in data-collection and tackling uncertainty for CFR assessments in SIDS, we recommend to extend this analysis to other locations. Furthermore, more input sources could be tested, like the combination of the peak of the storm surge with different phases of the tidal cycle (Vousdoukas et al., 2018a).

5.6.2. INTERPOLATION TECHNIQUES

Different interpolation techniques for scattered data are available, either for the process of downscaling and upscaling. Interpolation may be necessary when an higher resolution is necessary and thus new data points have to be estimated, as well as when a smaller resolution is preferred, for example for computational expenses and thus points at a larger spacing have to be extrapolated from measured data. Considering the latter process, trying to reproduce the same information as precisely as possible can be challenging. Different interpolation techniques exist that vary for computational expenses and accuracy.

A preliminary investigation was conducted in our study and is described in Appendix D. The results did not allow for any early conclusion, but indicate that developing some further knowledge on how each technique impacts the topography and coastal flood risk assessments should be encouraged. Indeed, it was found that, although on average very little variation in flooding extents was computed, in some cases significant differences could arise. These differences were especially found when the starting point of the extrapolated grid was shifted. It is therefore recommended to investigate more robustly the consequences of applying one interpolation technique over the others, with the goal in mind to provide a selection of methods that gives robust sampling. Their effects have already been investigated by (Guo et al., 2013) , (Aguilar et al., 2013), (Weng, 2002), although in these studies, the differences are measured with regards to variations in estimated elevation. A sound understanding of how such differences then translate in computing flooding could potentially reduce the epistemic uncertainty that arises from the application of DEM in CFR analyses.

5.6.3. IMPROVE DAMAGE MODELING

Damage modeling proves to be one of the weakest links in risk assessments, and its impacts on predictions is expected to not decrease for future scenarios (Section 4.4). For these reasons, future research efforts may focus on improving the current approach to damage modeling. A possible way to derive new damage function is to conduct laboratory experiments. This approach has the advantage that all physical conditions and characteristics of the assets at risk are controlled. However, the review of the literature suggests that this approach is rarely used (Schultz et al., 2010). Varying the hydrodynamic conditions and asset vulnerability, could allow for the extrapolation of DDF fitted to different buildings characteristics and strengths. One benefit of laboratory experiments over field observations is that they allow for a thorough assessment of the time-dependency of damages. One of the biggest limitation of available DDFs is that they do not include any correlation of the damages with the duration of the flood. A building that undergoes the same water depth would most likely incur in larger damages if the flood lasts for longer. Indeed, the impact of inundation duration on flood damages has

possibly been overlooked (Merz et al., 2013). Developing curves that depend on multiple variables (e.g. flood duration, flood depth, average water velocity) would largely increase the accuracy of damage assessment, as modeling damages including multiple variables has already been found to bring substantial improvement(Schröter et al., 2014), (Merz et al., 2013). Another aspect of coastal flooding that is often not included in damage modeling is the action of waves. Waves can exert high forces on structures that should be accounted for. According to (Schröter et al., 2014) the use of additional explanatory variables would increase the level of accuracy of the model, alongside with, as these variables would be uncertain, the level of assessment of uncertainty in the output. A possible and simple approach to multi-variate damage modeling are tree-based models (Merz et al., 2013). These models are based on dividing binarily the data according to the behaviour of a state variable, which leads to the creation of sub-branches, where further division for other variables follows. Figure 5.8 below show a qualitative example of a simplified tree-based model to estimate damage factors based on flooding depth and inundation duration.

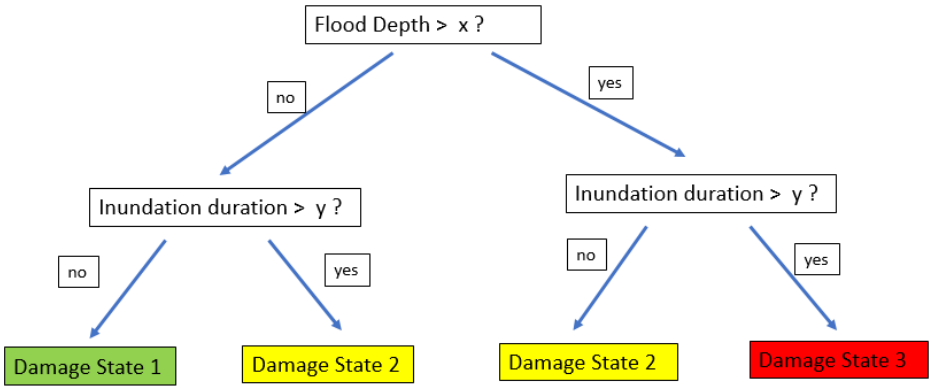

Figure 5.8: A simplified tree-based model for estimating CFR damages dependign on two variables. A real case model could include multiple values for each variable, as well as more variables. See (Merz et al., 2013) for a more complex example of tree-based multi-variate flood damage model.

The consideration of including more variables also comes from the fact that such information is already available in most risk studies, but is not being exploited. Hydrodynamic models require small temporal steps to reproduce the hydrodynamics accurately, where for each time step water levels and flow velocities are computed. Collecting these data, for example the hourly distribution of maximum water depths and flow velocities over the flooded area and couple it with experimentally derived functions could greatly benefit the assessment of damages, especially if compared to the current practice, where a single variable (maximum water depth) over the whole time domain is used to compute damages. A possible drawback of increasing the complexity of damage models is the increase in calibration efforts required to set them model up. A very complex damage models that depends on several value may work extremely well for the conditions

on which it has been calibrated and validated. However, as flood damage characteristics can largely vary from one location to another, such complex model may perform terribly for a different case and the application of a simple model (a DDF) may be preferable. In order to develop an appropriate damage model, a good balance between its complexity and its applicability should be found.

Such implementation could be more beneficial if the hydrodynamic and damage modeling are merged. The model FIAT is based on a simple approach, that computes the damages using the same grid of the hydrodynamic model, or an aggregation of it. A possible development would be to merge the two models, therefore including the damage assessment directly in SFINCS. This would first remove the need for the post-processing and pre-processing steps currently necessary for SFINCS and FIAT, respectively. Furthermore, if a multi-variate damage function as suggested above is to be used, the information it requires is already in SFINCS.

6

Conclusions and Recommendations

Conclusions

Uncertainty in flood damage estimates is well reproduced through our methodology, with a substantial spread of the output predictions for both locations. For the current time horizon, the main contributor to the output uncertainty are DDFs, followed by DEM. As climatic and socioeconomic variability is introduced, SLR projections become the major uncertainty source for future flood risk analyses, while DEM and DDF still have a considerable influence on the predictions. Socioeconomic changes can exponentially increase the total projected damages, despite carrying little uncertainty to the output, and should always be accounted for in risk analyses. Disregarding input combinations while conducting a local sensitivity analysis proves to significantly alter the assessment of inputs relative importance and a global analysis should be preferred. Low quality, publicly available dataset for bathymetry and topography introduce significant errors in the model assessment, alongside with affecting the output uncertainty, ultimately reducing the trustworthiness of the risk estimate.

Recommendations

Utilising a probabilistic framework and accounting for mitigation options are recommended improvements for the method of this study. To reduce the epistemic uncertainty surrounding DEM, new elevation data collection techniques, such as UAVs, that can achieve a satisfying level of accuracy, should be encouraged. Multi-variate damage models could be developed, that account for wave action and inundation time, to tackle damage-related uncertainty and improve the vulnerability assessment in the modeling scheme. To improve the communication of risk analyses to decision-makers, the development of an uncertainty framework that reproduces output uncertainty and allows to visualise the effect of underlying assumptions and inaccurate data is encouraged.

In this research, we investigated the development of uncertainty in model output testing several sources of both epistemic and aleatory uncertainty for coastal flood risk studies. To estimate risk from coastal hazards, we coupled the models XBeach, SFINCS and FIAT. The key inputs that we considered, with their relative uncertainty are: (i) storm surge level, (ii) offshore significant wave height, (iii) bathymetry, (iv) topography information in a DEM and (v) the choice of DDF to compute damages. Moreover, to understand the temporal changes of flood risk under future conditions, we included two other inputs in the analysis: (vi) SLR predictions and (vii) SSP scenarios to predict economic growth.
The methodology was applied to two coastal communities in the islands of Sao Tome and Principe, a member state of the Small Island Developing States (SIDS).

6.1. CONCLUSIONS

The questions proposed in Section 1.3, are answered here, based on our analysis:

1. ***Can we estimate uncertainties by varying input distributions and data in a train of models?***

   Answer: The uncertainty sources included in the analysis are successful at reproducing uncertainty in the model output. This is indicated by the 50% confidence interval for the estimated damages, that, for the current time horizon, equals to 1.2-2.2·10^6 STD in Pantufo and to 0.74-1.8·10^6 STD in Praia Abade, where the reference damage estimates are 2.11·10^6 and 1.56·10^6 STD, respectively.

   Elaboration: Input uncertainties are reproduced by either fitting a probability distribution in the case of H_s and storm surge level, or by varying the model or dataset used for bathymetry, DEM and DDF. The uncertainty in future risk estimations is also reproduced, testing different sea level rise scenarios and socioeconomic trends. Despite having room for improvement, the applied methodology allows us to weight the sensitivity of each input, both for local and global analyses. Through literature review and preliminary sensitivity tests, the number of inputs and thus model simulations necessary was minimised. Nevertheless, the computational expenses of testing all possible combinations determine a limit on the number of uncertainty sources that can be investigated.

2. ***What are the most important inputs that drive uncertainties in coastal flood risk assessment?***

   Answer: For the current time horizon, the choice of DDF, followed by topography information, are the main contributors affecting the uncertainty of coastal flood risk. Indeed, DDF and DEM can vary the estimated damages from the reference scenario with a multiplying factor that ranges between 0.25-4 and 0.3-2.5 respectively (see Figure 4.18).

Elaboration: Regarding damage analysis, knowledge is lacking on how building damages occur, particularly for SIDS. The understanding of the physical processes involved, let alone their model implementation, is far from being detailed enough. Such limitations, elucidated by many studies in literature, are reflected in the results, where DDFs give the largest spread of predictions for the present scenario. Despite the numerous of curves developed, linking them based on similar characteristics proves to be a challenging task. For developing countries and SIDS, a depth damage curve that yields significant damages already at small depths may be the preferable approach, being conservative and representing weaker buildings.

Digital Elevation Models also heavily contribute to the output uncertainty. Publicly available DEMs prove in most cases to give tremendously unreliable results, as they tend to overestimate elevation. The epistemic uncertainty of DEMs is the most straight forward to reduce, as adopting more accurate remote sensing techniques, like UAVs, would lead to a higher quality DEM. Unfortunately, SIDS are often in remote places with little technical equipment to be used. For this reason, higher accuracy satellite-based measurement may be more accessible.

With this analysis we were further able to identify some dissimilarities in the sensitivity to the inputs for the two villages of Praia Abade and Pantufo, despite having similar hydrodynamic conditions and social systems. Surprisingly, Pantufo was significantly more sensitive to the hydrodynamic conditions, as well as changes in the bathymetry and DEM. This highlights the need for uncertainty analyses in CFR studies, as they may provide useful insights and reveal underlying divergences.

3. ***How important are inputs interactions to estimate uncertainties and how do they vary under future conditions?***

   How important are inputs interactions to estimate uncertainties...

   Answer: Investigating uncertain inputs within a global sensitivity analysis significantly augments the estimated output uncertainty. Inputs interactions yield a greater impact on the estimated damages, alongside with affecting their relative importance. A local sensitivity analysis may not portray the whole picture and provide only limited knowledge of the system.

   Elaboration: In the global analysis, the weight on the output prediction of bathymetry, H_s and storm surge becomes more significant, whereas it diminishes for DEM. The increased sensitivity of H_s and storm surge has been linked to steeper damage curves, as well as lower quality data for bathymetry and DEMs. This demonstrates that an uncertain input increases the output sensitivity from other inputs as well, which emphasises the importance of minimising the uncertainty surrounding input data.

...and how do they vary under future conditions?

Answer: For long term future conditions, SLR prediction becomes the input with the highest impact on damages estimates. DEM and DDF still carry considerable uncertainty and are ranked second and third in importance (see Figure 4.22).

Elaboration: Sea level rise but especially economic and population growth drive enormous increases in future expected risk, with mean damage estimates increasing up to a factor 50. For closer time horizons (2050) their impact is rather low, growing exponentially as the time horizons increase (2100). Socioeconomic changes have a somewhat smaller uncertainty compared to other inputs. Nevertheless, they are responsible for exponentially increasing the mean value of damages, therefore, disregarding their effect in coastal flood impact analyses would lead to considerably underestimate the overall risk. Finally, the relative importance of other inputs does not vary significantly with time, and we can conclude that similar patterns are identified for each time horizon.

4. ***What is the minimum required quality of input data to have a satisfactory assessment of risk?***

Answer: A quantification of the minimum data quality necessary for a robust assessment cannot be defined. Nevertheless, we have proven that publicly available datasets for bathymetry and topography are not accurate enough for small scale CFR analyses and introduce substantial errors due to their low vertical accuracy. Moreover, increasing the resolution of the computational grid leads to an underestimation of the flooding, as the surface variability reproduced in the model is decreased. Therefore, only relatively small grid cell sizes should be used for micro-scale studies (1-5 m)

Elaboration: Comparing the damages distributions obtained using two different datasets for bathymetry and DEM, we noticed a substantial variation in the mean and likely range of results (see Figure 5.5 and 5.6), resulting in unreliable and inaccurate model predictions. Using the GEBCO dataset yields an increase in the mean damage prediction of approximately 45%, and the 50% confidence interval increases its width by 20%. On the other hand, the low quality DEM TANDEM results in an almost halved mean damage prediction and decreased size of the 50% confidence interval. However, the low accuracy of publicly available DEMs can be improved by correcting for buildings and trees, as this leads to 10-20% improvement in the damage estimate (see Section 4.3.4). The usefulness of a model can be measured by the uncertainty in its output, which ultimately describe its reliability. Using low-quality data has proven to not only decrease the accuracy of the model but also to change the output uncertainty. This would likely lead to a wrong level of confidence in the estimate, ultimately giving an unreliable assessment of risk and nullifying the trustworthiness of complex hydrodynamic models.

Furthermore, decreasing the grid resolution in SFINCS, using the high quality drone-derived DEM, leads to an underestimation of the flooding volumes. At larger resolution, the spatial variability is reduced and hydrodynamic processes are modeled less accurately. The minimal spatial scale that is required for a robust assessment (less than 10% error in the predicted flood volume) is 5m. On top of that, coarser resolutions also cause a higher sensitivity of the results and thus a greater output uncertainty, as the spread of the predictions increases (see Figure 4.30).

An overall ranking of the tested inputs, based on their influence on damage estimate uncertainty (see Figure 5.1), is as follows:

- Current time horizon:
  1. Depth Damage Function
  2. Digital Elevation Model
  3. Significant Wave Height
  4. Bathymetry
  5. Storm Surge
- Year 2100:
  1. Sea Level Rise prediction
  2. Digital Elevation Model
  3. Depth Damage Function
  4. Shared Socioeconomic Pathway
  5. Significant Wave Height
  6. Bathymetry
  7. Storm Surge

6.2. RECOMMENDATIONS

Here we propose some future research topics following our findings, together with some recommendations for the practice of coastal flood risk assessment:

a **Improve and extend the methodology to other locations** To further verify the findings of this study, the methodology should be extended to other locations, possibly accounting for mitigation and adaptation measures and adopting a fully probabilistic framework as suggested in Section 5.6. The findings in another location could substantially vary. Indeed, already for the two communities of Praia Abade and Pantufo, with similar hydrodynamic conditions and social system, we found some dissimilarities.

b **Increase the use of high-resolution remote sensing data collection techniques**
To tackle the paucity of high quality data in SIDS, the application of new data collection techniques should be encouraged, as well as the exploitation of local knowledge and crowdsourced information (see Section 4.2). UAVs are now able to collect extremely high resolution topography data that substantially improve the assessment of risk if compared to publicly available satellite-based DEMs. While the cost of these techniques is decreasing, their application is expanding to different fields of coastal engineering. Some possible applications include the measurement of sediment distribution and coral health.

c **Correct DEMs for buildings and trees**
Correcting DEM for buildings and trees largely improved the prediction using publicly available DEMs, making it a recommendable practice when utilising these datasets for hydrodynamic modeling. Nevertheless, the correction should be made with a conservative approach. Over-correcting a DEM would lead to biased flooding damages and enough care should be put into selecting the value of the correction factor.

d **Investigate interpolation technique uncertainty for flood modeling**
Improve the knowledge of the consequences of applying different interpolation techniques for downscaling purposes. Identifying the most suitable technique for hydrodynamic modeling would improve the confidence in the model results. This could be achieved by testing how several interpolation methods perform in reproducing the topography and estimate the errors introduced in the flooding estimate, by comparing them with the results using the original high resolution DEM. Another factor that could affect the results is the choice of the location of the sample points, for which preliminary tests were conducted, as well as for different interpolation techniques and are described in Section E.

e **Use 1 to 5 m resolution for SFINCS in micro-scale studies**
The SFINCS model grid resolution has a considerable effect on prediction accuracy. To accurately model single waves in small-scale studies small cell sizes are recommended, as using a resolution larger than 5m already underestimates flooding volumes up to 20%, compared to a finer resolution of 0.5m. Using a resolution of 2-5m already highly improves the accuracy (less than 10% error) without losing much in computational efficiency. However, these differences may be less pronounced at larger scales, where the computational burden of a finer grid may be too high.

f **Develop multi-variate flood damage models**
Multi-variate damage models have been found to bring improvements to damage estimation. Although the dynamics of flood damages are complex and difficult to include in numerical models, a simple tree-based model that allows for the implementation of more flooding variables like inundation duration and flood velocities would benefit the robustness of the risk analysis. A tree-based model with variables flood depth and inundation duration that leads to different damage states, each with a different damage curve based on the two variables (see Figure 5.8),

could be easily implemented in the modeling scheme. The damage curves could be developed from laboratory experiments or field data. This could be achieved by recreating up-to-code buildings in large scale facilities and test their resistance under varying forcing conditions, to then fit empirical relations to the measured data.

g **Prioritise global sensitivity analysis over local**
Testing the sensitivity of one model varying only one input at a time, only leads to a limited estimation of its weight. When inputs are varied simultaneously, non-linear interactions occur and their influence on the output may vary substantially. It is recommended that a global sensitivity analysis should always be preferred over a local analysis.

h **Develop an uncertainty analysis framework for coastal flood risk studies**
The uncertainty surrounding some inputs, like the hydrodynamic forcing or sea level rise predictions, cannot be reduced in the short term. However, ignoring such uncertainty may lead to a wrong estimation of risk. Developing an uncertainty framework to apply in risk studies would improve the information given to decision-makers for risk management, by better communicating the consequences of underlying model assumptions and uncertain data. Moreover, such framework would allow to identify threshold exceedances and improve the understanding of the system. A possible methodology could include probability distributions fitted to the parameters of interest and sampled within a MC framework, similar to the approach adopted by (De Moel et al., 2012).

i **Implement a methodology to reproduce depth damage curve uncertainty**
To represent the large uncertainty in damage curves, it is recommended to implement a method that accounts for different types of buildings and underlying assumptions. The methodology of (Egorova et al., 2008), which is described in Section 3.5.4 and was applied for the functions shape uncertainty proved successful in emulating the range of depth damage functions available in literature. If little knowledge is available for a specific location, this methodology could be used to model different building strengths.

j **Include socioeconomic changes for future risk estimates**
Not including socioeconomic changes has been demonstrated to lead to significantly underestimate future coastal flood risk predictions. Although a commonly accepted guideline on how to include them is not available yet, practitioners and engineers could adopt simple approaches to give estimates. A possible approach has been used in this research, where population growth and Gross Domestic Product projections were used as multiplying factors for future asset values. A more sophisticated approach could account for the local perception of risk, relating it to the income of the population, which would most likely be spatially heterogeneous. Including urbanisation and migrating patterns would also lead to an improvement of the risk estimate.

When thinking of a tropical island, people's imagination goes to a beautiful landscape, similar to the one depicted in the back cover of this report. In reality, the future of many islands around the world looks uncertain, vulnerable and at threat. The substantial uncertainty surrounding risk estimates, leads to a fragmented picture of different possible scenarios, more like the front cover of this report. If we want to leave the same first beautiful image of many world's islands for future generations to come, tackling the largest inaccuracies in flood risk studies and management is our first priority.

REFERENCES

Aguilar, F. J., Agüera, F., Aguilar, M. A., and Carvajal, F. (2013). Effects of Terrain Morphology, Sampling Density, and Interpolation Methods on Grid DEM Accuracy. *Photogrammetric Engineering & Remote Sensing*, 71(7):805–816.

Amante, C. J. (2018). Estimating Coastal Digital Elevation Model Uncertainty. *Journal of Coastal Research*, 34(6):1382.

Amidror, I. (2002). Scattered data interpolation methods for electronic imaging systems: a survey. *Journal of Electronic Imaging*, 11(2):157.

Apel, H., Thieken, A. H., Merz, B., and Bl, G. (2004). Flood risk assessment and associated uncertainty.

Apel, H., Thieken, A. H., Merz, B., and Blöschl, G. (2006). A probabilistic modelling system for assessing flood risks. *Natural Hazards*, 38(1-2):79–100.

Baldock, T. E., Huntley, D. A., Bird, P. A., O'Hare, T., and Bullock, G. N. (2000). Breakpoint generated surf beat induced by bichromatic wave groups. *Coastal Engineering*, 39(2-4):213–242.

Battjes, J. A. (2004). Shoaling of subharmonic gravity waves. *Journal of Geophysical Research*, 109(C2):1–15.

Benassai, G., Aucelli, P., Budillon, G., De Stefano, M., Di Luccio, D., Di Paola, G., Montella, R., Mucerino, L., Sica, M., and Pennetta, M. (2017). Rip current evidence by hydrodynamic simulations, bathymetric surveys and uav observation. *Nat. Hazards Earth Syst. Sci*, 17:1493–1503.

Bertin, X., de Bakker, A., van Dongeren, A., Coco, G., André, G., Ardhuin, F., Bonneton, P., Bouchette, F., Castelle, B., Crawford, W. C., Davidson, M., Deen, M., Dodet, G., Guérin, T., Inch, K., Leckler, F., McCall, R., Muller, H., Olabarrieta, M., Roelvink, D., Ruessink, G., Sous, D., Stutzmann, É., and Tissier, M. (2018). Infragravity waves: From driving mechanisms to impacts. *Earth-Science Reviews*, 177(June 2017):774–799.

Biésel, F. (1952). Equations générales au second ordre de la houle irrégulière. General 2nd order equations of irregular waves. *La Houille Blanche*, (3).

Booij, N., Holthuijsen, L., and Ris, R. (2015). The "Swan" Wave Model for Shallow Water. pages 668–676.

Bosboom, J. and Stive, M. (2011). *Coastal Dynamics : Part 1 (version 2011-0.2)*, volume Part 1 (version 2011-0.2). VSSD. Lecture Notes CT4305.

Bouwer, L. M., Bubeck, P., and Aerts, J. C. J. H. (2010). Changes in future flood risk due to climate and development in a Dutch polder area. *Global Environmental Change*, 20(3):463–471.

Bouziotas, D. (2016). Upscaling coastal flood risk assessment. (April).

Caires, S. (2011). Extreme Value Analysis : Wave Data. *Joint WMO/IOC Technical Commission for Oceanography and Marine Meteorology (JCOMM) Technical Report 57 (2011)*, (57):33.

Cammerer, H., Thieken, A. H., and Lammel, J. (2013). Adaptability and transferability of flood loss functions in residential areas. *Natural Hazards and Earth System Sciences*, 13(11):3063–3081.

Candela, J., Mazzola, S., Sammari, C., Limeburner, R., Lozano, C. J., Patti, B., and Bonanno, A. (2002). The â€œMad Seaâ€ Phenomenon in the Strait of Sicily. *Journal of Physical Oceanography*, 29(9):2210–2231.

Cannon, T. (2000). Vulnerability analysis and disasters. *Floods*, 1:45–55.

Carey, J. M. and Burgman, M. A. (2008). Linguistic uncertainty in qualitative risk analysis and how to minimize it. *Annals of the New York Academy of Sciences*, 1128(1):13–17.

Cea, L. and French, J. R. (2012). Bathymetric error estimation for the calibration and validation of estuarine hydrodynamic models. *Estuarine, Coastal and Shelf Science*, 100:124–132.

Chilunga, F. P., Rodriguez-Llanes, J. M., and Guha-Sapir, D. (2017). Rapid urbanization is linked to flood lethality in the small island developing states (sids): A modeling study. *Prehospital and Disaster Medicine*, 32(S1):S190–S190.

Colby, J. D. and Dobson, J. G. (2010). Flood modeling in the coastal plains and mountains: Analysis of terrain resolution. *Natural Hazards Review*, 11(1):19–28.

Cook, A. and Merwade, V. (2009). Effect of topographic data, geometric configuration and modeling approach on flood inundation mapping. *Journal of Hydrology*, 377(1-2):131–142.

Curray, J. (1964). Transgressions and regressions. *In Miller, R.L. eds, Marine Geology*, pages 175–203.

de Moel, H. (2012). *Uncertainty in Flood Risk*. Phd thesis, Vrije Universiteit Amsterdam.

De Moel, H., Asselman, N. E., and Aerts, J. C. (2012). Uncertainty and sensitivity analysis of coastal flood damage estimates in the west of the Netherlands. *Natural Hazards and Earth System Science*, 12(4):1045–1058.

De Moel, H., Bouwer, L. M., and Aerts, J. C. (2014). Uncertainty and sensitivity of flood risk calculations for a dike ring in the south of the Netherlands. *Science of the Total Environment*, 473-474:224–234.

de Moel, H., Jongman, B., Kreibich, H., Merz, B., Penning-Rowsell, E., and Ward, P. J. (2015). Flood risk assessments at different spatial scales. *Mitigation and Adaptation Strategies for Global Change*, 20(6):865–890.

de Ridder, M. (2018). Non-hydrostatic wave modelling of coral reefs with the addition of a porous in- canopy model. page 156.

Egorova, R., van Noortwijk, J. M., and Holterman, S. R. (2008). Uncertainty in flood damage estimation. *International Journal of River Basin Management*, 6(2):139–148.

ESRI (2014). Arcgis desktop: release 10. Redlands, CA: Environmental Systems Research Institute.

Frigerio, S., Bianchizza, C., Schenato, L., and Del Bianco, D. (2017). A mobile application to engage citizens and volunteers. Crowdsourcing within natural hazard. *Rendiconti Online Societa Geologica Italiana*, 42:70–72.

Fund, I. M. (2018). World economic outlook database april 2018.

GFDRR The World Bank (2014). Understanding Risk in an Evolving World: A Policy Note. *World Bank Publications*, pages 1–15.

GFDRR; The World Bank; ISDR (2016). Bringing resilience to scale. *Global Facility for Disaster Reduction and Recovery*, (1):1–5.

Giardino, A., Vandebroek, E., Torres Duenas, L., Ottow, B., and Pronker, J. (2018). Geomorphology, coastal dynamics, and adaptation options for eight coastal communities in São Tomé and Príncipe -Field Visit Report.

Gorokhovich, Y. and Voustianiouk, A. (2006). Accuracy assessment of the processed SRTM-based elevation data by CGIAR using field data from USA and Thailand and its relation to the terrain characteristics. *Remote Sensing of Environment*, 104(4):409–415.

Groffman, P. M., Baron, J. S., Blett, T., Gold, A. J., Goodman, I., Gunderson, L. H., Levinson, B. M., Palmer, M. A., Paerl, H. W., Peterson, G. D., et al. (2006). Ecological thresholds: the key to successful environmental management or an important concept with no practical application? *Ecosystems*, 9(1):1–13.

Guo, Q., Li, W., Yu, H., and Alvarez, O. (2013). Effects of Topographic Variability and Lidar Sampling Density on Several DEM Interpolation Methods. *Photogrammetric Engineering & Remote Sensing*, 76(6):701–712.

Hancock, G. (2006). The impact of different gridding methods on catchment geomorphology and soil erosion over long timescales using a landscape evolution model. *Earth Surface Processes and Landforms*, 31(8):1035–1050.

Hare, R., Eakins, B., and Amante, C. (2011). Modelling bathymetric uncertainty. *INTERNATIONAL HYDROGRAPHIC REVIEW*, 1(November):31–42.

Hashemi-Beni, L., Jones, J., Thompson, G., Johnson, C., and Gebrehiwot, A. (2018). Challenges and opportunities for uav-based digital elevation model generation for flood-risk management: A case of princeville, north carolina. *Sensors*, 18(11):3843.

Hawker, L., Rougier, J., Neal, J., Bates, P., Archer, L., and Yamazaki, D. (2018). Implications of Simulating Global Digital Elevation Models for Flood Inundation Studies. *Water Resources Research*, 54(10):7910–7928.

Helton, J. C. and Davis, F. J. (2003). Latin hypercube sampling and the propagation of uncertainty in analyses of complex systems. *Reliability Engineering & System Safety*, 81(1):23–69.

Hemer, M. A., Fan, Y., Mori, N., Semedo, A., and Wang, X. L. (2013). Projected changes in wave climate from a multi-model ensemble. *Nature climate change*, 3(5):471.

Heritage, G. L., Milan, D. J., Large, A. R., and Fuller, I. C. (2009). Influence of survey strategy and interpolation model on dem quality. *Geomorphology*, 112(3-4):334–344.

Hibiya, T. and Kajiura, K. (1982). Origin of the Abiki phenomenon (a kind of seiche) in Nagasaki Bay. *Journal of the Oceanographical Society of Japan*, 38(3):172–182.

Hinkel, J., Lincke, D., Vafeidis, A., Perrette, M., Nicholls, R., Tol, R., Marzeion, B., Fettweis, X., Ionescu, C., and Levermann, A. (2014). Coastal flood damage and adaptation costs under 21st century sea-level rise. *Proceedings of the National Academy of Sciences*, 111(9):3292–3297.

Hoeke, R. K., McInnes, K. L., Kruger, J. C., McNaught, R. J., Hunter, J. R., and Smithers, S. G. (2013). Widespread inundation of Pacific islands triggered by distant-source wind-waves. *Global and Planetary Change*, 108:128–138.

Holthuijsen, L. (2009). *Waves in oceanic and coastal waters*. Cambridge University Press.

Hongbo, W. (2014). Sids action platform: Third international conference on sids - mr. wu's blog on economic vulnerabilities. united nations - department of economic and social affairs (desa), september 2014.

Horan, R. D., Fenichel, E. P., Drury, K. L., and Lodge, D. M. (2011). Managing ecological thresholds in coupled environmental–human systems. *Proceedings of the National Academy of Sciences*, 108(18):7333–7338.

Hsu, Y.-C., Prinsen, G., Bouaziz, L., Lin, Y.-J., and Dahm, R. (2016). An investigation of dem resolution influence on flood inundation simulation. *Procedia Engineering*, 154:826–834.

Huizinga, J., de Meol, H., and Szewczyk, W. (2017). *Global flood depth-damage functions : Methodology and the Database with Guidelines*.

Hurtado, J. and Barbat, A. H. (1998). Monte carlo techniques in computational stochastic mechanics. *Archives of Computational Methods in Engineering*, 5(1):3.

INE (2012). Iv recenseamento geral da população e da habitação 2012 (iv rgph 2012). São Tomé e Príncipe: Instituto Nacional de Estatística (INE).

IPCC (2001). Climate change 2001: impacts, adaptation and vulnerability, technical summary. *Report of Working Group II of the IPCC, 13â€“16 February 2001*.

IPCC (2013). IPCC, 2013: climate change 2013: the physical science basis. *Contribution of working group I to the fifth assessment report of the intergovernmental panel on climate change*.

Jacobsen, K. (2005). Analyses of SRTM elevation models. *Proceedings of the EARSeL Workshop 3D-Remote Sensing*, (figure 1):10–11.

Jongman, B., Kreibich, H., Apel, H., Barredo, J. I., Bates, P. D., Feyen, L., Gericke, A., Neal, J., Aerts, J. C., and Ward, P. J. (2012). Comparative flood damage model assessment: Towards a European approach. *Natural Hazards and Earth System Science*, 12(12):3733–3752.

Jonkman, S. N., Bočkarjova, M., Kok, M., and Bernardini, P. (2008). Integrated hydrodynamic and economic modelling of flood damage in the Netherlands. *Ecological Economics*, 66(1):77–90.

Jonkman, S. N., Vrouwenvelder, A. C. W. M., Steenbergen, R. D. J. M., Morales-nápoles, O., and Vrijling, J. K. (2016). Probabilistic Design: Risk and Reliability Analysis in Civil Engineering. page 271.

Kaly, U., Pratt, C., Howorth, R., Pacific, S., and Geoscience, A. (2002). A framework for managing environmental vulnerability in small island developing states. 58:1–10.

Kelman, I. and West, J. J. (2009). Climate change and SIDS - a critical review. 5(1).

Kok, M., Huizinga, H. J., Vrouwenvelder, A., and Barendregt, A. (2005). Standaardmethode2004â€"Schade en Slachtoffers als gevolg van overstromingen. *HKV report PR999*, 10(november 2004).

Kron, W. (2005). Flood risk = hazard â€¢ values â€¢ vulnerability. *Water International*, 30(1):58–68.

Lashley, C. H., Roelvink, D., van Dongeren, A., Buckley, M. L., and Lowe, R. J. (2018). Nonhydrostatic and surfbeat model predictions of extreme wave run-up in fringing reef environments. *Coastal Engineering*, 137.

Leijnse, T. (2018). Computationally Efficient Modelling of Compound Flooding due to Tropical Cyclones with the Explicit Inclusion of Wave-Driven Processes Research into the required processes and the Computationally Efficient Modelling of Compound Flooding due to Tropical Cy. page 145.

Leitão, J. P., Moy de Vitry, M., Scheidegger, A., and Rieckermann, J. (2016). Assessing the quality of digital elevation models obtained from mini unmanned aerial vehicles for overland flow modelling in urban areas. *Hydrology and Earth System Sciences*, 20(4):1637–1653.

Leone, F., Lavigne, F., Paris, R., Denain, J. C., and Vinet, F. (2011). A spatial analysis of the December 26th, 2004 tsunami-induced damages: Lessons learned for a better risk assessment integrating buildings vulnerability. *Applied Geography*, 31(1):363–375.

Li, Z., Zhu, Q., and Gold, C. (2006). *Digital Terrain*.

Loucks, D. P. and Van Beek, E. (2017). *Water resource systems planning and management: An introduction to methods, models, and applications*. Springer.

MATLAB Mapping Toolbox (2018). Matlab mapping toolbox.

McGranahan, G., Balk, D., and Anderson, B. (2007). The rising tide: Assessing the risks of climate change and human settlements in low elevation coastal zones. *Environment and Urbanization*, 19(1):17–37.

McKay, M. D., Beckman, R. J., and Conover, W. J. (1979). Comparison of three methods for selecting values of input variables in the analysis of output from a computer code. *Technometrics*, 21(2):239–245.

Méheux, K., Dominey-Howes, D., and Lloyd, K. (2007). Natural hazard impacts in small island developing states: a review of current knowledge and future research needs. *Natural hazards*, 40(2):429–446.

Mercer, J., Kelman, I., Alfthan, B., and Kurvits, T. (2012). Ecosystem-based adaptation to climate change in caribbean small island developing states: integrating local and external knowledge. *Sustainability*, 4(8):1908–1932.

Merz, B., Kreibich, H., and Lall, U. (2013). Multi-variate flood damage assessment: a tree-based data-mining approach. *Natural Hazards and Earth System Sciences*, 13(1):53–64.

Merz, B., Kreibich, H., Schwarze, R., and Thieken, A. (2010). Review article" assessment of economic flood damage". *Natural Hazards and Earth System Sciences*, 10(8):1697–1724.

Merz, B., Kreibich, H., Thieken, A. H., and Schmidtke (2004). Estimation uncertainty of direct monetary flood damage to buildings. *Natural Hazards and Earth System Science*, 4(1):153–163.

Merz, B. and Thieken, A. H. (2009). Flood risk curves and uncertainty bounds. *Natural Hazards*, 51(3):437–458.

Merz, B., Thieken, A. H., and Gocht (2007). Flood risk mapping at the local scale: Concepts and challenges. *Advances in Natural and Technological Hazards Research*, 25:231–251.

Messner, F. and Meyer, V. (2005). Flood damage, vulnerability and risk perception â€“ challenges for flood damage research. In Schanze, J., Zemn, E., and Marsalek, J., editors, *Flood Risk Management â€“ Hazards, Vulnerability and Mitigation Measures*. Nato scien edition.

Mitrovica, J. and Milne, G. (2002). On the origin of late holocene sea-level highstands within equatorial ocean basins. *Quaternary Science Reviews*, 21(20):2179 – 2190.

Molinari, D., De Bruijn, K. M., Castillo-Rodríguez, J. T., Aronica, G. T., and Bouwer, L. M. (2019). Validation of flood risk models: Current practice and possible improvements. *International Journal of Disaster Risk Reduction*, 33(October 2018):441–448.

Monioudi, I. N., Asariotis, R., Becker, A., Bhat, C., Dowding-Gooden, D., Esteban, M., Feyen, L., Mentaschi, L., Nikolaou, A., Nurse, L., et al. (2018). Climate change impacts on critical international transportation assets of caribbean small island developing states (sids): the case of jamaica and saint lucia. *Regional environmental change*, 18(8):2211–2225.

Moore, W. R. (2010). The impact of climate change on caribbean tourism demand. *Current Issues in Tourism*, 13(5):495–505.

Morss, R. E., Wilhelmi, O. V., Downton, M. W., and Gruntfest, E. (2005). Flood risk, uncertainty, and scientific information for decision making: lessons from an interdisciplinary project. *Bulletin of the American Meteorological Society*, 86(11):1593–1602.

Muis, S., Verlaan, M., Winsemius, H. C., Aerts, J. C. J. H., and Ward, P. J. (2016). A global reanalysis of storm surges and extreme sea levels. *Nature Communications*, 7(May):1–11.

Munk, W. H. (1949). Surf beats. *Transactions, American Geophysical Union*, 30(6):849.

Nicholls, R., Hanson, S., Herweijer, C., Patmore, N., Hallegatte, S., Corfee-Morlot, J., Château, J., and Muir-Wood, R. (2007). Ranking port cities with high exposure and vulnerability to climate extremes: exposure estimates. *OECD Environment Working Papers, No 1*, (December):14–16.

Nichols, M. M. (1989). Sediment accumulation rates and relative sea-level rise in lagoons. *Marine Geology*, 88(3-4):201–219.

OECD World Bank (2016). Climate and Disaster Resilience Financing in Small Island Developing States. *A report jointly authored by the Organization for Economic Cooperation and Development (OECD) and the Small Island States Resilience Initiative (SISRI) team in the Climate Change Group of the World Bank.*, page 76.

Olsen, A. S., Zhou, Q., Linde, J. J., and Arnbjerg-Nielsen, K. (2015). Comparing methods of calculating expected annual damage in urban pluvial flood risk assessments. *Water*, 7(1):255–270.

O'Neill, B. C., Kriegler, E., Ebi, K. L., Kemp-Benedict, E., Riahi, K., Rothman, D. S., van Ruijven, B. J., van Vuuren, D. P., Birkmann, J., Kok, K., Levy, M., and Solecki, W. (2017). The roads ahead: Narratives for shared socioeconomic pathways describing world futures in the 21st century. *Global Environmental Change*, 42:169–180.

OpenEarthTools (2013). Deltares public wiki openearth.

OpenStreetMap contributors (2017). Planet dump retrieved from https://planet.osm.org . https://www.openstreetmap.org.

Paprotny, D., Morales-Nápoles, O., Vousdoukas, M. I., Jonkman, S. N., and Nikulin, G. (2019). Accuracy of pan-european coastal flood mapping. *Journal of Flood Risk Management*, 12(2):e12459.

Parsons, M., Bratanov, D., Gaston, K., and Gonzalez, F. (2018). Uavs, hyperspectral remote sensing, and machine learning revolutionizing reef monitoring. *Sensors*, 18(7):2026.

Paulik, R., Smart, G., Turner, R., and Bind, J. (2015). Development of preliminary depth-damage functions for samoa buildings. *National Institute of Water and Atmospheric Research*.

Pearson, S. (2016). Predicting wave-induced flooding on low-lying tropical islands using a Bayesian network. page 232.

Pearson, S. G., Storlazzi, C. D., van Dongeren, A. R., Tissier, M. F., and Reniers, A. J. (2017). A Bayesian-Based System to Assess Wave-Driven Flooding Hazards on Coral Reef-Lined Coasts. *Journal of Geophysical Research: Oceans*, 122(12):10099–10117.

Pelling, M. and Uitto, J. I. (2001). Small island developing states: natural disaster vulnerability and global change. *Global Environmental Change Part B: Environmental Hazards*, 3(2):49–62.

Penning-rowsell, E. C. (2004). Evaluating flood damages : guidance and recommendations on principles and methods. (January).

Phillips, J. D. (2003). Sources of nonlinearity and complexity in geomorphic systems. *Progress in Physical Geography*, 27(1):1–23.

Pickands, J. (1975). Statistical inference using extreme order statistics. *The Annals of Statistics*, 15(4):1580–1592.

Pidgeon, N. and Fischhoff, B. (2011). The role of social and decision sciences in communicating uncertain climate risks. *Nature climate change*, 1(1):35.

Plant, N. G. and Holland, K. T. (2011a). Prediction and assimilation of surf-zone processes using a bayesian network: Part i: Forward models. *Coastal engineering*, 58(1):119–130.

Plant, N. G. and Holland, K. T. (2011b). Prediction and assimilation of surf-zone processes using a Bayesian network. Part II: Inverse models. *Coastal Engineering*, 58(3):256–266.

Plant, N. G., Holland, K. T., and Puleo, J. A. (2002). Analysis of the scale of errors in nearshore bathymetric data. *Marine Geology*, 191(1-2):71–86.

Prahl, B. F., Rybski, D., Boettle, M., and Kropp, J. P. (2016). Damage functions for climate-related hazards: Unification and uncertainty analysis. *Natural Hazards and Earth System Sciences*, 16(5):1189–1203.

Purvis, M. J., Bates, P. D., and Hayes, C. M. (2008). A probabilistic methodology to estimate future coastal flood risk due to sea level rise. *Coastal engineering*, 55(12):1062–1073.

Ramirez, J. A., Lichter, M., Coulthard, T. J., and Skinner, C. (2016). Hyper-resolution mapping of regional storm surge and Tide Flooding : Comparison of Static and Dynamic Models. *Natural Hazards*, 82(1):571–590.

Reese, S., Bradle, B., Bind, J., SMart, G., Power, W., and Sturman, J. (2011). Empirical building fragilities from observed damage in the 2009 South Pacific tsunami. *Earth-Science Reviews*, 107(1-2):156–173.

Regan, H. M., Colyvan, M., and Burgman, M. A. (2002). A taxonomy and treatment of uncertainty for ecology and conservation biology. *Ecological Applications*, 12(2):618–628.

Riahi, K., van Vuuren, D. P., Kriegler, E., Edmonds, J., O'Neill, B. C., Fujimori, S., Bauer, N., Calvin, K., Dellink, R., Fricko, O., Lutz, W., Popp, A., Cuaresma, J. C., KC, S., Leimbach, M., Jiang, L., Kram, T., Rao, S., Emmerling, J., Ebi, K., Hasegawa, T., Havlik, P., HumpenÃ¶der, F., Silva, L. A. D., Smith, S., Stehfest, E., Bosetti, V., Eom, J., Gernaat, D., Masui, T., Rogelj, J., Strefler, J., Drouet, L., Krey, V., Luderer, G., Harmsen, M., Takahashi, K., Baumstark, L., Doelman, J. C., Kainuma, M., Klimont, Z., Marangoni, G., Lotze-Campen, H., Obersteiner, M., Tabeau, A., and Tavoni, M. (2017). The shared socioeconomic pathways and their energy, land use, and greenhouse gas emissions implications: An overview. *Global Environmental Change*, 42:153–168.

Roelvink, D., McCall, R., Mehvar, S., Nederhoff, K., and Dastgheib, A. (2018). Improving predictions of swash dynamics in XBeach: The role of groupiness and incident-band runup. *Coastal Engineering*, 134(February):103–123.

Roelvink, D., van Dongeren, A., McCall, R., Hoonhout, B., van Rooijen, A., van Geer, P., de Vet, L., Nederhoff, K., and Quataert, E. (2015). XBeach Technical Reference: Kingsday Release. page 141.

Roelvink J.A. (2009). XBeach : Non-hydrostatic model.

Saksena, S. and Merwade, V. (2015). Incorporating the effect of dem resolution and accuracy for improved flood inundation mapping. *Journal of Hydrology*, 530:180–194.

Saltelli, A., Ratto, M., Andres, T., Campolongo, F., Cariboni, J., Gatelli, D., Saisana, M., and Tarantola, S. (2008). *Global sensitivity analysis: the primer*. John Wiley & Sons.

Scawthorn, C., Flores, P., Blais, N., Seligson, H., Tate, E., Chang, S., Mifflin, E., Thomas, W., Murphy, J., Jones, C., and Lawrence, M. (2006). HAZUS-MH Flood Loss Estimation Methodology. II. Damage and Loss Assessment. *Natural Hazards Review*, 7(2):72–81.

Schnebele, E., Cervone, G., and Waters, N. (2014). Road assessment after flood events using non-authoritative data. *Natural Hazards and Earth System Sciences*, 14(4):1007–1015.

Schröter, K., Kreibich, H., Vogel, K., Riggelsen, C., Scherbaum, F., and Merz, B. (2014). How useful are complex flood damage models? *Water Resources Research*, 50(4):3378–3395.

Schultz, M. T., Gouldby, B. P., Simm, J. D., and Wibowo, J. L. (2010). Beyond the Factor of Safety : Developing Fragility Curves to Characterize System Reliability Geotechnical and Structures Laboratory Beyond the Factor of Safety : Developing Fragility Curves to Characterize System Reliability. (July).

Short, A. (2005). Sandy coasts. *in Schwartz , M.L ed. Encyclopedia of Coastal Science*.

Sobol, I. M. (2001). Global sensitivity indices for nonlinear mathematical models and their monte carlo estimates. *Mathematics and computers in simulation*, 55(1-3):271–280.

Steetzel, H. (1993). Crossh-shore Transport during Storm Surges.

Stockdon, H. F., Holman, R. A., Howd, P. A., and Sallenger, A. H. (2006). Empirical parameterization of setup, swash, and runup. *Coastal Engineering*, 53(7):573–588.

Storlazzi, C. D., Gingerich, S. B., Van Dongeren, A., Cheriton, O. M., Swarzenski, P. W., Quataert, E., Voss, C. I., Field, D. W., Annamalai, H., Piniak, G. A., and McCall, R. (2018). Most atolls will be uninhabitable by the mid-21st century because of sea-level rise exacerbating wave-driven flooding. *Science Advances*, 4(4):1–10.

Sweet, W. V. and Park, J. (2014). From the extreme to the mean: Acceleration and tipping points of coastal inundation from sea level rise. *Earth's Future*, 2(12):579–600.

Symonds, G., Huntley, D. A., and Bowen, A. J. (1982). Two-dimensional surf beat: long wave generation by a time-varying breakpoint. *Journal of Geophysical Research*, 87(C1):492–498.

Tamminga, A. D., Eaton, B. C., and Hugenholtz, C. H. (2015). Uas-based remote sensing of fluvial change following an extreme flood event. *Earth Surface Processes and Landforms*, 40(11):1464–1476.

Tarbotton, C., Dall'Osso, F., Dominey-Howes, D., and Goff, J. (2015). The use of empirical vulnerability functions to assess the response of buildings to tsunami impact: Comparative review and summary of best practice. *Earth-Science Reviews*, 142:120–134.

Tauro, F., Porfiri, M., and Grimaldi, S. (2016). Surface flow measurements from drones. *Journal of Hydrology*, 540:240–245.

Thompson, K. M. (2002). Variability and uncertainty meet risk management and risk communication. *Risk Analysis*, 22(3):647–654.

Tucker, M. (1950). Surf beats: sea waves of 1 to 5 min. period. *Proceedings of the Royal Society of London. Series A, Mathematical and Physical Sciences*, 202(1071):565–573.

UN-OHRLLS (2015). Small Island Developing States In Numbers: Climate Change Edition 2015. page 41.

UNISDR (2016). Report of the open-ended intergovernmental expert working group on indicators and terminology relating to disaster risk reduction. *United Nations General Assembly*, 41(December):1–44.

Uusitalo, L., Lehikoinen, A., Helle, I., and Myrberg, K. (2015). An overview of methods to evaluate uncertainty of deterministic models in decision support. *Environmental Modelling and Software*, 63:24–31.

Van de Sande, B., Lansen, J., and Hoyng, C. (2012). Sensitivity of coastal flood risk assessments to digital elevation models. *Water (Switzerland)*, 4(3):568–579.

van Vuuren, D. P., Edmonds, J., Kainuma, M., Riahi, K., Thomson, A., Hibbard, K., Hurtt, G. C., Kram, T., Krey, V., Lamarque, J. F., Masui, T., Meinshausen, M., Nakicenovic, N., Smith, S. J., and Rose, S. K. (2011). The representative concentration pathways: An overview. *Climatic Change*, 109(1):5–31.

Vogel, K., Riggelsen, C., Korup, O., and Scherbaum, F. (2014). Bayesian network learning for natural hazard analyses. *Natural Hazards and Earth System Sciences*, 14(9):2605–2626.

Voice, M., Harvey, N., Walsh, K., et al. (2006). Vulnerability to climate change of australia's coastal zone: Analysis of gaps in methods, data and system thresholds. *Report to the Australian Greenhouse Office, Canberra, Australia*.

Vojinovic, Z., Ediriweera, J. C. W., and Fikri, A. K. (2008). An approach to the model-based spatial assessment of damages caused by urban floods. *11th International Conference on Urban Drainage*, (1977):1–10.

Vousdoukas, M., Voukouvalas, E., Verlaan, M., and Feyen, L. (2016). Extreme sea level - rcp45 and rcp85. European Commission, Joint Research Centre (JRC), http://data.europa.eu/89h/e9e42344-119d-479e-9bc7-57400d12a8a2.

Vousdoukas, M. I., Bouziotas, D., Giardino, A., Bouwer, L. M., Mentaschi, L., Voukouvalas, E., and Feyen, L. (2018a). Understanding epistemic uncertainty in large-scale coastal flood risk assessment for present and future climates. *Natural Hazards and Earth System Sciences*, 18(8):2127–2142.

Vousdoukas, M. I., Mentaschi, L., Voukouvalas, E., Verlaan, M., Jevrejeva, S., Jackson, L. P., and Feyen, L. (2018b). Global probabilistic projections of extreme sea levels show intensification of coastal flood hazard. *Nature Communications*, 9(1):1–12.

Wagenaar, D. J., De Bruijn, K. M., Bouwer, L. M., and De Moel, H. (2016). Uncertainty in flood damage estimates and its potential effect on investment decisions. *Natural Hazards and Earth System Sciences*, 16(1):1–14.

Wahl, T., Haigh, I. D., Nicholls, R. J., Arns, A., Dangendorf, S., Hinkel, J., and Slangen, A. B. (2017). Understanding extreme sea levels for broad-scale coastal impact and adaptation analysis. *Nature Communications*, 8(May):1–12.

Weatherall, P., Marks, K. M., Jakobsson, M., Schmitt, T., Tani, S., Arndt, J. E., Rovere, M., Chayes, D., Ferrini, V., and Wigley, R. (2015). Earth and Space Science.

Wechsler, S. P. and Kroll, C. N. (2006). Quantifying dem uncertainty and its effect on topographic parameters. *Photogrammetric Engineering & Remote Sensing*, 72(9):1081–1090.

Weng, Q. (2002). Quantifying Uncertainty of Digital Elevation Models Derived from Topographic Maps. *Advances in Spatial Data Handling*, pages 403–418.

White, I. and Falkland, T. (2010). Management of freshwater lenses on small pacific islands. *Hydrogeology Journal*, 18(1):227–246.

Yamazaki, D., Ikeshima, D., Tawatari, R., Yamaguchi, T., O'Loughlin, F., Neal, J. C., Sampson, C. C., Kanae, S., and Bates, P. D. (2017). A high-accuracy map of global terrain elevations. *Geophysical Research Letters*, 44(11):5844–5853.

A

XBeach Setup Preliminary Tests

A.1. Model setup & Sensitivity

In this XBeach setup, an added hydrostatic layer (XBNH+) is used to improve the dispersive behaviour of the model, so that the non-hydrostatic model can start in larger water depths. For this primary analysis, this reduced 2-layer model was used as it is expected to give the most accurate results compared to other modes (de Ridder, 2018). However, offshore boundary point at larger depths has the effect of increasing the length of the computational grid, and thus the model run times. Therefore, model parameters that could reduce the number of grid cells were also tested.

All the transects for each community are subjected to the same forcing, coming from the wave analysis (see Section3.5). For all the communities, the average significant wave height is 120 cm, with very little variation. This primary sensitivity analysis has a twofold purpose: to identify the parameters to which the modeled coastal flooding hazard is most sensitive to and to identify a model setup that reduces the computational expense as much as possible without sacrificing too much accuracy in the predictions. Moreover, this primary analysis was used to see whether there are large differences in the outputs from the different transects within the communities. Several parameters were considered as they were recognized as most important from literature and previous studies (Lashley et al., 2018), (Pearson, 2016), (Roelvink et al., 2018), which identified grid spacing as one of the most important parameters in the model, both for computational expense and for predictive accuracy. The table shows the parameters and the purpose of the analysis for each one of them.

The range of values for the significant wave height (H_s) and water level are justified by the 99th percentile confidence interval of their cdf. Indeed a 15% variation for H_s yields to values that are at the boundaries of the 99% confidence interval (see Figure 4.2 and Figure 4.3). The values for the Jonswap spectrum peakedness factor ($\gamma_{JONSWAP}$) are taken

A

Table A.1: Parameters included in the XBeach primary sensitivity analysis.

Parameters	Range of values	Purpose
Significant wave height	± 15% from reference value	Hazard sensitivity
Water level	100 -110 -120 [cm]	Hazard sensitivity
Chezy bed friction coefficient	20 - 55 - 70 [$m^{0.5}/s$]	Hazard sensitivity
Jonswap spectrum peakedness	2 - 3.3 - 7 [/]	Hazard sensitivity
Storm length	3-6 [hours]	Hazard sensitivity & reduce computational expense
grid points per wave length	40-45-50	Reduce computational expense

arbitrarily within the possible range, Chezy bed friction coefficient values are chosen arbitrarily within the range in the XBeach manual, where 55 is the default value (Roelvink et al., 2015). Only a maximum of 6 hour storm length was modeled as modeling longer storm periods would have not been feasible computationally, as the goal was to run a large number of simulations. A 6 hour storm on average takes approximately 1 hour to run, longer run times would make a sensitivity analysis with multiple runs unfeasible. Another condition that was tested is the shape of the storm. Initially, storms with a total length of three hours were modeled. This means that the water level begins to increase due to the tide and storm surge at the beginning of the simulation, starting from the mean sea level (MSL), and it decreases back to MSL towards the end of the storm. This was later considered potentially unrealistic, therefore model runs with a different time distribution of the storm were also compared. This comparison was only made for 6 hours storms where the 6 hours of simulation represent the peak of a longer period storm (24 hours), therefore at the beginning of the simulation the water level are already very close to the peak. Such an approach may lead to an underestimation of the flooding, since the whole 24 hours of the storm are not modeled. Nevertheless, the peak hours would lead to the majority of the flooding and this assumption was considered necessary to run a large number of simulations. The results of the comparison between the different scenarios is based on the runup, which is represented by the $R_{2\%}$, the runup value which is exceeded only 2 percent of the times. To reduce the number of simulations, the analysis on storm length, type of forcing and bed friction was done only for some location and certain transects.

The parameter *grid points per wave length* (PPWL) was included in the analysis for a different reason. This is a model parameter that determines the number of grid points used to model the wavelength of the peak period wave. For the study case, PPWL was set to 50 points. In combination with *dxmin* (minimum grid size) and *vardx* (boolean parameter for varying grid size), PPWL determines the number of grid cells and thus influences the computational time. The parameter *dxmin* was set equal to 1 as this has been proven to give a sufficient amount of modeling accuracy (Roelvink et al., 2018), (Pearson et al., 2017)and to accurately model waves. *Vardx* was set to 1, indicating a varying grid size. This allows the model to find the optimum cell size according to the cross-shore position, larger cell sizes for more offshore points where less computational accuracy is required

and decreasing as the grid moves onshore.

PPWL was tested comparing simulations with values set to 40, 45 and 50. The number of grid cells, a proxy to estimate the computational expense of the model, for the different PPWL values is shown in Table A.2. The comparison was based on the offshore significant wave height and nearshore, at a water depth of approximately -2 m.

Table A.2: Number of grid points for different PPWL inputs for one transect in Praia Abade.

Input	Number of grid points	Computational time for a 3 hour storm
50 PPWL	1150	30 min
45 PPWL	1062	27 min
40 PPWL	977	24min

A.2. RESULTS

A.2.1. GRID SENSITIVITY

To assess whether the reduction of grid points would still give reliable result, the offshore wave height and the runup to offshore wave height ratio were used to compare the different scenarios. The results are shown in Table A.3 below for two transects of Praia Melao and indicate how there is a very little change in the runup prediction of the model to PPWL. Therefore, for the larger sensitivity analysis, the grid spacing will be use as input 40 PPWL. At the same time, there is some discrepancy with the modeled offshore significant wave height. Indeed, for all the transects, the 50 PPWL scenario gives a lower value compared to the other two. Nevertheless, this value is generally smaller than what given as input from the Jonswap spectrum file (1.35m), which means that the other two scenarios (40 and 45 PPWL), are better at simulating the offshore wave height.

Table A.3: Model comparison for the different PPWL input scenarios.

Transect #1	Offshore H_s [m]	$R_{2\%}/H_{s_{off}}$	Transect #2	Offshore H_s [m]	$R_{2\%}/H_{s_{off}}$
50 PPWL	1.30	1.43	50 PPWL	1.31	1.36
45 PPWL	1.36	1.40	45 PPWL	1.36	1.38
40 PPWL	1.35	1.44	40 PPWL	1.36	1.33

A.2.2. PRIMARY SENSITIVITY

The following results indicate how sensitive are the runup and overtopping to changes in the input parameters introduced before. First, the model runs for the different transect in each location showed very little variation in the output. Indeed, in each community, the forcing to each transect is identical and the bathymetry does not vary much. Considering this, in the following larger sensitivity analysis, only one transect per each community will be considered.

The comparison and visualization is made through tables where the reference case is compared to its lower and higher counterparts. The results from each transect are aver-

aged, in order to have a single value per scenarios. For each location, the impacts on the coastal flooding given by the different parameters are compared between each other. More intense red and green colours represent larger differences (see Figure A.1). For Praia Abade, the comparison was made through the overtopping volume, measured as the amount of water flowing past the highest point on the profile. This different comparison was necessary because of the very low topography of this community where many waves overtop and make the measurement of runup at the beach not representative for the flooding.

In the tables included in Figure A.1 below it can be seen how for all the locations, the influence of $\gamma_{JONSWAP}$ is strongly limited. Both the significant wave height and the water levels show larger influence, especially in Praia Abade, the most flooding prone community. Significant wave height has the largest impact on all communities except for Pantufo, where water level has a slightly larger influence.

Praia Abade	Hs	Water level	$\gamma_{jonswap}$
small	0,56	0,70	1,04
reference	1	1	1
large	1,40	2,11	0,99

Pantufo	Hs	Water level	$\gamma_{jonswap}$
small	0,95	0,90	1,02
reference	1	1	1
large	1,03	1,11	0,98

Micolo	Hs	Water level	$\gamma_{jonswap}$
small	0,90	0,95	0,96
reference	1	1	1
large	1,07	1,00	1,02

Praia Melao	Hs	Water level	$\gamma_{jonswap}$
small	0,90	0,95	1,02
reference	1	1	1
large	1,08	1,05	1,01

Figure A.1: Tables showing the results from the sensitivity analysis for each location on significant wave height, water levels and the peakedness of the Jonswap spectrum, compared to the reference scenario.

The impact of bed friction is almost negligible. Indeed, the largest change given from varying this parameter is approximately 2% percent different from the reference case with the default value. This may be due to the steepness of the beach profile, which could mean that most of the wave energy dissipation is through breaking and bottom friction has a very low impact on wave energy. Also, bottom friction is a dominant factor for reef and rocky coastlines, where the roughness of the bed can have a very large impact in dissipating wave energy, on sandy coastlines the hydrodynamic roughness of the bed and its frictional dissipation of wave energy are reduced.
The shape and the length of the storm strongly influences the flooding. In Table A.4 below it can be seen how, simulating 6 hours of storm yields much larger volumes of flooding, generally more than a factor 2 if compared to a storm length of only 3 hours. The results are only shown for the transect where some overtopping occurred. At the same time, simulating only the peak of a storm with approximately a constant forcing in the water levels and wave heights also generates larger amounts of overtopping.

Table A.4: Overtopping volumes throughout the whole storm in m3/m Simulation comparison for storm of 3 and 6 hours.

transect	3 hours storm m^3/m	6 hours storm m^3/m
Praia Melao #1	3	8
Pantufo #1	3	6
Micolo #1	1	5
Praia Abade #1	23	70
Praia Abade #2	144	438

To better assess the relation between the modeled storm length and the amount of overtopping, a set of different simulations with varying storm length from 2 to 6 hours was run. The forcing was made constant for the whole duration of the storm, to understand and search for possible non linear behaviours of the model in reproducing the water level oscillations. Five runs were made (2-3-4-5-6 hours storms) and the results are shown in Figure A.2. As it can be seen, with a constant forcing, the relation between overtopping and modeled storm length is approximately linear. This means that, at first analysis, non-linear behaviour are not particularly strong.

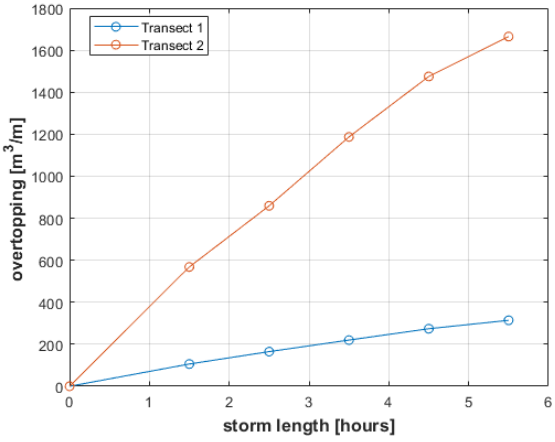

Figure A.2: Computed overtopping under constant forcing conditions for the two transects at Praia Abade.

Given the primary sensitivity results, only the communities of Pantufo and Praia Abade have shown some coastal flooding, therefore only these two will be included in the hinterland flood modeling with SFINCS. Moreover, all the locations have shown very little variation in the model outputs between the different transects, thus, for the larger sensitivity analysis, only one transect per community will be considered. The inputs significant wave height and water level have proven to be the ones to which the flooding is most sensitive to and will be the only one included in the larger sensitivity. In order to represent a more realistic storm, for future XBeach simulations, the modeled length will be of 6 hours, with a storm shape derived from (Steetzel, 1993). The total storm length is assumed to be 24 hours, but only the peak central 6 hours are modeled, as they are

expected to give the largest contribution to the flooding. Figure A.3 shows the hydrographs for the 24 hours storm. Only the hours from 9 to 15 are modeled. Both the significant wave height and peak period distributions during the storm are discretized into bins of single hours, during which the offshore forcing is constant.

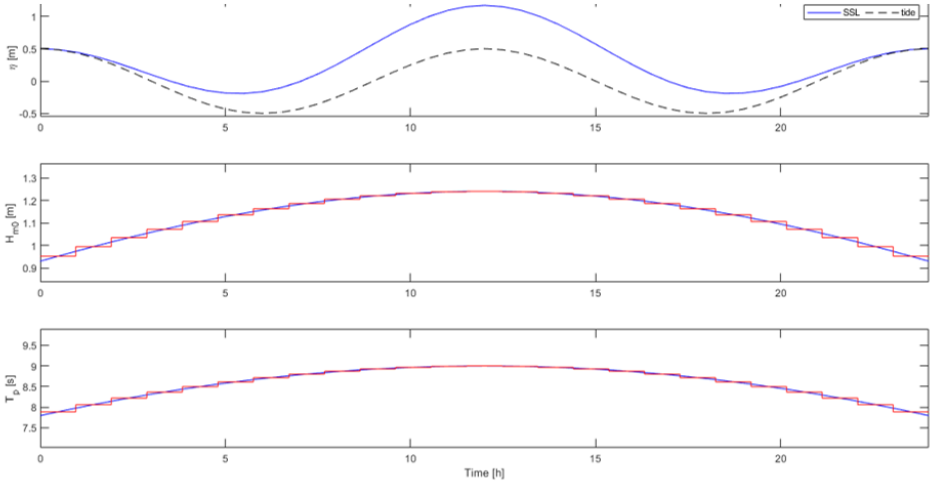

Figure A.3: Modeled water levels significant wave height and wave peak period for coastal storms.

B

SFINCS AND DEMS SET UP AND PRIMARY ANALYSIS

B.1. SFINCS SET UP AND PRIMARY ANALYSIS

The sensitivity for the input parameters of the SFINCS model directly follows the result of the sensitivity on the XBeach outputs. Only the runs varying the parameters identified as most sensitive in the previous section were carried forward and used as input for SFINCS. As explained in Section 3, SFINCS takes the water level time series from the XBeach runs at a water depth of approximately -2 m, therefore before most of the wave breaking has occurred. In conclusion, wave height, storm length, storm shape, storm surge height were considered for the sensitivity from the hydrodynamic forcing in SFINCS. Nevertheless, the output of SFINCS also relies on the elevation grid, which is retrieved from elevation models. To test how the model responds to different elevation inputs, the drone images were compared with the DEm TerraSar-X in Pantufo and SRTM in Praia Abade.

Looking at the preliminary results of the storm surge impact, very little flooding occurs for the two locations of Micolo and Praia Melao, even at much larger water levels. For this reason, the two locations were discarded from the analysis and only the locations of Pantufo and Praia Abade were considered. This choice is also supported from the XBeach simulation results, which showed that Praia Melao and Micolo would not experience overtopping during the storms.

B.1.1. SFINCS PRIMARY SENSITIVITY

Before addressing the results, is important to remember that these simulations were run with a storm length of only 3 hours as reference case, in order to reduce the computational time, whereas in the global analysis, the simulated storm is of six hours.
The maps shown in Figure B.1 illustrate the maximum water depth during the storm for each grid cell. This is the reference case, for the 100 years return period wave height and

water level, with no variation in the input parameter. As it can be seen, Pantufo experiences very little flooding, on the right of the maps where some houses are located. In the case of Praia Abade, a larger volume of flooding occurs, this is due to the lower mean elevation of this community.

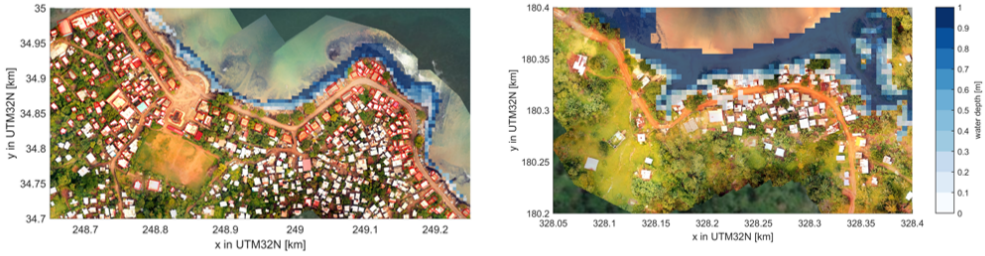

Figure B.1: Maximum computed inundation depths for Pantufo (left) and Praia Abade (right), for the reference scenario.

As it can be expected, larger water levels and significant wave height contribute to larger flooding extent. This is shown in Figure B.2 where the results for increased water level for both the locations are shown. Once again, it is possible to notice how Praia Abade is more sensitive to changes than Pantufo, being more prone to flooding. With the increased water level Pantufo also experiences more flooding, although this is largely limited to some houses on the headland, visible on the map.

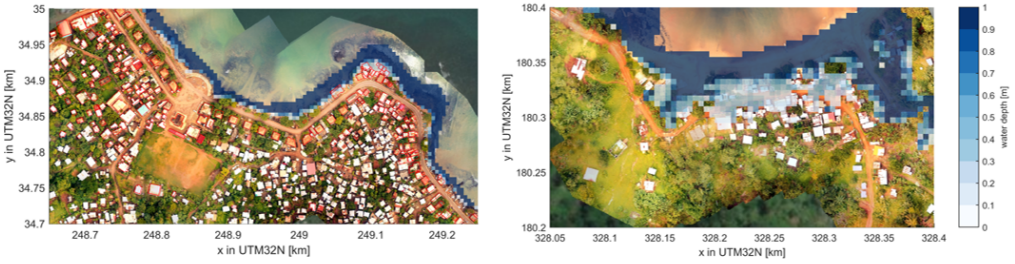

Figure B.2: Maximum computed inundation depths for Pantufo (left) and Praia Abade (right), for the increased water level scenario.

If, instead of a three hours storm, one of six hours is simulated, the flooding in Pantufo increases, although the sensitivity is not too high, see Figure B.3.

With SFINCS it was possible to start testing the impact of different elevation models. For Pantufo, TerraSar data was available and in Figure B.4 is compared with the drone map. The much higher resolution is clearly visible in the drone image. Regarding Praia Abade, unfortunately the TerraSar-X was not available and data from the SRTM had to be used. The quality of the data is very low and shows a lot of discrepancy with the

Figure B.3: Maximum computed inundation depths for Pantufo for a storm of six hours.

drone image (see Figure B.5). The elevation from TerraSar-X is generally smoother and less detailed. Another distinguished feature is the generally lower elevation model by TerraSar-X, especially on the western side of the coastal community (the darker blue area).

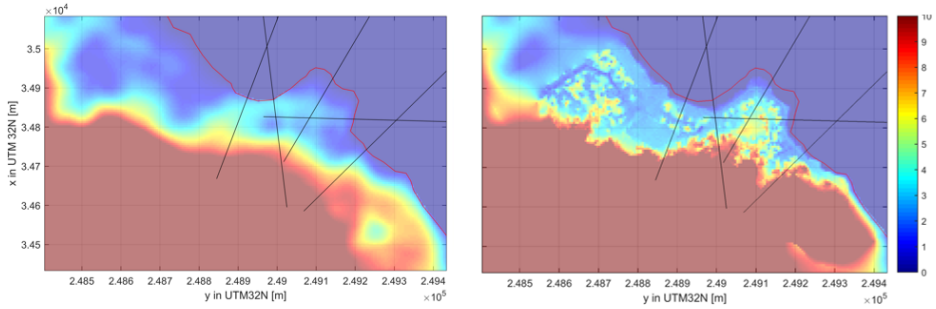

Figure B.4: (Left) TerraSar elevation map.(Right) drone image elevation map for Pantufo.

The results from the scenario with TerraSar-X elevation data for Pantufo are shown in Figure B.6. Two different simulations were made, one with the reference scenario (left in the figure) and one with the increased water level scenario. The flood maps show the higher sensitivity of the results to changes in the hydrodynamic forcing due to the different elevation input. This clearly shows the high importance of the quality in the data used for the elevation.

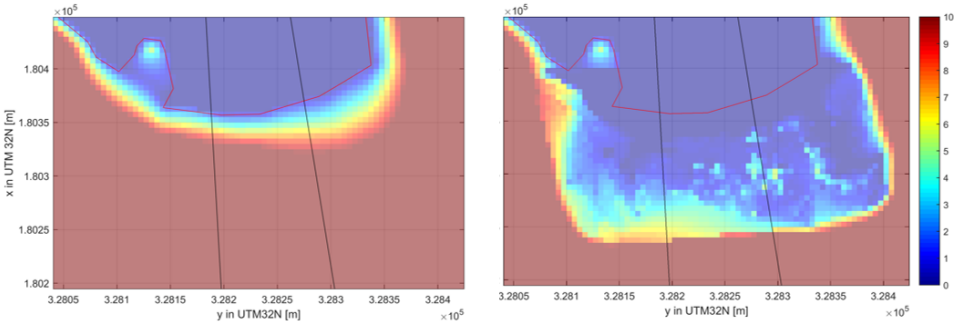

Figure B.5: (Left) TerraSar elevation map.(Right) drone image elevation map for Praia Abade.

Figure B.6: Maximum computed inundation depths in Pantufo with the reference scenario (left) and for the increased water level scenario (right) with TerraSar.

C

DEM Tests & Processing

C.1. Comparison of DEMs

One of the first step before choosing which DEMs to include in the analysis was to compare the globally available DEMs with the drone-derived DEM. The DEMs ASTER, MERIT and TANDEM are shown in Figure C.1, for the location of Pantufo, with a resolution of 5 m. To have this resolution, all the topographic dataset were resampled from their original tile size, using the bilinear method to interpolate between the points. Since most of the data points along the coastline were larger than 0, the coastline position taken from OpenStreetMaps was assumed as ground truth and used to represent the elevation of 0 m, shown as a red line in the figure.

As shown from the elevation maps, all the global DEMs tend to overestimate the elevation, having high values close to the coastline. The ASTER derived DEM is the one with more spurious points and seems the most unreliable. MERIT and TANDEM are both smoother and reproduce a more realistic terrain, although MERIT still contains some spurious points close, especially close to the headland, where an elevation of approximately 5 m is modeled right next to the coastline. From these figures, all the DEMs are expected to underestimate the flooding, with potentially TANDEM being the best of them.

The DEM were compared also for Abade and are illustrated in Figure C.2. Once again, TANDEM represent the local terrain more accurately than MERIT, which has high elevations close to the coastline.

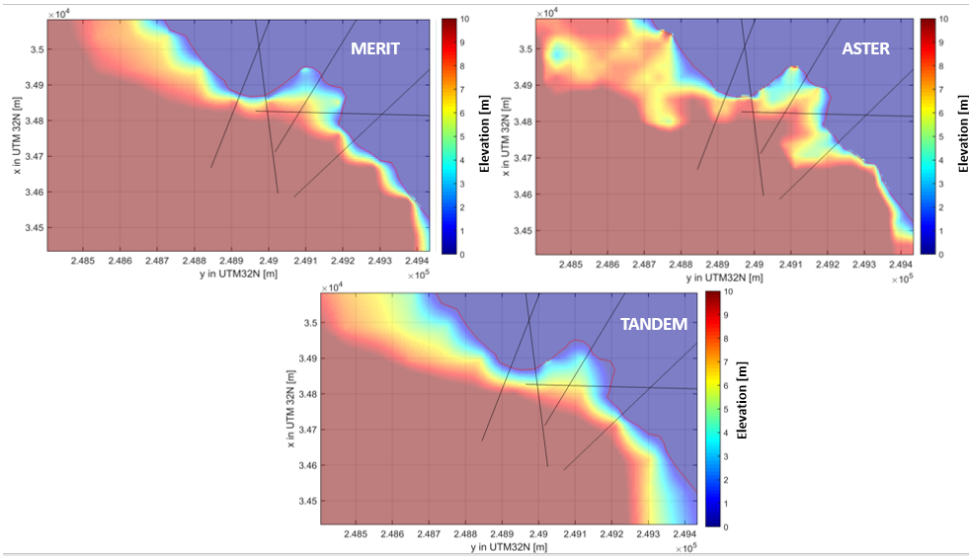

Figure C.1: Pantufo elevation models with a 5 m resolution derived from MERIT, ASTER and TANDEM. The red line represent the coastline.

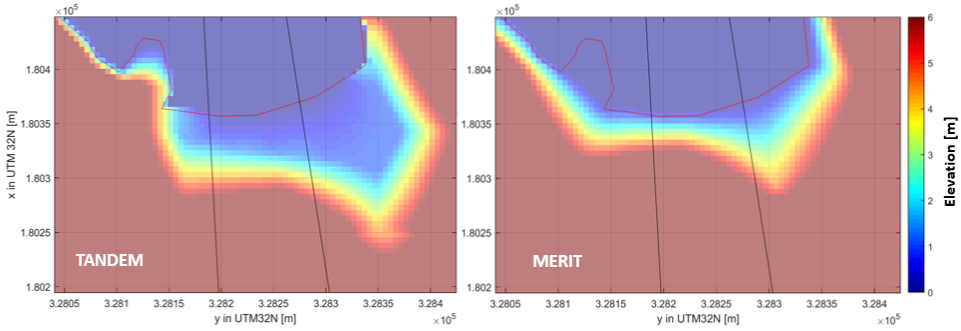

Figure C.2: Abade elevation models with a 5 m resolution derived from MERIT, and TANDEM. The red line represent the coastline.

C.1.1. COMPARISON WITH THE DRONE DEM

The elevation model retrieved from the drone aerial imagery is considered as ground truth for this study. This choice is based on the higher accuracy of UAVs derived DEM compared to satellite-derived (see Section 2.6) as well as the fact that the drone-derive DEM was calibrated using ground GPS measurements (Giardino et al., 2018). In ArcGIS, the elevation reproduced from the global DEMs TanDEM and MERIT was subtracted of the drone DEM elevation. Figure C.3 shows the result of the comparison, where a positive difference (red) indicates that the global DEM is higher than the drone DEM, whereas a negative difference (white) indicates the opposite. Generally, both DEMs are overestimating the elevation of the area, as it can be seen from the larger presence of the red colour, for both locations. For all the four figures, smaller or negative differences are present where the buildings are located (lighter colours). This is because the global DEM elevation values are averaged over different measurement points within the tile (see Section 2.6), which yields a value in between the bare earth surface and objects surface. This pattern is clear When the satellite DEMs are compared to the drone elevation, which has a much smaller resolution and allows to distinguish between the bare surface and, for example, the buildings roofs.

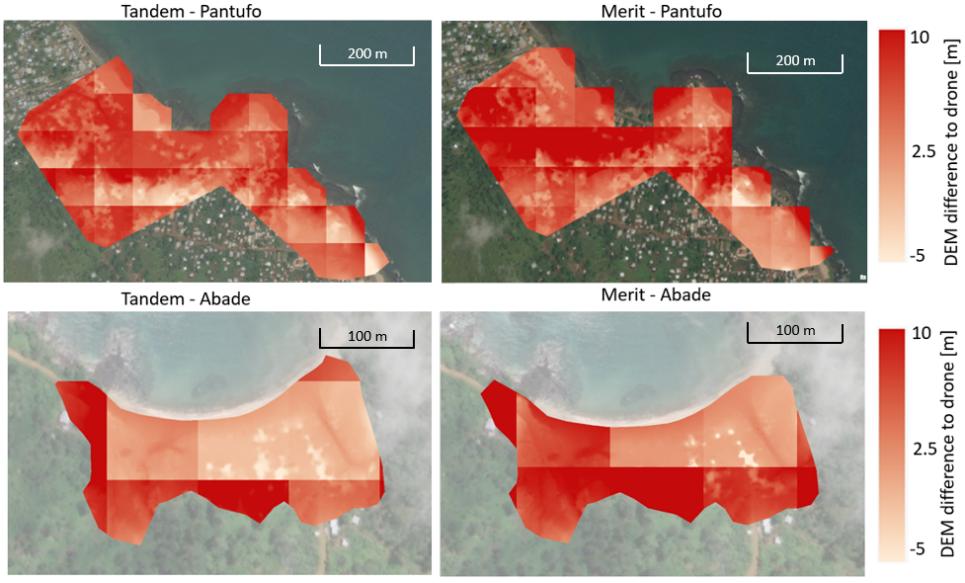

Figure C.3: Comparison of the two global DEMs TanDEM (left) and MERIT (right) with the drone-derived DEM, both for Abade (lower panels) and Pantufo (upper panels). The figures indicate the elevation difference between the two DEMs.

To quantify the inaccuracy in representing the elevation of the global DEMs, error metrics were retrieved.

C

ERROR QUANTIFICATION

Considering the drone DEM values as ground truth, the error in global satellite DEMs can be retrieved. (Wechsler and Kroll, 2006) suggest to use the mean error (ME) and the error standard deviation (SD) of the DEM to have a statistical representation of its inaccuracy. These two metrics can be more representative of the DEM inaccuracy than the root mean squared error, in cases where the mean error is unequal to zero (Wechsler and Kroll, 2006). The ME and SD are defined as follows:

$$ME = \frac{\sum_{i=1}^{n}(Z_{DEM} - Z_{ref})}{n} \tag{C.1}$$

$$SD = \sqrt{\frac{\sum_{i=1}^{n}[(Z_{DEM} - Z_{ref}) - ME^2]}{n}} \tag{C.2}$$

where Z_{DEM} and Z_{ref} are the elevations measured by the satellite and drone DEMs respectively. n is the number of measured elevation points within the two datasets, over which the ME and SD are measured. The comparison is made with both the dataset at a resolution of 5m. The choice of this resolution is based on the fact that is the resolution used for the computational grid of SFINCS. Table C.1 and C.2 below shows the results of the comparison for SRTM, MERIT, ASTER and TANDEM for Praia Abade and Pantufo, respectively.

Table C.1: Error Quantification of satellite based DEMs for Praia Abade.

	SRTM	MERIT	TANDEM	ASTER
ME [m]	6.43	6.35	3.23	6.9
SD [m]	0.95	0.55	0.54	0.73

Table C.2: Error Quantification of satellite based DEMs for Pantufo.

	SRTM	MERIT	TANDEM	ASTER
ME [m]	4.63	4.48	2.9	5.8
SD [m]	0.97	0.89	0.68	0.69

All the DEMs have a positive ME, thus overestimating the elevation. The global DEM that performs the best is TANDEM, having the smallest ME, both in Pantufo and in Praia Abade. MERIT and SRTM show similar results which suggests that MERIT,a vegetation corrected version of the SRTM model, has not improved much the modeled elevation for the area of Sao Tome. ASTER has the lowest accuracy compared to the drone, with the highest ME of 6.9 m in Praia Abade. One of the limits of these descriptive metrics is that they do not represent the spatial variability of a DEM, which can be qualitatively assessed in Figure C.3. Given these results, we expect TANDEM to perform best among the other satellite DEMs in reproducing the flooding and and thereby the damages in the two locations. the fact that the quality of a DEM is spatially varying

C.2. DEM PROCESSING

C.2.1. CORRECTION FOR BUILDINGS AND TREES

As it as previously been discussed in Section 3.5.3, there is a distinction in elevation models between terrain models and surface models. In many risk analyses, surface models that include buildings and vegetation are directly used as terrain models, meant to represent the bare earth surface (Van de Sande et al., 2012). For our case, it was important to test the sensitivity of our models to the use of DSMs or DTMs. MERIT, SRTM, ASTER, TanDEM models were therefore corrected as much as possible from trees and houses. The buildings and trees location were drawn as shape-files in ArcGIS Pro from the drone images. Then, the results using the corrected and not corrected elevation were both included in the overall sensitivity analysis to estimate the impacts of such correction. Trees and buildings were corrected assuming a constant height for trees and houses of 3 m. This value is rather conservative, especially regarding the tree height, nevertheless, our knowledge regarding the exact trees heights and their influence in the global DEMs was little for this location, thus a conservative approach is preferable. The correction was made in a similar manner to the process of transforming the shape-file into raster files explained in Section 3.4. First, trees and buildings shape-files were transformed into raster files. Then, the raster riles containing a tree or an house were assigned a value of 3, whereas the other tiles were assigned 0 as value. Figure C.4 shows the shape-files indicating buildings and trees in Praia Abade.

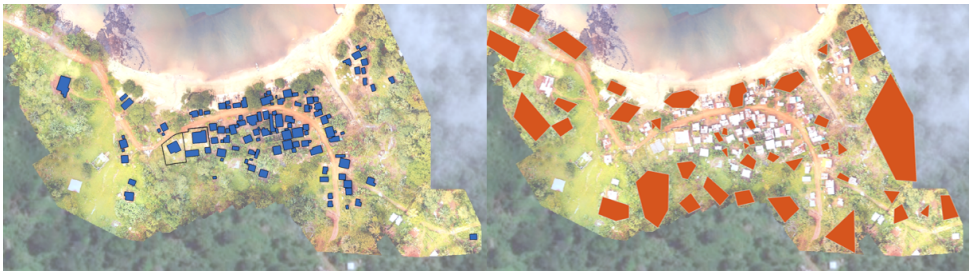

Figure C.4: Shape-files used to correct from houses (left) and trees canopy (left) elevations in Praia Abade.

The raster tiles were then aggregated at a larger resolution, equal to the global DEM (30 or 90 m accordingly to the specific DEM) and taking the mean representing value of each tile. After the aggregation, the larger raster cells would have a value varying from 0, representing no trees or building present in the tile area, to 3, representing the situation where all the area is comprised of trees or buildings. The raster representing the correction factor of trees for Abade is shown in Figure C.5 where darker tiles have a smaller correction value and lighter tiles a larger one. The value of the correction factor ranges from 0 to a maximum of 0.8 m for the tile where most trees canopies where identified. Such raster was used to correct the global satellite-based DEMs.

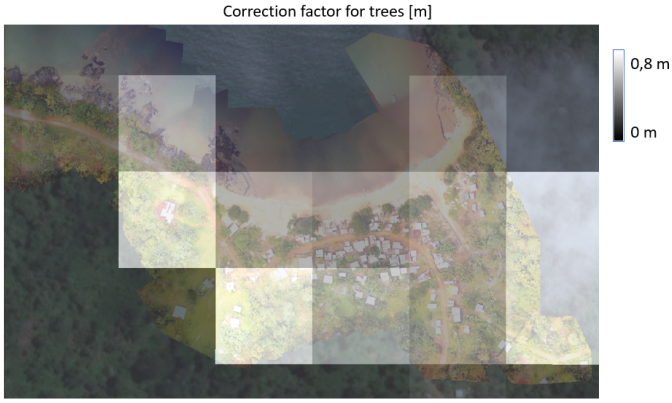

Figure C.5: Correction trees raster for Abade with a 90 m resolution, used to correct the global satellite-based DEMs.

C.2.2. CORRECTION FOR THE DRONE DEM

Although holding a high accuracy, the drone DEM also contained elevation points that measured roofs of houses and canopies of trees. Some of this grid cells were then modeled by SFINCS as dry points. This is visible in Figure C.6, where the orange points in the zoomed drone map represent higher elevations. These points are situated where buildings roofs and tree canopies are present. The resulting estimated flooding map shows dry points in these spots. These higher points were then partially lowered, so that the DEM could represent the bare earth terrain more accurately. However, in order to avoid sharp change in slope where the correction was made, the values were only reduced of 1m.

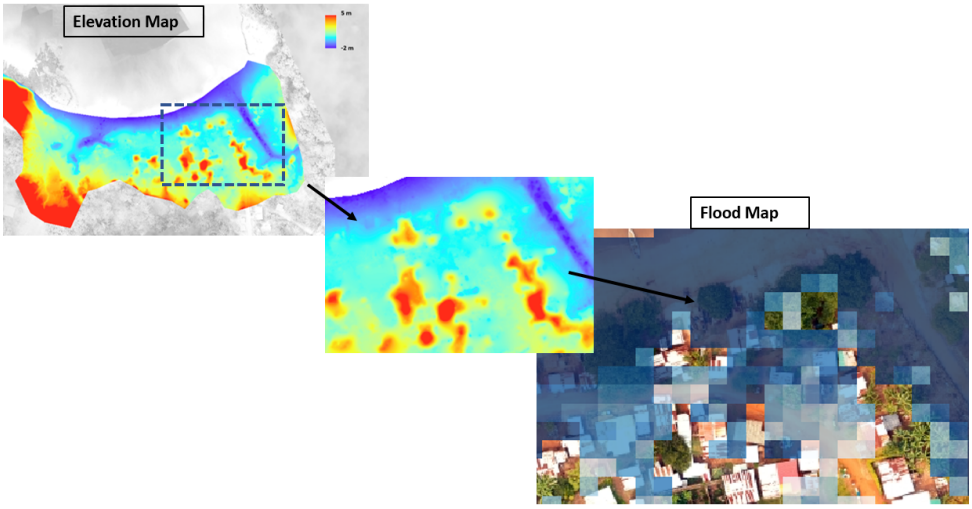

Figure C.6: Drone DEM points representing trees canopies and buildings roofs, in the right corner the computed flooding is plotted, where these points are dry.

D

MODEL PRE- AND POST-PROCESSING

This chapter includes a simple workflow showing the main necessary steps o process the data and run the models. Most of the function cited are available at (OpenEarthTools, 2013).

D.1. HAZARD MODELING PROCESSING

Figure D.1 shows the necessary steps followed to pre-process model inputs and post-process the outputs. The matlab functions *xb_grid_xgrid.m, xb_generate_model.m, bc_storm_surge.m, sfincs_initialize_input.m, sfincs_write-boundary_points.m, sfincs_write_input.m, sfincs_binary_output.m* are available on the open source platform Open Earth Tools developed by Deltares (OpenEarthTools, 2013). The matlab function *scatteredInterpolant.m* is found in Matlab[1].

The following three figures show an example of the input files compiled and used by Xbeach (D.2 and D.3) and SFINCS (D.4). The *params.txt* file contains the user specified parameters given to the model XBeach. For a detailed description of the parameters, the reader is referred to the manual (Roelvink et al., 2015). The two files *bcfile* and *zs0file* define the Jonswap spectrum parameters and the mean water levels during the simulation.

The input file *sfincs.inp* includes the values for the model parameters, as swell as the name of the files containing the water level time series. The incoming water level signal is split in two different components, a mean one *bzsfile*, and a deviation from the mean one, *bzifile*. The *depfile* and *mskfile* are used to specify the topography and distinguish between active and non active cells in the model.

[1] MATLAB 2018b, The MathWorks, Natick, 2018.

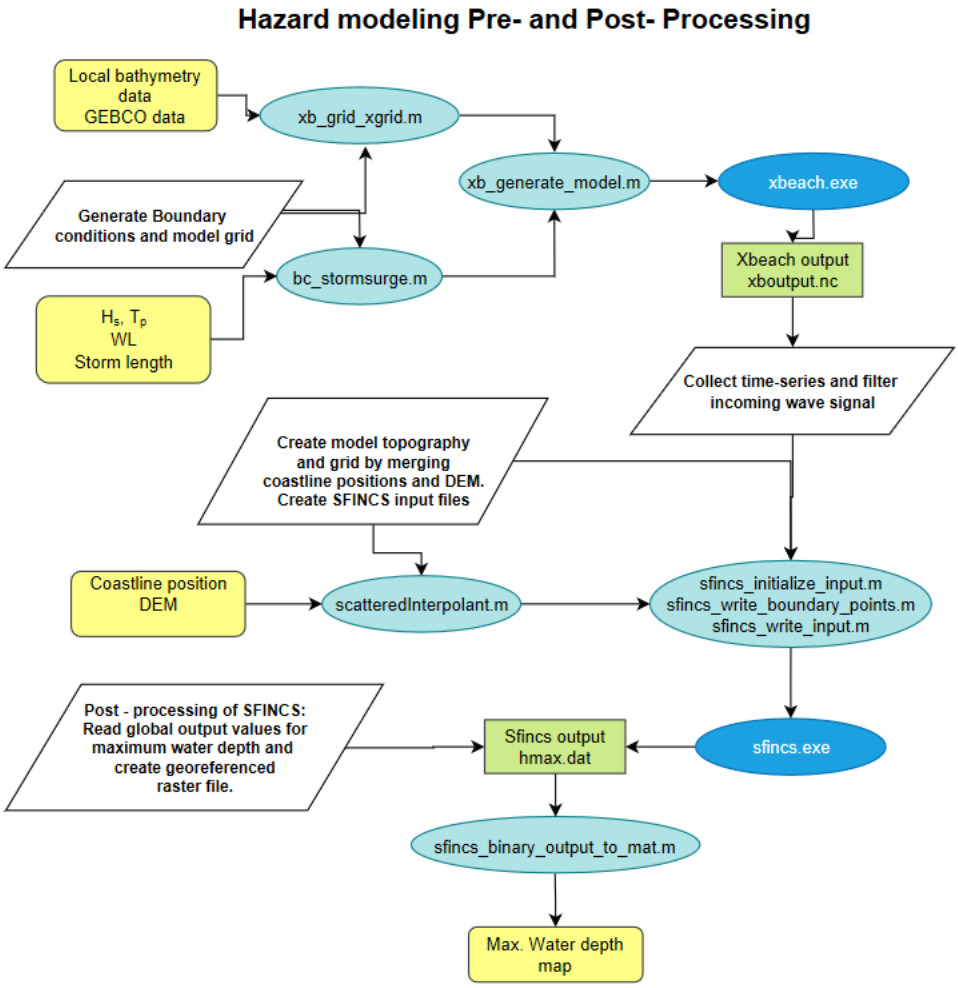

Figure D.1: Hazard modeling workflow, with the main processing steps.

```
%%%%%%%%%%%%%%%%%%%%%%%%%%%%%%%%%%%%%%%%%%%%%%%%%%%%%%%%%%%%%%%%%%%%%%%%
%%%%%%%%%%%%%%%%%%%
%%% XBeach parameter settings input file
%%%
%%%
%%%
%%% date:     11-Apr-2019 11:23:13
%%%
%%% function: xb_write_params
%%%
%%%%%%%%%%%%%%%%%%%%%%%%%%%%%%%%%%%%%%%%%%%%%%%%%%%%%%%%%%%%%%%%%%%%%%%%
%%%%%%%%%%%%%%%%%%%

%%% Flow boundary condition parameters
%%%%%%%%%%%%%%%%%%%%%%%%%%%%%%%%%%%%%%%%%%%%

front      = nonh_1d

%%% General
%%%%%%%%%%%%%%%%%%%%%%%%%%%%%%%%%%%%%%%%%%%%%%%%%%%%%%%%%%%%%%%%%%%%%%%%
%%%%%%

nonhq3d    = 1
tidelen    = 2

%%% Grid parameters
%%%%%%%%%%%%%%%%%%%%%%%%%%%%%%%%%%%%%%%%%%%%%%%%%%%%%%%%%%%%%%%%%%%%%%%%

depfile    = bed.dep
posdwn     = 0
nx         = 967
ny         = 0
alfa       = 0
vardx      = 1
xfile      = x.grd
yfile      = y.grd
xori       = 0
yori       = 0
thetamin   = 0
thetamax   = 360
dtheta     = 360

%%% Model time
%%%%%%%%%%%%%%%%%%%%%%%%%%%%%%%%%%%%%%%%%%%%%%%%%%%%%%%%%%%%%%%%%%%%%%%%
%%%

tstop      = 21600

%%% Physical processes
%%%%%%%%%%%%%%%%%%%%%%%%%%%%%%%%%%%%%%%%%%%%%%%%%%%%%%%%%%%%%%%%%%%%%%%%

swave      = 0
sedtrans   = 0
morphology = 0
nonh       = 1
```

Figure D.2: XBeach input file, first part.

```
%%% Tide boundary conditions
%%%%%%%%%%%%%%%%%%%%%%%%%%%%%%%%%%%%%%%%%%%%%%%%%%%

zs0file    = tide.txt
tideloc    = 2

%%% Wave boundary condition parameters
%%%%%%%%%%%%%%%%%%%%%%%%%%%%%%%%%%%%%%%%%

instat     = jons_table

%%% Wave-spectrum boundary condition parameters
%%%%%%%%%%%%%%%%%%%%%%%%%%%%%%%%

bcfile     = jonswap.txt

%%% Output variables
%%%%%%%%%%%%%%%%%%%%%%%%%%%%%%%%%%%%%%%%%%%%%%%%%%%%%%%%%%%

tintm      = 1800
tintp      = 0.250000
tintg      = 300

nglobalvar = 4
zs
zb
u
qx

nmeanvar   = 3
H
zs
zb

npointvar  = 2
zs
u

npoints    = 7
328020 181932 point1
328025 181905 point2
328270 180399 point3
328275 180369 point4
328249 180527 point5
328223 180690 point6
328263 180445 point7

nrugauge   = 1
328270 180399 point8
```

Figure D.3: XBeach input file, second part.

```
mmax            = 151
nmax            = 171
dx              = 5
dy              = 5
x0              = 248600
y0              = 34650
rotation        = 0
tref            = 20190101 000000
tstart          = 20190101 000000
tstop           = 20190101 060000
dtout           = 300
dthisout        = 300
dtwnd           = 1800
alpha           = 0.5
manning         = 0.02
manning_land    = 0.04
manning_sea     = 0.02
rgh_lev_land    = 0
zsini           = 0
qinf            = -1.3889e-06
rhoa            = 1.25
rhow            = 1024
cd_nr           = 0
depfile         = sfincs.dep
mskfile         = sfincs.msk
geomskfile      = sfincs.gms
indexfile       = sfincs.ind
bndfile         = sfincs.bnd
bzsfile         = waves_surge_zs.rp1
bzifile         = waves_surge_bzi_.rp1
hmaxfile        = hmax.dat
hmaxgeofile     = hmaxgeo.dat
zsfile          = zs.dat
vmaxfile        = vmax.dat
obsfile         = sfincs.obs
inputformat     = bin
outputformat    = bin
min_lev_hmax    = -5
huthresh        = 0.02
advection       = 2
theta           = 0.9
bndtype         = 1
```

Figure D.4: Sfincs input file.

D.2. DAMAGE MODELING PROCESSING

The following Figure D.5 includes the main steps taken to set up the excel configuration file, which contains all the input parameters that are given to FIAT. Since multiple simulations were necessary, FIAT was used through a python script that allows for a fast iteration of the model over different parameter values. The Matlab functions *mapraster-ref.m, imref2d.m* and *geotiffwrite.m* are available from the Mapping Toolbox developed by (MATLAB Mapping Toolbox, 2018) and are used to georeference the flood maps obtained from SFINCS.

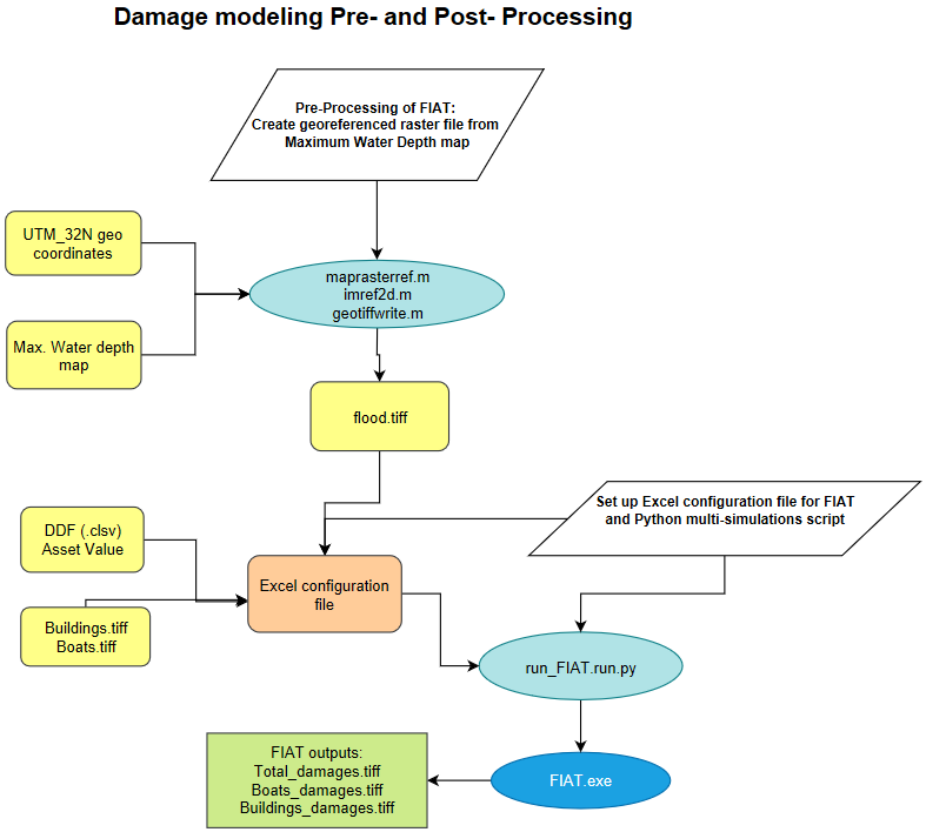

Figure D.5: Workflow of the damage processing steps for FIAT.

To create the raster files of buildings and boats from the shapefiles the following steps were performed. Given the fact that the flood maps had a 5 meter resolution and the shapefiles cell size was much smaller (approximately 10 cm), the latter ones had to be resampled to a larger resolution. The following steps use functions and tools from the software ArcGIS Pro (ESRI, 2014) and a work-flow summarizing the steps is shown in Figure D.6. Using the tool *polygon to raster* the shape-files were transformed into raster files and then the cell values were reclassified (with the *reclassify* tool)in such a way to

have cells representing the assets with value 1 and the other cells with value 0. Then, the cells were aggregated into larger cells of 5 by 5 meters with the *aggregate* tool, assigning to the larger resulting cell the mean value of the smaller cells. The result is a raster file with a 5 by 5 grid size that contains a value ranging from 0 to 1. These values indicate what fraction of the cell represents the asset. In other words, if a tile has a value of 0.4, 40% of the smaller cells that were aggregated represented an asset. The environment settings of ArcGIS Pro were set to have the output raster with the same extent of inundation map rasters.

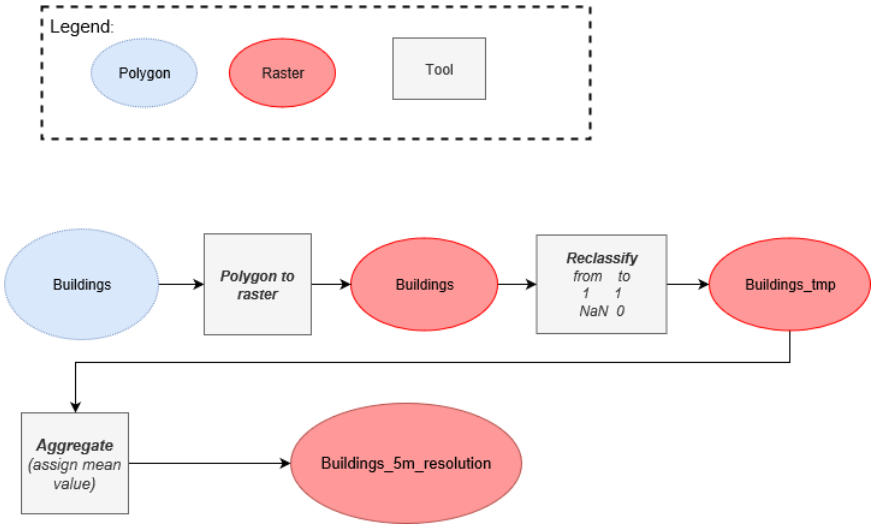

Figure D.6: Workflow followed in the analysis to transform the shape-files of the assets into raster files with a 5 m resolution, using ArcGIS Pro.

The three models had different simulation time and different number of simulations required, which are also summarised below in Table D.1.

Table D.1: Summary of necessary simulations and respective run times

Model	Single run [minutes]	number of runs	Total run time [hours]
XBeach - NH+	50	36	30
SFINCS	2	180	6
FIAT	0.1	1260	2.1

E

INTERPOLATION TECHNIQUES

E.1. BACKGROUND

In topography models, another source of uncertainty comes from the chosen resolution. For some applications, a very high resolution dataset may be available, but its use is constrained by the computational time of the flooding model. To not exceed acceptable computational expenses, the computational grid size may need to be one order of magnitude larger than the resolution of the DEM. Therefore, by applying an appropriate sampling technique to downscale the topography data, some of he initial information gets lost. Different techniques are available to interpolate between scattered data points and the choices change according to the application, considering different project time and computational power available (Amidror, 2002).
The range of interpolation techniques that are available differs for complexity, accuracy and computational effort required. In general, the methods can either be defined *global* or *local*. In a global approach, each interpolated value is influenced by all data and are limited to small datasets due to large computational effort. In a local method, only a subset of the surrounding points is used to compute the value at the interpolated point. They hold the advantage of being more affordable and can become rather complex too. A further distinction for local methods, is distance and area based methods. Distance based only compute the weights for each point based on the distances to the interpolated point. For area methods, the weights are based on areas and hold the advantage to be sensitive to data density.

In the field of environmental risk modeling, it may be well possible that the resolution at which a DEM is available overcomes the computational feasibility of a specific model. Numerous studies have approached the question of which interpolation technique would be best under certain circumstances and what parameters are they most sensitive to (Guo et al., 2013), (Weng, 2002), (Aguilar et al., 2013). (Guo et al., 2013) have investigated the consequence of terrain variability, as well as sampling density on different techniques, founding significant influences from both of them. They also linked

the increase of interpolation error to the surface roughness, indicating a positive correlation between the two parameters. According to the authors, increasing the density can largely reduce the dependency of the interpolation error on the different techniques.

E.2. METHODOLOGY

The drone-derived DEM was used as testing dataset for different interpolation techniques. The two resolution of 2 and 5 m were chosen in order to potentially assess dependency on the resolution of the sampling. The choice went on these two as they proved to give a good comprise between flooding prediction accuracy and computational time (see Section 4.5.2) and thus to continue the improvement of SFINCS. Since time was a limiting factor, Matlab was selected as software to extrapolate the different topography maps with the function *scatteredInterpolant.m*. With this function, the actual mathematical calculations cannot be varied to check and test different settings and therefore it is recommended that for future studies, other software and tools are used that include more functions, for example GDAL.
Three interpolation techniques are available in the function, from (Amidror, 2002):

- *Linear*, consists in linear triangulation-based interpolation, an area-base method.
- *Natural Neighbour*, similar to the *linear method*, but the areas of influence are drawn as Voronoi tiles. It is considered to be more robust than the linear method, but more expensive.
- *Nearest Neighbour*, where the closest data point from the interpolation point is taken as value.

Amongst all, Natural Neighbours is thought to be the most accurate while keeping a good level of accuracy, (Amidror, 2002). It was expected that Nearest Neighbour, being the simplest and crudest method, would yield to the largest differences.

The three different methods were tested under nine hydrodynamic conditions, combining three H_s values and three *storm surge* values, both for Pantufo and Praia Abade.

Another point of discrepancy was believed to be the starting coordinate of the interpolation points and hence the coordinates of the points at larger resolution. It is possible, that if we vary the footprint of each interpolating point, the interpolated value would change as well. The concept is illustrated in Figure E.1. The blue points are the measured points at a very fine resolution. The yellow diamonds indicate the locations of the extrapolated grid points with a resolution of 5m, for illustrative purposes. The grid points footprints, the area from which they averaged the measured points, are represented as shaded yellow circles. If the position of the grid points is shifted, (S_x in the graph, the points over which the interpolation is done, change. To test whether this could have a large impact on the modeled topography and ultimately on the model output, the starting point of the grid was shifted 5 times for the 5m resolution (each one meter apart) and 4 times for the 2m resolution (each half a meter apart). The shift are applied in both horizontal directions.

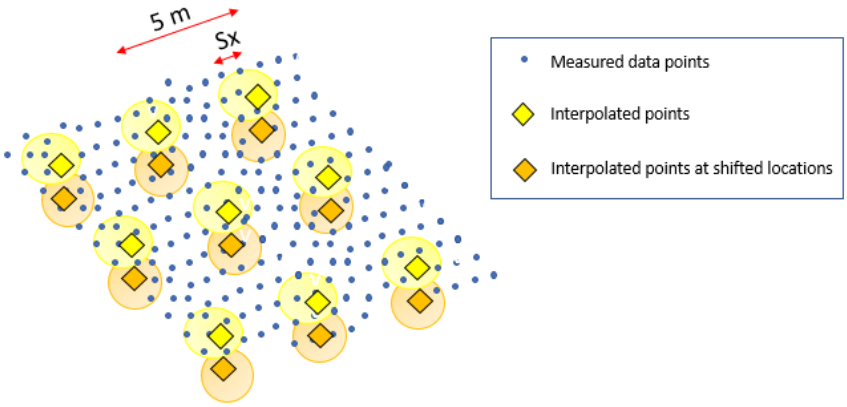

Figure E.1: Flooding volumes using different interpolation techniques in Praia Abade (left) and the estimated errors compared to the natural interpolation method, with a 2m (top panels) and 5m(resolution) .

In order to consider different combinations, each interpolation was considered for both resolutions and locations, as well as for each hydrodynamic condition and grid starting point step.

E.3. RESULTS & DISCUSSION

The following figures show the results, divided for interpolation techniques (Figures E.2 and E.3) and for different starting point shifts (Figures E.4 and E.5).

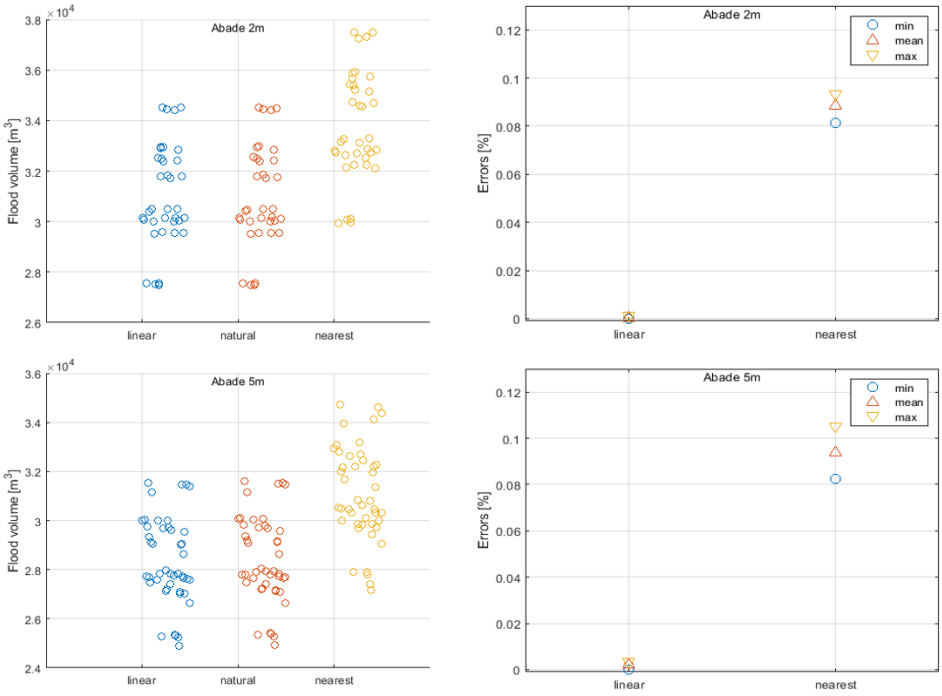

Figure E.2: Flooding volumes using different interpolation techniques in Praia Abade (left) and the estimated errors compared to the natural interpolation method, with a 2m (top panels) and 5m(resolution) .

Although a clear common conclusion could be drawn, it is clear that *nearest neighbour* method, as expected, gives the biggest differences in the computed flooding. This occurs for both resolution in Praia Abade and for the 5m resolution in Pantufo, where the differences between the *linear* and *natural* methods are always very small. However, the same does not occur for the resolution of 2m in Pantufo, where the *linear* method gives the larger errors.
Regarding the differences introduced by sampling the grid points at different locations, looking at the results, it can be said that generally it does not vary largely the topography. Indeed, in Abade, the errors are always smaller than 2%. The results are less consistent in Pantufo, where a shift of 0.5 m for the 2 m grid and a shift of 2 m for the 5m grid give a mean error of 5% and 8% respectively.

In Pantufo more unexpected results are found, such as the larger error given by the linear interpolation method, or the anomalies in the computed damages using a particular shift in the grid location. This could be linked to the higher spatial variability of the area, although a clear conclusion cannot be drawn at this preliminary stage. It is

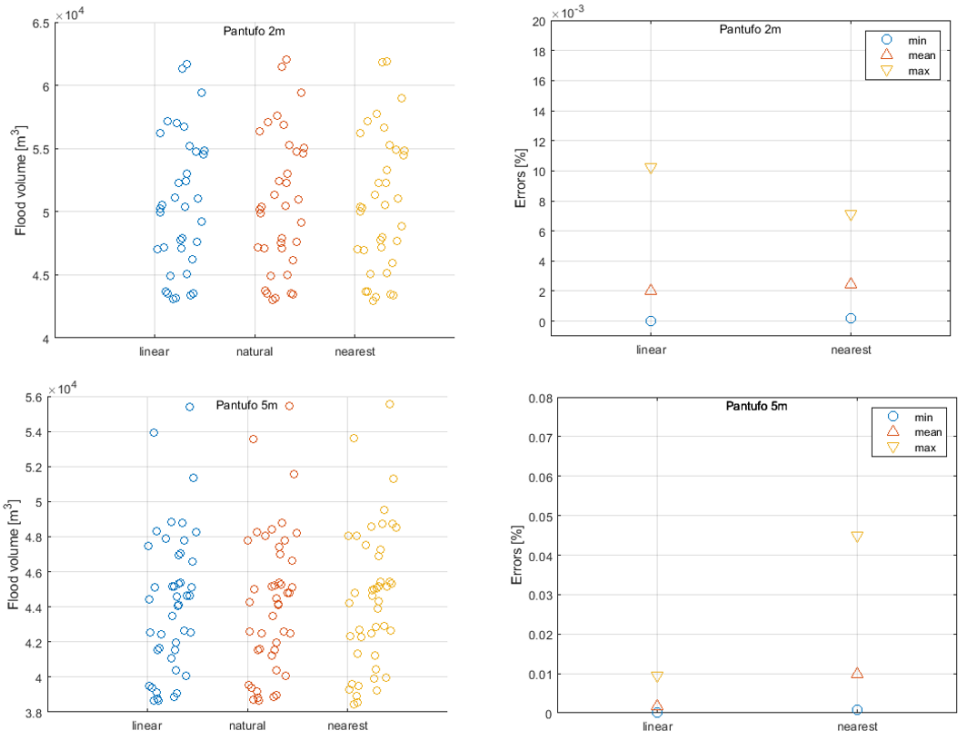

Figure E.3: Flooding volumes using different interpolation techniques in Pantufo (left) and the estimated errors compared to the natural interpolation method, with a 2m (top panels) and 5m(resolution) .

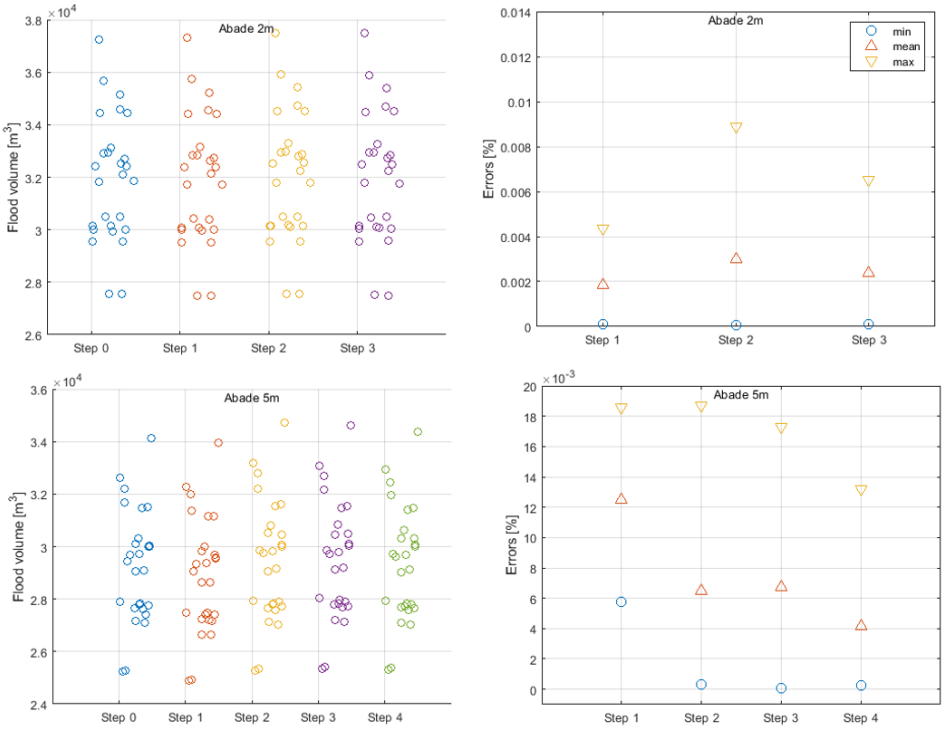

Figure E.4: Flooding volumes using different starting point steps in Praia Abade (left) and the estimated errors compared to the interpolation with no starting point step, with a 2m (top panels) and 5m(resolution) .

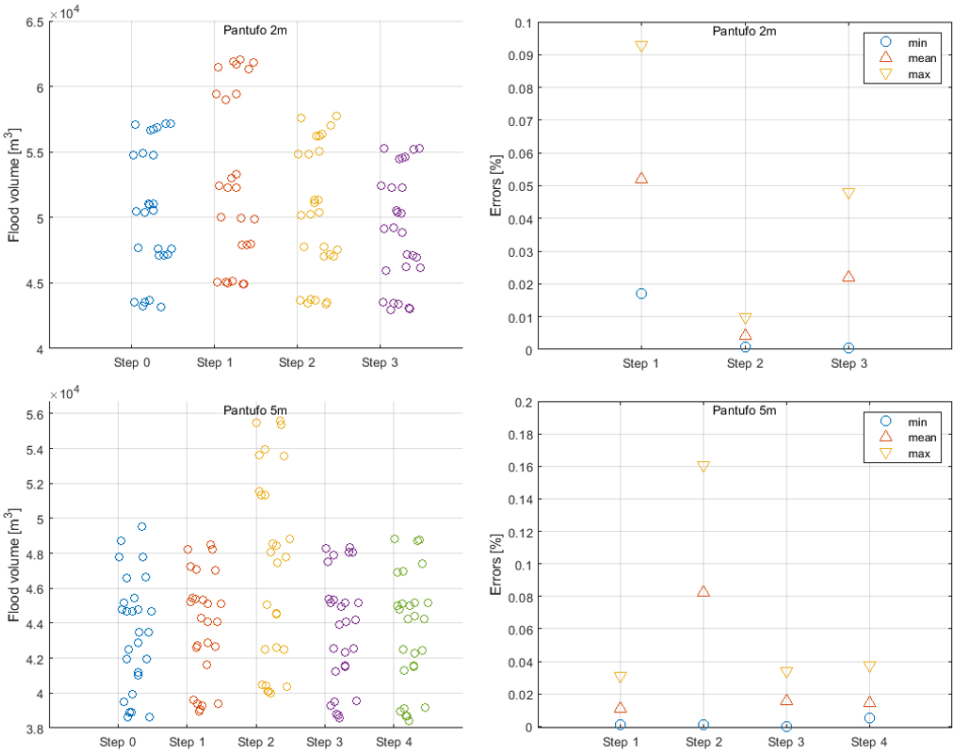

Figure E.5: Flooding volumes using different starting point steps in Pantufo (left) and the estimated errors compared to the interpolation with no starting point step, with a 2m (top panels) and 5m(resolution).

therefore recommended that a more thorough assessment of the effects of interpolation techniques on retrieving DEM for flood modeling is conducted.